AWARD NUMBER: W81XWH-12-1-0319

TITLE: VRPD Novel Combinatory Approaches to Repair Visual System After Optic Nerve Damage

PRINCIPAL INVESTIGATOR: Kevin K. Park

RECIPIENT: University of Miami, Coral Gables, FL 33146

REPORT DATE: May 2015

TYPE OF REPORT: Final

PREPARED FOR: U.S. Army Medical Research and Materiel Command
Fort Detrick, Maryland 21702-5012

REPORT DOCUMENTATION PAGE

Form Approved
OMB No. 0704-0188

1. REPORT DATE	2. REPORT TYPE	3. DATES COVERED
May 2015	Final	30 Aug 2012 – 28 Feb

4. TITLE AND SUBTITLE

VRPD Novel Combinatory Approaches to Repair Visual System After Optic Nerve Damage

5a. CONTRACT NUMBER

5b. GRANT NUMBER
W81XWH-12-1-0319

5c. PROGRAM ELEMENT NUMBER

6. AUTHOR(S)
Kevin Park

E-Mail: kpark@med.miami.ed

5d. PROJECT NUMBER

5e. TASK NUMBER

5f. WORK UNIT NUMBER

7. PERFORMING ORGANIZATION NAME(S) AND ADDRESS(ES)

University of Miami
Coral Gables, FL 33146

8. PERFORMING ORGANIZATION REPORT NUMBER

9. SPONSORING / MONITORING AGENCY NAME(S) AND ADDRESS(ES)

U.S. Army Medical Research and Materiel Command
Fort Detrick, Maryland 21702-5012

10. SPONSOR/MONITOR'S ACRONYM(S)

11. SPONSOR/MONITOR'S REPORT NUMBER(S)

12. DISTRIBUTION / AVAILABILITY STATEMENT

Approved for Public Release; Distribution Unlimited

13. SUPPLEMENTARY NOTES

14. ABSTRACT

Poor survival of retinal ganglion cells and axon regeneration poses major challenges to achieving functional recovery after optic nerve damage, which occurs in battlefield and post-combat in a delayed manner. In our studies, we have discovered that combining genetic modulations including PTEN deletion, to target multiple genes promotes striking neuronal survival and axon regeneration. Further, we observed that genetically modified RGCs exhibit relatively normal physiology, a critical aspect in our quest to achieve functional restoration after optic nerve damage. Technically, we have successfully developed and optimized AAV vectors, shRNA and imaging tools to better evaluate optic nerve regeneration. Overall, our study tested several combinatorial strategies and identified effective strategies to strongly promote RGC survival and axon regeneration after optic nerve injury.

15. SUBJECT TERMS
None provided

16. SECURITY CLASSIFICATION OF:			17. LIMITATION OF ABSTRACT	18. NUMBER OF PAGES	19a. NAME OF RESPONSIBLE PERSON
a. REPORT	b. ABSTRACT	c. THIS PAGE			USAMRMC
Unclassified	Unclassified	Unclassified	Unclassified	73	19b. TELEPHONE NUMBER *(include area code)*

Table of Contents

1. **INTRODUCTION:** Death of retinal ganglion cells (RGCs) and poor regeneration are major obstacles for treating traumatic optic neuropathy after road accident, falls or combat blasts. Optic nerve regeneration from many long-term surviving RGCs, reconnecting the brain could potentially restore vision after injury. We previously determined that deletion of two genes, PTEN and SOCS3 induces optic nerve regeneration (Park *et al.*, 2008; Smith *et al.*, 2009; Sun *et al.*, 2011). On the other hand, genetic modification of CHOP and XBP1 in RGCs render them highly resistant to injury-induced death (Hu *et al.*, 2012). We hypothesize that combined strategies to target PTEN/SOCS3 and CHOP/XBP1 will further enhance long-term RGC survival and regeneration, and RGCs in these animals exhibit normal physiological responses. In this proposal, we have used knockout mice and therapeutically relevant short hairpin RNA (shRNA) approaches to determine the combined effects of targeting PTEN/SOCS3 and CHOP/XBP1 on RGC survival and regeneration after injury. Further, we examined the integrity of RGC functions after modification of these genes using pattern electroretinogram (PERG). In addition, we have developed new imaging techniques to assess optic nerve regeneration in whole animal tissues without histological sectioning. Overall, this proposal investigates genetic interventions to rescue dying neurons and promote regeneration, and restore vision, with the potential to be administered to the clinic and battlefield.

2. **KEYWORDS:** Axon regeneration, PTEN, SOCS3, XBP1, CHOP, retinal ganglion cells, axotomy, axon injury, PERG, Axon growth.

3. **OVERALL PROJECT SUMMARY:**

Aim 1: Use knockout mice to examine the combined effects of targeting PTEN/SOCS3 and CHOP/XBP1 on RGC survival and regeneration. PTEN/SOCS3/CHOP knockout mice will receive AAV-assisted over-expression of XBP1, followed by nerve crush injury and assessment of RGC survival and regeneration.

In this Aim, we have mated PTEN/SOCS3$^{f/f}$ mice with CHOP KO mice to generate triple mutant mice, PTEN/SOCS3$^{f/f}$/CHOP KO mice. Adult mice received various AAV treatments as outlined in Table 1 below.

Groups (n=8-10/group)	**Intravitreal Viral Treatment**	**Outcome Measures**
PTEN/SOCS3$^{f/f}$	AAV-GFP (Control)	RGC staining and axon tracing
PTEN/SOCS3$^{f/f}$	AAV-Cre	" "
CHOP$^{-/-}$	AAV-XBP1	" "
CHOP$^{-/-}$ /PTEN/SOCS3$^{f/f}$	AAV-Cre/AAV-XBP1	" "

At different time points after intraorbital optic nerve crush, animals were analyzed for RGC survival and axon regeneration using immunohistochemistry and axon tracing methods used in our previous studies. At 4 and 8 weeks after injury, retinas were immunostained with an antibody against beta III tubulin (TUJ1) to estimate RGC survival. The degree of axon

regeneration, assessed by dye-labeled fibers was quantified and compared among the control animal groups. Using histology, axon regeneration into various visual targets including the lateral geniculate nucleus, superior colliculus, olivary pretectal nucleus and suprachiasmatic nucleus was assessed. As shown in Fig. 1, we have found that while manipulation of two genes (i.e. PTEN/SOCS3 or CHOP/XBP1) in combination resulted in some degree of neuroprotection after optic nerve injury, the ultimate combination targeting all four genes (PTEN/SOCS3/CHOP/XBP1) led to marked improvement in the rate of RGC survival at 4 and 8 weeks after injury. These results represent one of the most powerful genetic strategies that protect injured RGCs reported to date. Importantly, our unique approaches use gene therapy strategy which raises hope for treating damaged optic nerve.

In addition to RGC survival, we examined the rate of axon regeneration in the combinatorial treatment groups. Successful re-innervation of regenerated axons to their targets is of paramount interest. Thus, the next important question is whether the number of axons that regenerate long distances into the visual targets is also increased in these animals. In order to determine this, we are currently analyzing the sectioned brain tissues to identify and quantify the number of regenerated axons in various visual targets.

As shown in Fig. 2, we observed that combinatorial treatments result in enhanced axon regeneration along the damaged optic nerve.

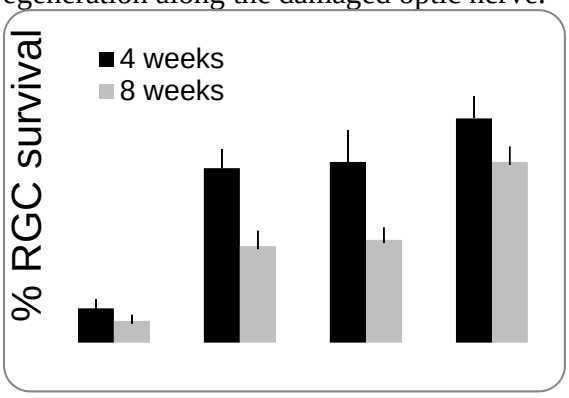

Figure 1. Combined modulation of PTEN/SOCS3/CHOP and XBP1 further enhances RGC survival after injury. Data are presented as mean % of RGC number compared to the uninjured contralateral eye at 4 and 8 weeks after injury. P/S KO, PTEN/SOCS3 KO; C/X, CHOP KO/XBP1 mice; P/S/C/X, PTEN/SOCS3/CHOP KO/XBP1 mice.

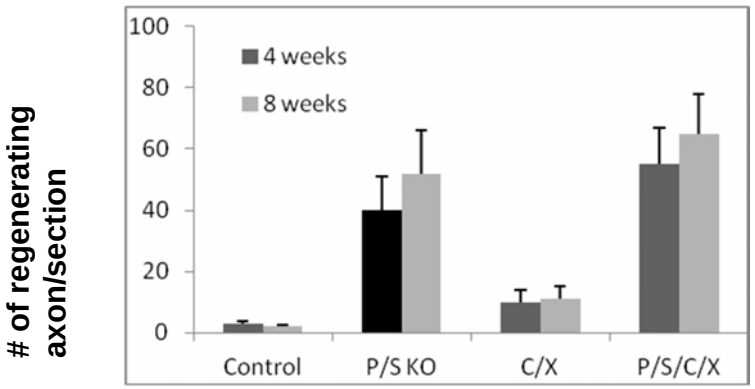

Figure 2. Combined modulation of PTEN/SOCS3/CHOP and XBP1 further enhances RGC axon regeneration. Data are presented as mean number of axons counted/ optic nerve section at 3 mm distal to the lesion site at 4 and 8 weeks after injury. Consistent with previous findings, control and C/X animals did not have regenerated axons. P/S KO, PTEN/SOCS3 KO; C/X, CHOP KO/XBP1 mice; P/S/C/X, PTEN/SOCS3/CHOP KO/XBP1 mice.

Aim 2: Integrity of RGC functions after genetic modification of PTEN/SOCS3 or CHOP/XBP1 will be evaluated using PERG.

In this Aim, we have used PERG to investigate whether RGCs subjected to different genetic manipulations exhibit normal physiological functions.

Groups (n=7-14/group)	**Outcome Measures**
PTEN/SOCS3 modified	PERG
WT control	" "

At different time points (0, 7, 40 and 60 days) after intraorbital optic nerve crush, PTEN/SOCS3-modified or control animals were analyzed for PERG measurement. The PERG amplitude in PTEN/SOCS3-modified animals decreased 7 days after injury but in 4 eyes out of 7, the PERG signal then progressively tended to a recovery. In control animals PERG did not show any obvious recovery (data not shown).

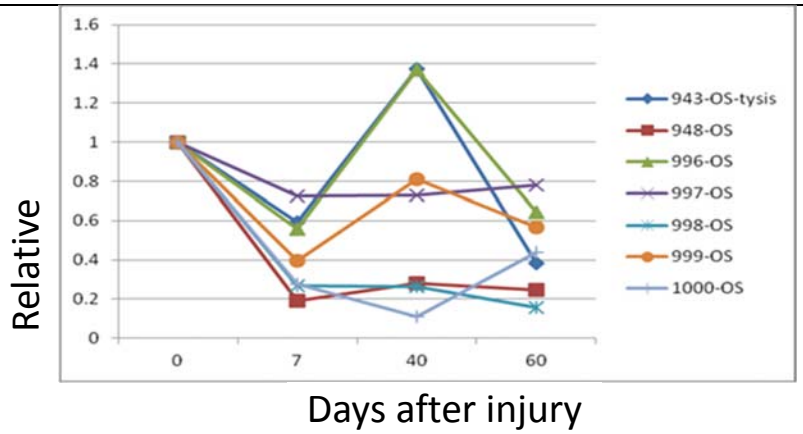

Figure 3. Mean PERG amplitude in Pten/Socs3-modified mice before and at different times after injury. All data were normalized to mean baseline values.

In addition, we have recently developed new methods to analyze optic axon regeneration in animal tissues without physical sectioning.

Traditional methods of assessing RGC axon regeneration rely on histological sectioning. However, tissue sections provide fragmentary information about axonal trajectory and termination. To unequivocally evaluate regenerating RGC axons, we apply tissue clearance and light sheet fluorescence microscopy (LSFM) to image axons in whole optic nerve and brain without histological sectioning. In this way, we demonstrate the strength of LSFM for comprehensive assessment of RGC axon regeneration, and unequivocally reveal significant axon misguidance after injury. This work (Luo *et al.*, 2013) has been published in **Experimental Neurology (2013 September Cover Issue)** titled, *Three-dimensional evaluation of retinal ganglion cell axon regeneration and pathfinding in unsectioned tissue after optic nerve injury.*

Aim 3: Optimize shRNA approach to promote RGC survival and regeneration. PTEN, SOCS3 and CHOP will be knocked down alone or in combination using shRNAs to improve RGC survival and regeneration.

In this Aim, we harness shRNA approach to knockdown CHOP, PTEN or SOCS3 in RGCS to promote RGC survival and axon regeneration.
Using concatenated shRNA construct methods (Chung et al., Nucleic Acids Res. 2006; 34(7): e53), we generated shRNA plasmid targeting CHOP. This shRNA method allows insertion of multiple sets of shRNA sequences into one vector, thus providing high degree of knockdown efficacy. After confirming plasmid knockdown efficacy in HEK 293 cells

subjected to ER stress (treatment with ER stress inducer thapsigargin), we generated AAV2-shRNA CHOP to test CHOP knockdown effects on RGC survival in optic nerve crush injury model. Our AAV2 at certain titer allows infection of RGC specifically, with minimum infection of non-RGC cells. RGCs infected with AAV2-shRNA CHOP show reduction CHOP expression using immunohistochemistry (unpublished data).

Adult mice received AAV-shRNA CHOP injection intravitreously. At 14 days after injection, animals received intraorbital optic nerve crush injury. At 14 days after crush, CHOP knockdown (Kd) animals were analyzed for RGC survival and axon regeneration. Immunostaining using RGC-specific marker was used to examine RGC survival. Our preliminary results show that there is approximately two fold increase in RGC survival (42% RGC survival in shRNA CHOP treated animals, compared to 18% in control animals).

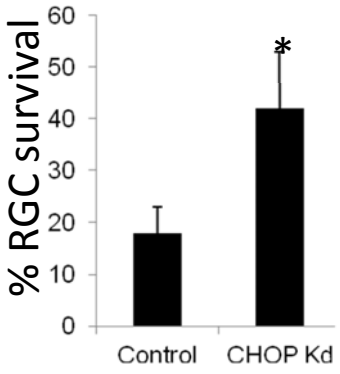

CHOP knockdown promotes RGC survival following axotomy. Data are presented as mean % of RGC number compared to the uninjured contralateral eye at 2 weeks after injury. CHOP Kd, adult mice subjected to AAV-shRNA CHOP injection two weeks prior to crush injury. Control, Adult mice subjected to AAV-shRNA targeting luciferase (control AAV). N=3/group. *<0.05, Student t test.

Thus, our data demonstrate enhanced RGC survival following optic nerve damage by targeting ER stress using a shRNA viral approach. We are in the process of examining whether AAV administered days after optic nerve injury will also result in enhanced RGC survival.

In addition to CHOP shRNA, we have used the same shRNA strategy to knockdown PTEN (Fig, 4). Using in vivo model of optic nerve crush injury, we show, for the first time, extensive RGC axon regeneration using AAV-shRNA approach (Fig. 5).

In the last several months, we have submitted our results on shRNA in different journals. Recently, parts of these results were accepted for publication in *Gene Therapy*.

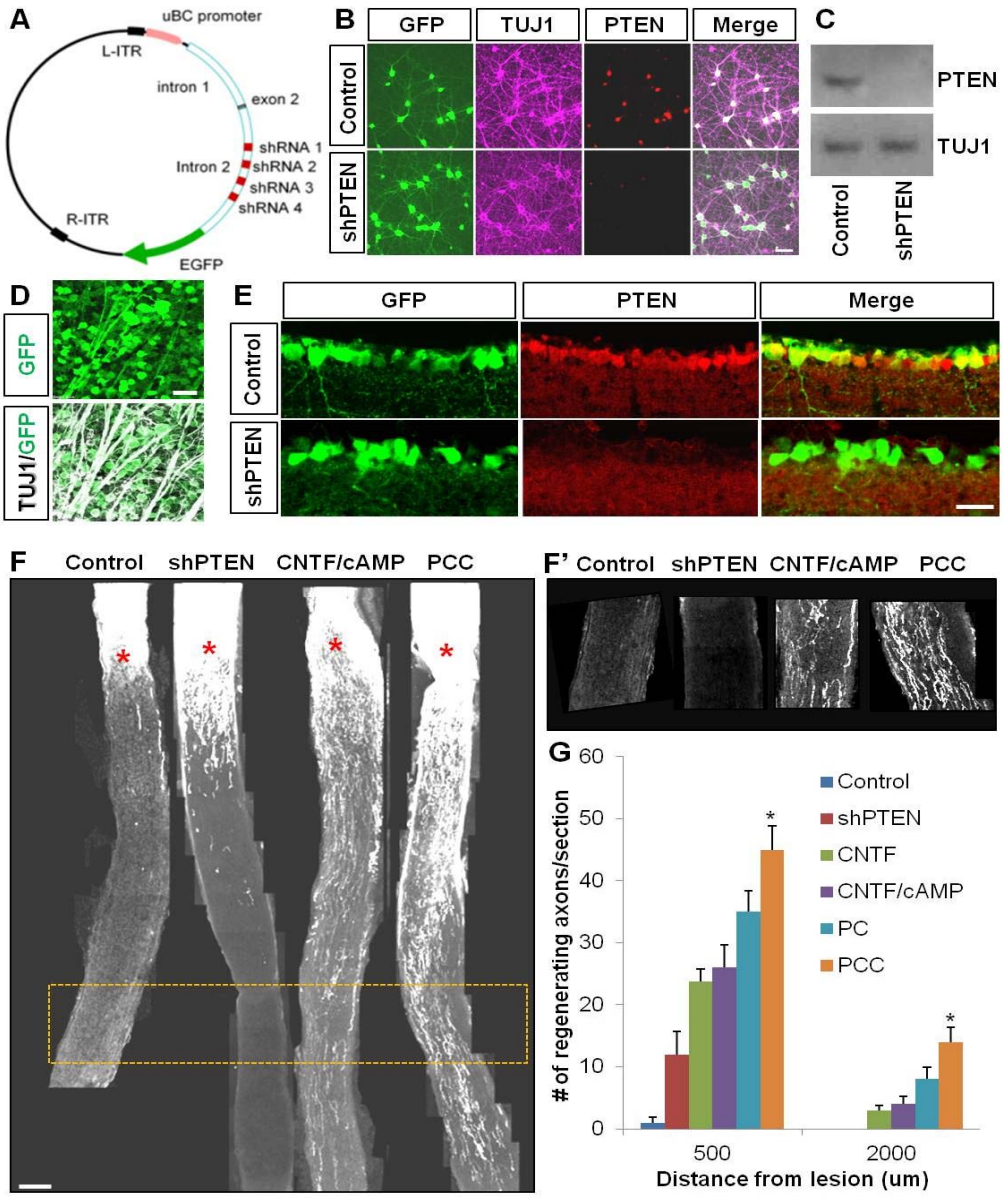

Figure 5. AAV modulation of PTEN combined with other growth inducing factors improve axon regeneration. (**A**) AAV2-shPTEN construct map. Control and shPTEN constructs contain EGFP reporter (**B**) PTEN knockdown shown by immunocytochemistry in cultured cortical neurons. (**C)** Western blot of protein lysates from treated cortical neurons. (**D**) Flat-mounted retina 2 weeks following intravitreal injection of AAV2-shPTEN, and staining with antibodies against GFP and TUJ1 (i.e. RGC-marker) shows >90% transduction efficacy in RGCs. (**E**) Retina sections following control AAV or AAV2-shPTEN injection show PTEN knockdown in ganglion cell layer. (**F**) Representative sectioned optic nerves of mice receiving various AAV treatments. Control, AAV-anti-Luc/EGFP; shPTEN, AAV2-PTEN; CNTF/cAMP, AAV2-CNTF/cpt-cAMP; PC, AAV2-shPTEN/AAV2-CNTF; PCC, AAV2-shPTEN/AAV2-CNTF/cpt-cAMP. Asterisk: lesion site. (**F'**) Higher-magnification images of the boxed area in (**F**). (**G**) Quantification of regenerating axon (n=6-8/group). *:

$p<0.05$, Bonferroni test (PCC significantly different to all treatment groups except to PC). Error bars, SEM. Scale bars: B-E, 20 µm; F, 100 µm.

4. KEY RESEARCH ACCOMPLISHMENTS:

- Successful generation of triple knockout mice (i.e. PTEN/SOCS3/CHOP knockout mice) required for Aim 1 of the proposal.
- Successful assessment of retinal ganglion cell survival and axon regeneration in different animal groups subjected to combinatory PTEN/SOCS3/CHOP and XBP1 manipulation.
- Successful assessment of retinal ganglion cell survival and axon regeneration in different animal groups subjected to combinatory PTEN/SOCS3/CHOP and XBP1 manipulation.
- Successful assessment of pattern electroretinograph (PERG) on animals subjected to PTEN/SOCS3 pathway manipulation.
- Establishment of novel methods (tissue clearance and light sheet fluorescent microscopy) to assess optic axon regeneration in whole mouse tissues.
- Successful generation of shRNA plasmid against CHOP.
- Successful generation of adeno-associated virus (AAV)-shRNA against CHOP.
- Initiation of assessment of gene therapy (AAV) approach to target CHOP to promote RGC survival.
- Successful generation of adeno-associated virus (AAV)-shRNA against PTEN.
- Paper presentation at the 2013 ARVO and 2013, 2014 Society for Neuroscience (SFN) meetings on our data pertaining to axon regeneration and new imaging techniques.
- Demonstrated that there is a high degree of axon misguidance in regenerate adult mice.
- Publications in multiple journals (listed below).

5. CONCLUSION:

In summary, we have had a very successful and fruitful year undertaking the proposed studies. Mostly importantly, we have performed large parts of the Proposed Aims from which we have obtained extremely interesting and promising results. We have discovered that combining genetic modulations to target multiple genes, namely PTEN, SOCS3, CHOP and XBP1 promotes striking neuronal survival and axon regeneration. Further, we observed that genetically modified RGCs exhibit relatively normal physiology, a critical aspect in our quest to achieve functional restoration after optic nerve damage. In addition, we have successfully developed and optimized AAV and shRNA approaches to target multiple genes, and promote RGC survival and axon regeneration. This is extremely exciting because we now show for the first that a non-transgenic approach can induce extensive optic nerve regeneration in post-injury treatment paradigm. This part of work has been submitted for publication, and is currently being reviewed. We also established new imaging methodologies using tissue clearing and light sheet fluorescent microscope to evaluate optic nerve regeneration without histological sectioning. This technique will change the way researchers assess optic nerve regeneration in animal models. We anticipate more publications in the near future and we expect to submit for additional publications in the months to come.

6. PUBLICATIONS, ABSTRACTS, AND PRESENTATIONS:

a. List all manuscripts submitted for publication during the period covered by this report resulting from this project. Include those in the categories of lay press, peer-reviewed scientific journals, invited articles, and abstracts. Each entry shall include the author(s), article title, journal name, book title, editors(s), publisher, volume number, page number(s), date, DOI, PMID, and/or ISBN.

(1) Lay Press:
(2) Peer-Reviewed Scientific Journals:

1. Yungher, B.J., Luo, X, Salgueiro, Y, Blackmore, M.G., **Park, K.K.** (2015) Viral vector based improvement of optic nerve regeneration: characterization of individual axons' growth patterns and synaptogenesis in a visual target. ***Gene Therapy***, in press

2. Soderblom, C., Lee, D.H., Dawood, A., Carballosa, M., Santamaria, A.J., Benavides, F.D., Jergova, S., Grumbles, R.M., Thomas, C.K., **Park, K.K**., Guest, J.D., Lemmon, V.P., Lee, J.K.*, Tsoulfas, P.* (2015) 3D imaging of transparent spinal cords from rodents and nonhuman primates. ***eNeuro.*** 2(2):1-24. *Co-corresponding authors

3. Lee, D., Luo, X., Yungher, B., Bray, E., Lee, J.K., **Park, K.K.** mTOR's distinct roles and effectiveness in promoting compensatory axonal sprouting in the injured CNS. ***Journal of Neuroscience***, 34(46):15347-55, 2014.

4. Luo, X., Salgueiro, Y., Beckerman, S.R., Lemmon, V.P., Tsoulfas, P., Park, K.K., Three-dimensional evaluation of retinal ganglion cell axon regeneration and path-finding in whole mouse tissue after injury. ***Experimental Neurology,*** 247:653-62, 2013 ***(Issue Cover)***

5. Chou, T.H., Park, K.K., Luo, X., Porciatti, V., Retrograde signaling in the optic nerve is necessary for electrical responsiveness of retinal ganglion cells. ***Invest. Ophthalmol. Vis. Sci.,*** 54:1236-43, 2013.

6. Soderblom C, Luo X, Blumenthal E, Bray E, Lyapichev K, Ramos J, Krishnan V, Lai-Hsu C, **Park K.K**., Tsoulfas P, Lee JK. Perivascular fibroblasts form the fibrotic scar after contusive spinal cord injury. ***Journal of Neuroscience***, 33(34):13882-7, 2013.

7. Kuboyama T, Luo X, **Park K**, Blackmore MG, Tojima T, Tohda C, Bixby JL, Lemmon VP, Kamiguchi H. Paxillin phosphorylation counteracts proteoglycan-mediated inhibition of axon regeneration. ***Experimental Neurology,*** 248C:157-169, 2013.

8. Hu, Y*., **Park, K.K***., Yang, L*., Wei X*., Yang, Q., Thielen, P., Lee, A.H., Cartoni, R., Glimcher, L.H., Chen D.F., He, Z., Differential Effects of Unfolded Protein Response Pathways on Axon Injury-induced Death of Retinal Ganglion Cells. ***Neuron***, 9;73(3):445-52, 2012, *; equal contribution.

(3) Invited Articles:

1. Luo X., Yungher, B., **Park, K.K**. Application of Tissue Clearing and Light Sheet Fluorescence Microscopy to Assess Optic Nerve Regeneration in Unsectioned Tissues. ***Methods in Molecular Biology*** Volume 1162, pp 209-217, 2014.

2. Luo, X., **Park, K.K**., Neuron-intrinsic inhibitors of axon regeneration: PTEN and SOCS3. ***Int. Rev. Neurobiol.,*** 105:141-73, 2012.

(4) Abstracts:

1. Lee, D., Luo, X., Yungher, B., Lee, J.K., **Park, K.K.** Evaluating the role and effect of specific neuron-intrinsic pathways that mediate collateral axonal sprouting after CNS injury. Soc. Neurosci. Abstr. 2014
2 Bray, E., Lyapichev, K., Luo, X., Lee, J.K., **Park, K.K.**, Translational analysis of retinal ganglion cells undergoing axon regeneration, Soc. Neurosci. Abstr. 2014
3. Yungher, B., Schmidt, T., Chew, K., Luo, X., Lyapichev, K., Chou, T.-H., Porciatti, V., Blackmore, M., Hattar, S., **Park**, **K.K.** Characterization of AAV vectors' potentials to promote long distance optic nerve regeneration, path-finding, and restoration of visual functions after injury, Soc. Neurosci. Abstr. 2014
4. Hackett, A., Lee, D., Dawood, A., Tsoulfas, P., **Park**, **K.K.,** Lee, J.K. NG2 cell fate after contusive spinal cord injury, Soc. Neurosci. Abstr. 2014
5. Luo, X., Yungher, B., Salgueiro, Y., Beckerman, S.R., Lemmon, V.P., Tsoulfas, P., **Park**, **K. K.** Investigation into axonal pathfinding of injured retinal ganglion cells in intact animal tissues, Soc. Neurosci. Abstr. 2013
6. Schmidt, T., Rupp, A., Chew, K., Yungher, B., **Park**, **K. K.,** Hattar, S. ipRGCs mediate ipsilateral pupil constriction, Soc. Neurosci. Abstr. 2013
7. Lyapichev, L., Soderblom, C., Luo, X., **Park**, **K. K.,** Lee, J.K. Macrophage specific translational profile after spinal cord injury, Soc. Neurosci. Abstr. 2013
8. Lee, D., Hackett, A., Dawood, A., Tsoulfas, P., **Park**, **K. K.,** Lee, J.K. NG2 cells contribute to the astroglial scar after contusive spinal cord injury, Soc. Neurosci. Abstr. 2013
9. Luo, X., Salgueiro, S., Beckerman, S., Lemmon, V., Tsoulfas, P., **Park**, **K. K.** Three-dimensional Evaluation of Retinal Ganglion Cell Axon Regeneration, Pathfinding and Glial Reaction in Unsectioned Tissue, Association for Research in Vision and Ophthalmology. Abstr. 2013
10. Rupp, A., Tchmidt, T., Chew, K., Yungher,D., **Park**, **K. K.,** Hattar, S. ipRGCs mediate ipsilateral pupil constriction, ARVO Abstr. 2013

b. List presentations made during the last year (international, national, local societies, military meetings, etc.). Use an asterisk (*) if presentation produced a manuscript.

- 2014 Invited speaker, "*Investigating Regeneration and Reconnection of Retinal Ganglion Cell Axons"*, Bascom Palmer Eye Institute, Miami, FL
- 2013 Invited speaker, "*Promoting axon regeneration: Insights from the retinal neurons"*, Association of Korean Neuroscientists, Washington, DC
- 2013 Invited speaker, "*Promoting axon regeneration: Insights from the retinal neurons"*, Ajou University, Republic of Korea
- 2013 Invited speaker, "*Promoting axon regeneration: Insights from the retinal neurons"*. Drexel University, Philadelphia, PA

- 2013 Invited speaker, "*Modulation of neuron-intrinsic factors to induce axon regeneration in the central nervous system"*, U.S. Kavli Frontiers of Science Symposium, Irvine, CA

7. INVENTIONS, PATENTS AND LICENSES: Nothing to report

8. REPORTABLE OUTCOMES:

- Triple knockout mice (i.e. PTEN/SOCS3/CHOP knockout mice)
- Establishment of novel methods (tissue clearance and light sheet fluorescent microscopy) to assess optic axon regeneration in whole mouse tissues.
- shRNA plasmid against CHOP.
- Adeno-associated virus (AAV)-shRNA against CHOP.
- Successful generation of adeno-associated virus (AAV)-shRNA against PTEN.

9. OTHER ACHIEVEMENTS:

2014 3D optic pathway visualization method featured in NIH Director's blog (7-24-2014)

2014 Federation of American Societies for Experimental Biology, BioArt Award, (Video category awarded to Xueting Luo and Kevin Park).

10. REFERENCES:

Hu Y, Park KK, Yang L, Wei X, Yang Q, Cho KS, Thielen P, Lee AH, Cartoni R, Glimcher LH, Chen DF, He Z (2012) Differential effects of unfolded protein response pathways on axon injury-induced death of retinal ganglion cells. Neuron 73:445-452.

Luo X, Salgueiro Y, Beckerman SR, Lemmon VP, Tsoulfas P, Park KK (2013) Three-dimensional evaluation of retinal ganglion cell axon regeneration and pathfinding in whole mouse tissue after injury. Exp Neurol 247:653-662.

Park KK, Liu K, Hu Y, Smith PD, Wang C, Cai B, Xu B, Connolly L, Kramvis I, Sahin M, He Z (2008) Promoting axon regeneration in the adult CNS by modulation of the PTEN/mTOR pathway. Science 322:963-966.

Smith PD, Sun F, Park KK, Cai B, Wang C, Kuwako K, Martinez-Carrasco I, Connolly L, He Z (2009) SOCS3 deletion promotes optic nerve regeneration in vivo. Neuron 64:617-623.

Sun F, Park KK, Belin S, Wang D, Lu T, Chen G, Zhang K, Yeung C, Feng G, Yankner BA, He Z (2011) Sustained axon regeneration induced by co-deletion of PTEN and SOCS3. Nature 480:372-375.

11. APPENDICES: Attach all appendices that contain information that supplements, clarifies or supports the text. Examples include original copies of journal articles, reprints of manuscripts and abstracts, a curriculum vitae, patent applications, study questionnaires, and surveys, etc.

NOTE:

TRAINING OR FELLOWSHIP AWARDS: For training or fellowship awards, in addition to the elements outlined above, include a brief description of opportunities for training and professional development. Training activities may include, for example, courses or one-on-one work with a mentor. Professional development activities may include workshops, conferences, seminars, and study groups.

COLLABORATIVE AWARDS: For collaborative awards, independent reports are required from BOTH the Initiating Principal Investigator (PI) and the Collaborating/Partnering PI. A duplicative report is acceptable; however, tasks shall be clearly marked with the responsible PI and research site. A report shall be submitted to **https://ers.amedd.army.mil** for each unique award.

QUAD CHARTS: If applicable, the Quad Chart (available on https://www.usamraa.army.mil) should be updated and submitted with attachments.

MARKING OF PROPRIETARY INFORMATION: Data that was developed partially or exclusively at private expense shall be marked as "Proprietary Data" and Distribution Statement B included on the cover page of the report. Federal government approval is required before including Distribution Statement B. The recipient/PI shall coordinate with the GOR to obtain approval. REPORTS NOT PROPERLY MARKED FOR LIMITATION WILL BE DISTRIBUTED AS APPROVED FOR PUBLIC RELEASE. It is the responsibility of the Principal Investigator to advise the GOR when restricted limitation assigned to a document can be downgraded to "Approved for Public Release." DO NOT USE THE WORD "CONFIDENTIAL" WHEN MARKING DOCUMENTS. See term entitled "Intangible Property – Data and Software Requirements" and https://mrmc.amedd.army.mil/index.cfm?pageid=researcher_resources.technical_reporting for additional information.

Experimental Neurology 247 (2013) 653–662

Contents lists available at SciVerse ScienceDirect

Experimental Neurology

journal homepage: www.elsevier.com/locate/yexnr

Three-dimensional evaluation of retinal ganglion cell axon regeneration and pathfinding in whole mouse tissue after injury

Xueting Luo, Yadira Salgueiro, Samuel R. Beckerman, Vance P. Lemmon, Pantelis Tsoulfas, Kevin K. Park *

Miami Project to Cure Paralysis, University of Miami, Miller School of Medicine, Miami, FL, 33136, USA
Department of Neurosurgery, University of Miami, Miller School of Medicine, Miami, FL, 33136, USA

ARTICLE INFO

Article history:
Received 2 February 2013
Revised 25 February 2013
Accepted 1 March 2013
Available online 16 March 2013

Keywords:
PTEN
SOCS3
Axon regeneration
Axon growth
Retinal ganglion cell
Axotomy

ABSTRACT

Injured retinal ganglion cell (RGC) axons do not regenerate spontaneously, causing loss of vision in glaucoma and after trauma. Recent studies have identified several strategies that induce long distance regeneration in the optic nerve. Thus, a pressing question now is whether regenerating RGC axons can find their appropriate targets. Traditional methods of assessing RGC axon regeneration use histological sectioning. However, tissue sections provide fragmentary information about axonal trajectory and termination. To unequivocally evaluate regenerating RGC axons, here we apply tissue clearance and light sheet fluorescence microscopy (LSFM) to image whole optic nerve and brain without physical sectioning. In mice with PTEN/SOCS3 deletion, a condition known to promote robust regeneration, axon growth followed tortuous paths through the optic nerve, with many axons reversing course and extending towards the eye. Such aberrant growth was prevalent in the proximal region of the optic nerve where strong astroglial activation is present. In the optic chiasms of PTEN/SOCS3 deletion mice and PTEN deletion/Zymosan/cAMP mice, many axons project to the opposite optic nerve or to the ipsilateral optic tract. Following bilateral optic nerve crush, similar divergent trajectory is seen at the optic chiasm compared to unilateral crush. Centrally, axonal projection is limited predominantly to the hypothalamus. Together, we demonstrate the applicability of LSFM for comprehensive assessment of optic nerve regeneration, providing in-depth analysis of the axonal trajectory and pathfinding. Our study indicates significant axon misguidance in the optic nerve and brain, and underscores the need for investigation of axon guidance mechanisms during optic nerve regeneration in adults.

Introduction

Retinal ganglion cells (RGCs) do not regenerate their axons, leading to loss of visual functions in glaucoma and after trauma or stroke. Studies on the limited regenerative capacity of RGCs have identified several strategies that stimulate axon regeneration. These include enhancing the intrinsic growth capacity as well as neutralizing repulsive cues in the environment (Cho et al., 2005; Duffy et al., 2012; Leaver et al., 2006; Lingor et al., 2008; Liu et al., 2006; Muller et al., 2007; Qiu et al., 2002; Su et al., 2008; Winzeler et al., 2011; Wong et al., 2003). We and others have used knockout (KO) mice to demonstrate that RGC-specific deletion of PTEN (phosphatase and tensin homolog), SOCS3 (suppressor of cytokine signaling 3) or KLF4 (Krüppel like factor 4) induces RGC axon regeneration (Moore et al., 2009; Park et al., 2008; Smith et al., 2009). More recent studies have shown that combining PTEN KO mice with either SOCS3 deletion, or Zymosan and a cAMP analogue leads to substantially more regeneration than targeting them individually (de Lima et al., 2012; Kurimoto et al., 2010; Sun et al., 2011), pointing to the importance of targeting multiple factors to induce extensive regeneration.

With the recent progress made in promoting RGC axon regeneration, it is becoming increasingly important to investigate whether regenerating RGC axons can find their targets in the brain. While appropriate pathfinding of RGC axons has been documented comprehensively in regeneration-competent species including fish and amphibians (Beazley et al., 1997; Becker and Becker, 2007; Stelzner et al., 1986), the degree to which RGC axons in adult mammals correctly reinnervate their targets is unclear.

A common method for assessing optic nerve regeneration is histological sectioning. However, tissue sections provide incomplete spatial information. For instance, it is difficult to determine the precise trajectory of axons or their final destinations. In this study, we applied a tetrahydrofuran (THF) based-clearing method that renders tissues relatively transparent (Becker et al., 2012; Erturk et al., 2012), and combined it with LSFM, allowing deep tissue fluorescence imaging in unsectioned optic nerve and brain. Using these methods, we found in PTEN/SOCS3 KO mice that regenerating axons follow circuitous paths, with many axons

* Corresponding author at: Miami Project to Cure Paralysis, University of Miami, Miller School of Medicine, Miami, FL, 33136, USA.
E-mail addresses: Xluo@med.miami.edu (X. Luo), Ysalgueiro@med.miami.edu (Y. Salgueiro), Sbeckerman@med.miami.edu (S.R. Beckerman), Vlemmon@med.miami.edu (V.P. Lemmon), Ptsoulfa@med.miami.edu (P. Tsoulfas), Kpark@med.miami.edu (K.K. Park).

0014-4886/$ – see front matter © 2013 Elsevier Inc. All rights reserved.
http://dx.doi.org/10.1016/j.expneurol.2013.03.001

making multiple turns and extending back to the eye. Axon turning was prevalent in nerve regions with strong astroglial activation. Many RGC axons generated branches in the optic nerve and brain as they re-grow. In the optic chiasm, a major decision point en route to visual targets, high numbers of regenerating axons in PTEN/SOCS3 KO mice or PTEN KO/Zymosan/cAMP analogue-treated mice diverge into the ipsilateral optic tract or to the opposite optic nerve. Following bilateral optic nerve crush, a similar growth pattern is seen at the optic chiasm compared to unilateral crush. Centrally, axonal projection is limited primarily to the hypothalamus. In summary, we demonstrated the combined application of tissue clearance and LSFM for comprehensive analysis of optic nerve regeneration, providing in-depth assessment of the axonal trajectory. Our study shows substantial misdirection of RGC axon growth in adult mice, and underscores the need for investigation into the mechanisms that underlie misguidance during regeneration in adults.

Materials and methods

All experimental procedures were performed in compliance with animal protocols approved by the IACUC at the University of Miami Miller School of Medicine. For all surgical procedures, mice were anaesthetized with ketamine and xylazine. Eye ointment containing atropine sulfate was applied preoperatively to protect the cornea during surgery, and Buprenorphine (0.05 mg/kg, Bedford Lab) was administrated as post-operative analgesic.

Mice, optic nerve crush injury and intravitreal injection

SOCS3$^{f/f}$/PTEN$^{f/f}$ (Sun et al., 2011) mice (female; 4–6 week old) were intravitreally injected with 1–2 μl volume of AAV2-Cre in the left eyes at 2 weeks prior to crush injury. 1 μl (1 μg/μl) ciliary neurotrophic factor (CNTF; Pepro Tech) was intravitreally injected immediately after injury and at 3 days post-injury, and bi-weekly thereafter. PTEN KO/ZYM/cAMP mice, PTEN$^{f/f}$ (Groszer et al., 2001) (female; 8 week old) received intravitreal AAV2-Cre injection followed by optic nerve crush 2 weeks later. Zymosan (Sigma-Aldrich; 12.5 μg/μL) along with the cAMP analogue CPT-cAMP (Sigma; 50 μM, 3 μL) was injected as described (de Lima et al., 2012). Zymosan and CPT-cAMP were injected intravitreally immediately after crush injury, and additional Zymosan at half the original dose plus CPT-cAMP at the original dose again 3 and 6 week later. For each intravitreal injection, a glass micropipette was inserted into the peripheral retina, just behind the ora serrata, and was deliberately angled to avoid damage to the lens. For optic nerve crush injury, the optic nerve was exposed intraorbitally and crushed with jeweler's forceps (Dumont #5; tip dimension, 0.1 × 0.06 mm) for 5 s approximately 1 mm behind the optic disc. Using retrograde and anterograde experiments, completeness of axotomy has been confirmed in our previous study (Park et al., 2008). Two to 7 days before sacrifice, l–2 μl of cholera toxin β subunit (CTB)-Alexa 555 (2 μg/μl, Invitrogen) was injected into the vitreous with a Hamilton syringe (Hamilton) to anterogradely label regenerating RGC axons. *ALDH1L1-EGFP* (Doyle et al., 2008; Yang et al., 2011), *PLP-EGFP* (Mallon et al., 2002) and *CX3CR1-EGFP* mice (Jung et al., 2000) received unilateral optic nerve crush. At 14–17 days later, optic nerves from these transgenic mice were treated for tissue clearance and analyzed for the distribution of glial cells in the injured optic nerve. Uninjured mice (C57BL/6 at 5 week old) with bilateral CTB tracing received intravitreal CTB-555 injection in the right eye and CTB-488 injection in the left eye.

AAVs

cDNA of Cre was inserted downstream of the CMV promoter/β-globin intron enhancer in the plasmid pAAV-MCS (Stratagene), containing the AAV2 inverted terminal repeats and a human growth hormone polyA signal. pAAV-RC (Stratagene) that encodes the AAV2 genes (rep and cap) and the helper plasmid (Stratagene) that encodes E2A, E4 and VA were used for co-transfection of 293T cells to generate recombinant AAV. AAV2 viral particles were prepared by the University of Miami Viral Vector Core using an FPLC method to produce titers of approximately 4×10^{13} particles/mL.

Tissue preparation and clearing

Mice were perfused transcardially with PBS followed by 4% paraformaldehyde (PFA) in phosphate buffered saline (PBS) at 5 ml/min. The optic nerve and the brain were dissected and post-fixed with 4% PFA in PBS overnight. For histological sectioning, samples were cryoprotected by incubating in 30% sucrose overnight. For tissue clearing, samples were rinsed with PBS and stored at 4 °C until needed. Tissue clearing was performed as described (Becker et al., 2012; Erturk et al., 2012), with minor modifications. Samples underwent dehydration by incubation in increasing concentration of THF (Sigma-Aldrich) solutions under constant rocking. Optic nerves were incubated in 50% THF (diluted in water v/v), 80% THF (v/v) and 100% THF for 15 min each. Dehydrated optic nerve was rendered clear by incubating in BABB (a mixture of benzyl alcohol and benzyl benzoate (Sigma-Aldrich) at a ratio of 1:2) for 20 min. Adult mouse brain was incubated in 50% THF for 12 h, 80% THF for 12 h, 100% THF for 3 × 12 h, and BABB for 12 h before imaging.

LSFM (ultramicroscopy)

Ultramicroscope illuminates specimen with a thin sheet of light formed by two lenses, allowing imaging of large tissues, yet with cellular resolution (Fig. 1C). Ultramicroscopy was performed as previously described (Erturk et al., 2012). Between 100 and 500 optical slices were imaged. The scan speed was 0.5–1.5 s per section, which was about 2–3 min for the optic nerve and 5–10 min for the brain for a complete scan of the tissue. Images were collected at 2 to 5 μm increment in Z axis.

Image processing, neurite tracing and statistical analysis

Images, videos and 3D volume rendering were prepared using Imaris software v7.6.1 (Bitplane). CTB-labeled RGC axons in the optic nerve and brain were traced using Imaris Filament Tracer Module. To quantify the number of axons that regenerated long distances in the optic nerve, we counted the CTB-labeled fibers that crossed different distances from the lesion site after scanning through 100 to 200 individual horizontal optical slices. To quantify the number of axons that extended into different regions beyond the optic chiasm, we counted the CTB-labeled fibers that were found in the optic tracts, opposite optic nerve and hypothalamus after scanning through 100 to 300 individual horizontal optical slices. We used Student's *t* test for two group comparisons using SPSS statistics software.

Results

3D visualization of RGC axonal projections in uninjured mouse

In this study, we set out to apply tissue clearance and LSFM to evaluate regeneration of RGC axons without histological sectioning. Initially we visualized RGC axonal projections in the whole brain of uninjured animal. Adult mice received intravitreal injection of fluorophore-conjugated CTB, a lipophilic tracer used routinely to label CNS axons in regeneration studies. Seven days later, samples were processed for tissue clearance. THF-based clearing methods rendered mouse optic nerve and brain transparent to a large extent (Figs. 1A and B). A total of 1 h incubation in THF/BABB solutions was sufficient to clear the optic nerve, while it took approximately 3 days for the brain. Normally, RGCs send axons to central targets including the lateral geniculate nucleus (LGN) and superior colliculus (SC), which are

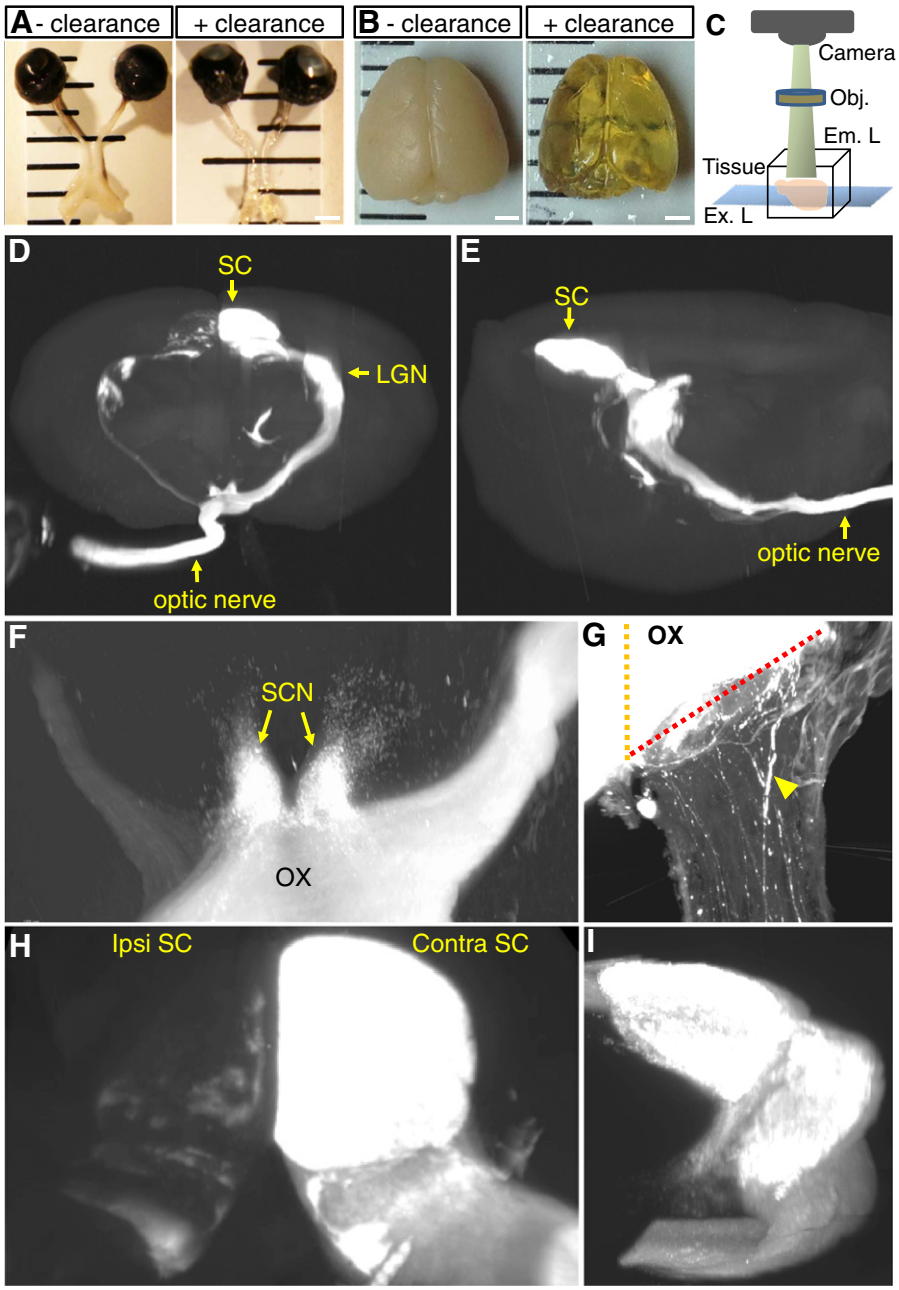

Fig. 1. Tetrahydrofuran (THF)-based tissue clearing and LSFM methods allow 3D visualization of RGC axonal projections in whole tissue. A, adult mouse optic nerve and chiasm, and B, whole brain before and after clearance with THF and BABB. C, principle of LSFM. Optic nerves and brains were cleared, and then imaged under an Ultramicroscope (LaVision Biotec). Horizontal optical slices were compiled using Imaris software for 3D reconstruction. D–I, snapshot images from 3D reconstruction video. Anterior, D and lateral, E views of a cleared brain displaying the trajectory of CTB-labeled RGC axons from the eye, through the chiasm and into the brain. All visual targets including the suprachiasmatic nucleus, lateral geniculate nucleus and superior colliculus both in the ipsilateral and contralateral sides of the brain can be clearly visualized. F–I, higher magnification images taken from 3D reconstruction showing axonal projections to the chiasm and SCN, and diverging into the ipsilateral and contralateral optic tracts in F, to the opposite optic nerve in G (arrowhead indicates CTB-labeled axons), ipsilateral and contralateral superior colliculus in H, and contralateral lateral geniculate nucleus in I. In G, yellow and red dotted lines represent the chiasm midline and the optic nerve-chiasm transition zone, respectively. Ex. L, excitation light; Em. L, emission light; Obj, objective; SC, superior colliculus; SCN, suprachiasmatic nucleus; LGN, lateral geniculate nucleus; ipsi, ipsilateral; contra, contralateral; OX, optic chiasm. Scale bars, 1 mm in A and B.

involved in image-forming visual functions. RGC axons also innervate the suprachiasmatic nucleus (SCN) and olivary pretectal nucleus (OPT) that are involved in non-image forming visual functions. After imaging the entire depth of the brain, approximately 500 optical slices (Movie 1) were compiled using Imaris software for 3D reconstruction. RGC axons can be visualized in 3D with remarkable detail along the entire visual pathway through the optic nerve, chiasm and optic tracts to the SCN, OPT, LGN, and SC (Figs. 1D–I, Movies 1 and 2). In mice, a small proportion of RGCs located in the ventro-temporal retina send their axons to the ipsilateral brain. The ipsilateral projection stemming from the optic chiasm to the various brain regions is clearly visible (Movie 2), with axons terminating in the dorsal and ventral LGN (Figs. 1D–I), and in the different layers of the SC (Fig. 1H). We also detected several RGC axons (10–30 axons; n = 4) that turn at the optic chiasm and project to the opposite optic nerve (Fig. 1G), confirming that some axons are misrouted at the chiasm during development (Bunt et al., 1983). Together, we show that tissue clearance combined with LSFM allows 3D visualization of the entire optic pathway as well as

single axons that leave the main bundle, providing excellent details regarding the paths taken by RGC axons.

3D assessment of regenerating axons shows high degree of axon turning

Next, we assessed regenerating RGC axons following injury. To this end, we analyzed animals with genetic deletion of PTEN/SOCS3 in adult RGCs, together with intravitreal injection of CNTF, a condition known to promote long distance regeneration of many RGC axons after an optic nerve crush (Sun et al., 2011). Adult PTEN/SOCS3$^{f/f}$ mice received intravitreal injection of AAV2-Cre to induce PTEN/SOCS3 deletion in adult RGCs, followed by an intraorbital crush injury 2 weeks later (Sun et al., 2011). Animals received CNTF injection on the day of injury, at 3 day post-injury, and bi-weekly thereafter. Previously, we have demonstrated that AAV2-Cre at appropriate viral titers infects the majority of RGCs in adult mice (Park et al., 2008; Sun et al., 2011). Control animals received AAV-GFP injection. Two days prior to sacrifice, animals received CTB injection to label regenerating RGC axons. In control animals, a few axons sprouted short distances at the lesion site, but no axons were found beyond 1 mm from the lesion site at 17 day post-injury (n = 5; Fig. 2A, Movie 3). On the other hand, many axons extended into and beyond the lesion in PTEN/SOCS3 KO mice (Figs. 2A and E, Movie 4). The use of LSFM allowed comprehensive evaluation of three different aspects

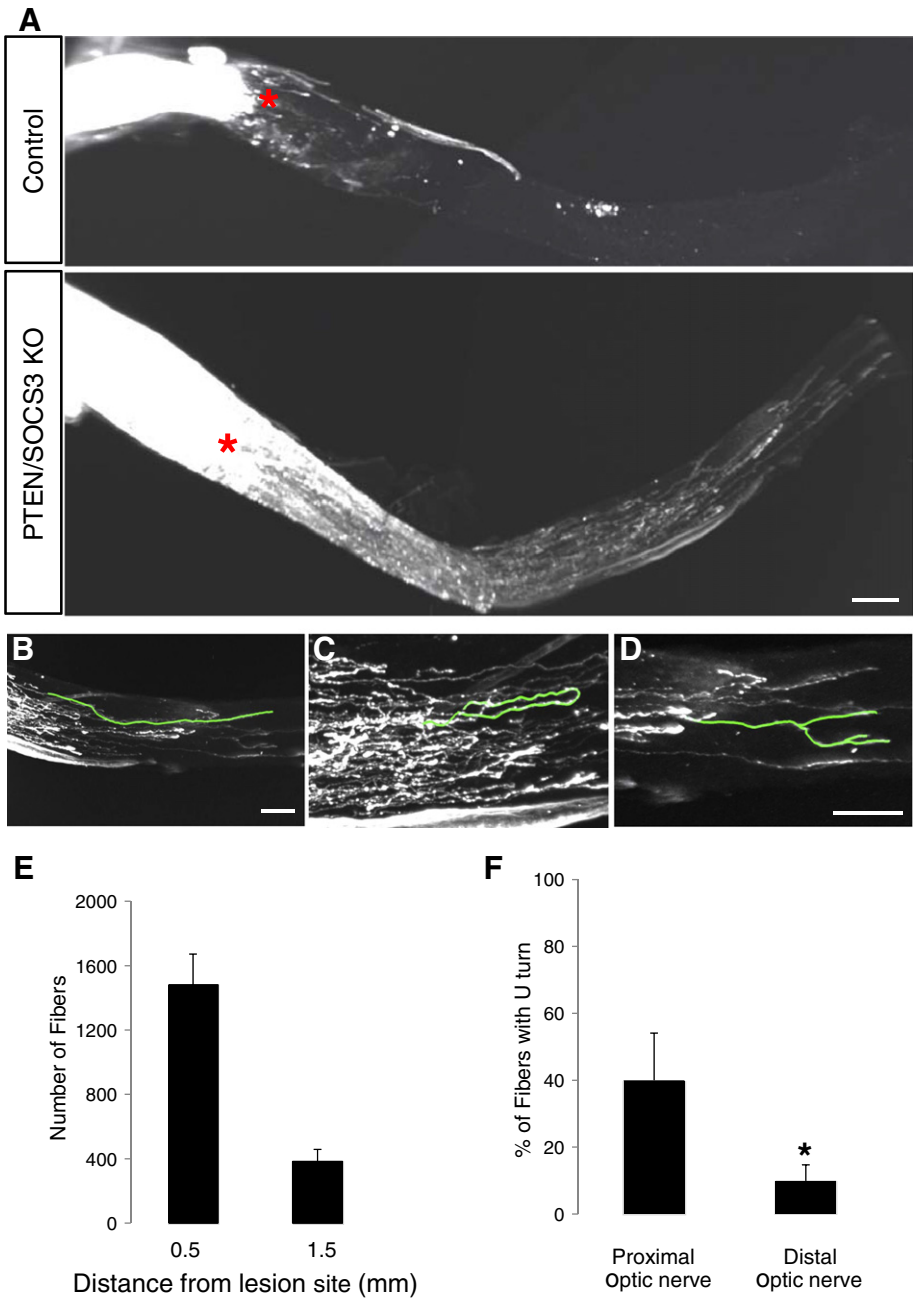

Fig. 2. 3D assessment of regenerated RGC axons in the cleared optic nerve. A, 3D reconstructed optic nerves of control AAV-GFP treated mice and PTEN/SOCS3 KO mice at 17 day post-injury. B–D, neurite tracing of single fiber showing different growth patterns. Some axons travel in a relatively straight along the optic nerve towards the chiasm (to the right side of the image) as shown in B, or loop back towards the eye (to the left side of the image) as shown in C. Some axons generate branches as they extend within the optic nerve as shown in D. E, quantification of the number of CTB-labeled axons found at different distances away from the lesion site (n = 5). Red asterisk, lesion site. *$p < 0.01$, Student's *t* test. Scale bars, 200 μm.

of axon growth that are difficult to obtain in histological sections. First, LSFM allowed direct counting of almost all fibers that have regenerated long distances through the optic nerve. By scanning through individual optical slices (i.e. z-stack images taken at 2–5 μm increments; a total of 150–200 optical slices/optic nerve), we could count individual CTB labeled fibers crossing different distances distal to the lesion site in PTEN/SOCS3 KO mice (n = 5; Fig. 2E). Second, it allowed unequivocal examination of the axonal trajectories along their regenerative paths, and where the regenerated axons terminate. Notably, we found that while a few RGC axons project relatively straight towards the brain (Fig. 2B), most axons have a meandering path. Many axons made sharp turns (often multiple occasions) with some axons reversing course and projecting towards the eye (Fig. 2C & Movie 4). These results are consistent with a recent study by Pernet et al., in which many axons that were induced to regenerate were shown to take circuitous paths in the optic nerve following elevation of CNTF (Pernet et al., 2012). We noticed in our study that these "turning events" seemed highly prevalent in the proximal nerve regions close to the lesion site. We traced the paths of axons (a total of 80 axons) within this proximal nerve region (i.e. a region covering 0.2–0.4 mm distal to the optic nerve head) and found that about 40% of axons made at least one U-turn (Fig. 2F). On the other hand, only about 10% of regenerating axons made U-turn in the more distal nerve region (i.e. 1–1.2 mm distal to the optic nerve head; Fig. 2F). We performed optic nerve crush in transgenic mice in which astrocytes, oligodendrocytes or microglial cells are labeled with EGFP to examine the correlation between the presence of glial cells and axon turning (Supplementary Fig. 1). After LSFM, we observed high astrocyte density in the proximal region of the optic nerve close to the lesion site in ALDH1L1-EGFP mice (n = 3; Supplementary Fig. 1). These results suggest that the nerve region with a high degree of axon turning may correspond to the areas with strong astroglial activation. Third, 3D visualization provided detailed examination of the axonal morphologies. For instance, it is clear that some RGC axons generate branches as they re-grow along the optic nerve (Fig. 2D & Movie 4), a morphogenetic process normally found in growing axons during nervous system development. Approximately 10–20% of axons traced in PTEN/SOCS3 KO showed at least one axonal branch. Together, we demonstrate that at present, tissue clearance combined with LSFM represents the most precise method to assess RGC axon regeneration, allowing unequivocal assessment of axonal trajectories and growth patterns in the optic nerve.

3D assessment of axonal projections to the brain

Recent studies from us and others demonstrated that PTEN KO alone or in combination with other strategies, such as SOCS3 deletion, promote long distance axon regeneration, with RGC axons projecting to the brain (de Lima et al., 2012; Kurimoto et al., 2010; Sun et al., 2011). Because histological sections provide incomplete spatial information about axonal trajectory and where RGC axons terminate in the brain, we applied LSFM to examine axonal projections in the brain. After imaging the entire brain, approximately 500 optical slices were compiled using Imaris software for 3D reconstruction. At 10 week post-injury, RGC axons were not detected in the optic chiasm or brain of AAV-GFP control animals (data not shown). In PTEN/SOCS3 KO animals however, many CTB-labeled regenerating axons reached the optic nerve/chiasm transition zone (OCTZ) (a mean of 119 fibers/animal; n = 8; SEM = 16.5). To evaluate the axonal projections through the optic chiasm and to the brain, we measured the number of axons projecting to different brain regions. In all animals examined (n = 8), similar or higher numbers of axons were found in the ipsilateral optic tract than in the contralateral optic tract (Figs. 3E and G, Movie 5). In all animals, we observed that a small percentage of RGC axons also extend into the opposite uninjured optic nerve (Figs. 3E and G, Movie 5). Some axons appeared to be inhibited from entering the OCTZ, or turn sharply at the OCTZ before continuing to project into the optic tracts (Fig. 3B). In the brain, a few axons extended medial-dorsally into the hypothalamic brain regions including the SCN and medial pre-optic area, while some axons exited the optic tracts to reach the lateral hypothalamus (Figs. 3C and D, Supplementary Fig. 2). In some animals, we found regenerating axons in abnormal regions that are not typically associated with the optic pathway including the fornix and extended amygdala (unpublished data). RGC axons were not detected in the more distant visual targets including LGN or SC (Fig. 3, Supplementary Fig. 2, Movie 5). We also examined axon regeneration in animals subjected to shorter and longer survival times (i.e. 8 and 16 weeks after injury; unpublished data). However, among these time points, we observed the greatest degree of axon regeneration (i.e. axon number and length in the brain) in the brain at 10 week post-injury time point.

To ensure that the axonal projections observed using LSFM are not under-represented by potential loss of CTB signal during the clearing procedure, LSFM results were corroborated by examining fibers in coronal brain sections from a separate set of animals (n = 8). In coronal sections, CTB-labeled RGC axons were found mainly in the hypothalamus region including the SCN, anterior hypothalamic area and ventromedial hypothalamus (Supplementary Fig. 2). Laterally, some axons travelled short distances within the degenerated optic tracts. RGC axons were not found in the more distant targets, LGN and SC (Supplementary Fig. 2). Immunohistochemical staining of the brain sections using CTB antibody to amplify the signal did not detect regenerated axons in midbrain targets, LGN and SC.

3D assessment of axonal projection in PTEN KO/Zymosan/cAMP analogue-treated mice

It was recently reported that PTEN KO combined with Zymosan and the cAMP analogue (PTEN KO/ZYM/cAMP) promotes extensive long distance regeneration of RGC axons. Strikingly, regenerating RGC axons in these mice were reported to re-innervate all the major visual targets including the OPT, LGN and SC (de Lima et al., 2012). Thus, we applied LSFM to examine axon regeneration to the brain in PTEN KO/ZYM/cAMP mice. Adult $PTEN^{f/f}$ mice received an intravitreal AAV-Cre injection 2 weeks prior to a crush injury, and Zymosan and the cAMP analogue were administered during the survival time as previously described (de Lima et al., 2012). At 10 to 12 weeks after injury, the optic nerves and brains were cleared using THF and imaged with the LSFM. Five to 7 days prior to sacrifice, CTB was injected to label the regenerating axons. As expected, many axons regenerated long distances in the optic nerve of the PTEN KO/ZYM/cAMP mice (Fig. 4B). Similar to the axon number reported previously (de Lima et al., 2012), many RGC axons (a mean of 112 fibers/animal; n = 9; SEM = 19.5) elongated long distances (4–5 mm distal to the lesion site) to reach the optic chiasm (Fig. 4B). In the brain, the axonal projection was similar to that of PTEN/SOCS3 KO mice. In general, similar or higher numbers of axons were found in the ipsilateral optic tract than in the contralateral optic tract (Figs. 4E and G). A few RGC axons extended into the opposite uninjured optic nerve (Figs. 4E and G), while others projected dorsally to the SCN (Supplementary Fig. 3). Some axons also exited the optic tracts and extended into the lateroanterior hypothalamic nucleus or supraoptic nucleus. RGC axons were not detected in the OPT, LGN and SC (Supplementary Fig. 3).

3D assessment of axonal projections following bilateral optic nerve crush

The optic chiasm is a region where RGC axons from each eye meet (Movie 6). As previously mentioned, some regenerating axons made sharp turns upon reaching the optic chiasm, suggesting that intact axons from the contralateral eye may affect the trajectory of regenerating axons in this region. To examine this possibility, we carried out a bilateral crush experiment. AAV-Cre/rCNTF was injected into the left eye of PTEN/SOCS3 floxed mice, followed by crush on both optic nerves 2 weeks later. At 10 weeks after bilateral crush

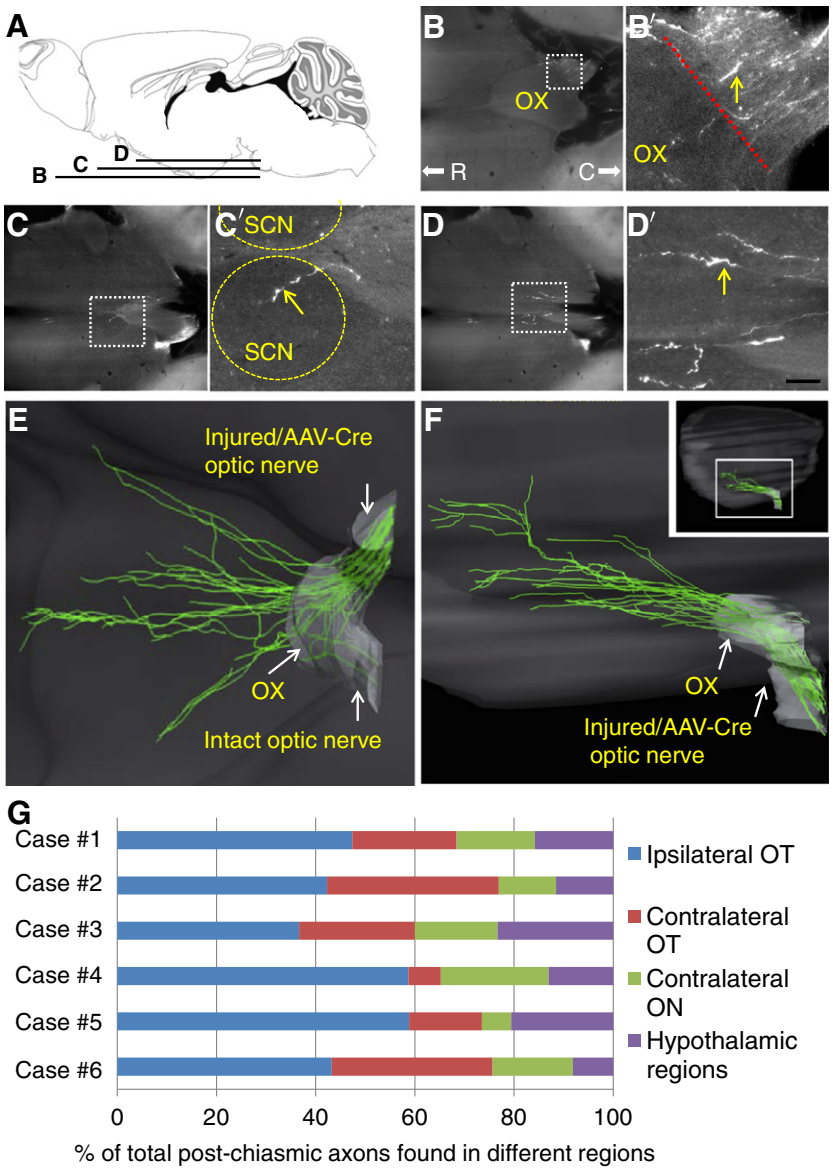

Fig. 3. 3D visualization of axonal projections in the brain. A, schematic diagram of mouse brain showing horizontal planes at which individual optical slices in B–D are derived from. B–D, several representative horizontal optical slices collected from an unsectioned brain of PTEN/SOCS3 KO animal following LSFM. B′–D′, higher magnification of the respective white boxed area in B–D. Yellow arrows indicate CTB-labeled axons. CTB-labeled axons are found immediately before the optic chiasm as shown in B. Some axons extended medial-dorsally into the hypothalamic brain regions including the SCN as shown in C, and medial pre-optic area as shown in D. E, ventral view of the 3D reconstruction of traced fibers near the optic chiasm. Neurite tracing and 3D volume rendering were done using Imaris software. F, lateral view of the 3D reconstruction of axonal projections into the brain. Inset shows low magnification of the whole brain following 3D reconstruction. G, quantification of axonal trajectory into different regions (i.e. ipsi/contralateral optic tracts, opposite optic nerve or hypothalamic regions). Values are presented as percentages of total axons that have exited the optic chiasm in 6 individual animals (case #1–6). C, caudal; ON, optic nerve; OT, optic tract; OX, optic chiasm; R, rostral; SCN, suprachiasmatic nucleus. Scale bar, 100 μm in D.

injury, we observed that while similar numbers of axons regenerated up to the optic chiasm compared to the animals receiving a unilateral crush, higher numbers of axons regenerated into and beyond the optic chiasm. However, the overall trajectory pattern at the optic chiasm was similar compared to unilateral crush. Similar or higher numbers of axons extended into the ipsilateral optic tract than to the contralateral optic tract, with a few axons extending also into the opposite optic nerve. Some axons projected dorsally to reach the SCN, or medial pre-optic area (Fig. 5).

Discussion

We have applied tissue clearance and LSFM to obtain a comprehensive assessment of RGC axon regeneration after injury. Using these methods, we were able to image the entire mouse optic nerve and brain, providing 3D visualization of the optic pathways from the eye through the brain. This approach allowed not only visualization of the main axon bundles that make up the visual pathway in normal animals, but it also enabled detection of single axons that leave the main pathway to stream into aberrant regions. For instance, in all uninjured control mice examined, between 10 and 30 axons were found to turn at the optic chiasm and project long distances into the contralateral optic nerve, confirming that some RGC axons are misrouted at the chiasm during development and persist in the adult (Bunt et al., 1983). Thus, these results highlight the strength of 3D imaging to detect small numbers of axons that would have been difficult to identify in histological sections. In addition to observing axonal trajectories, we also found that some RGC axons generate branches as they regenerate. During development, RGC axons generate branches to connect with multiple synaptic targets, a process

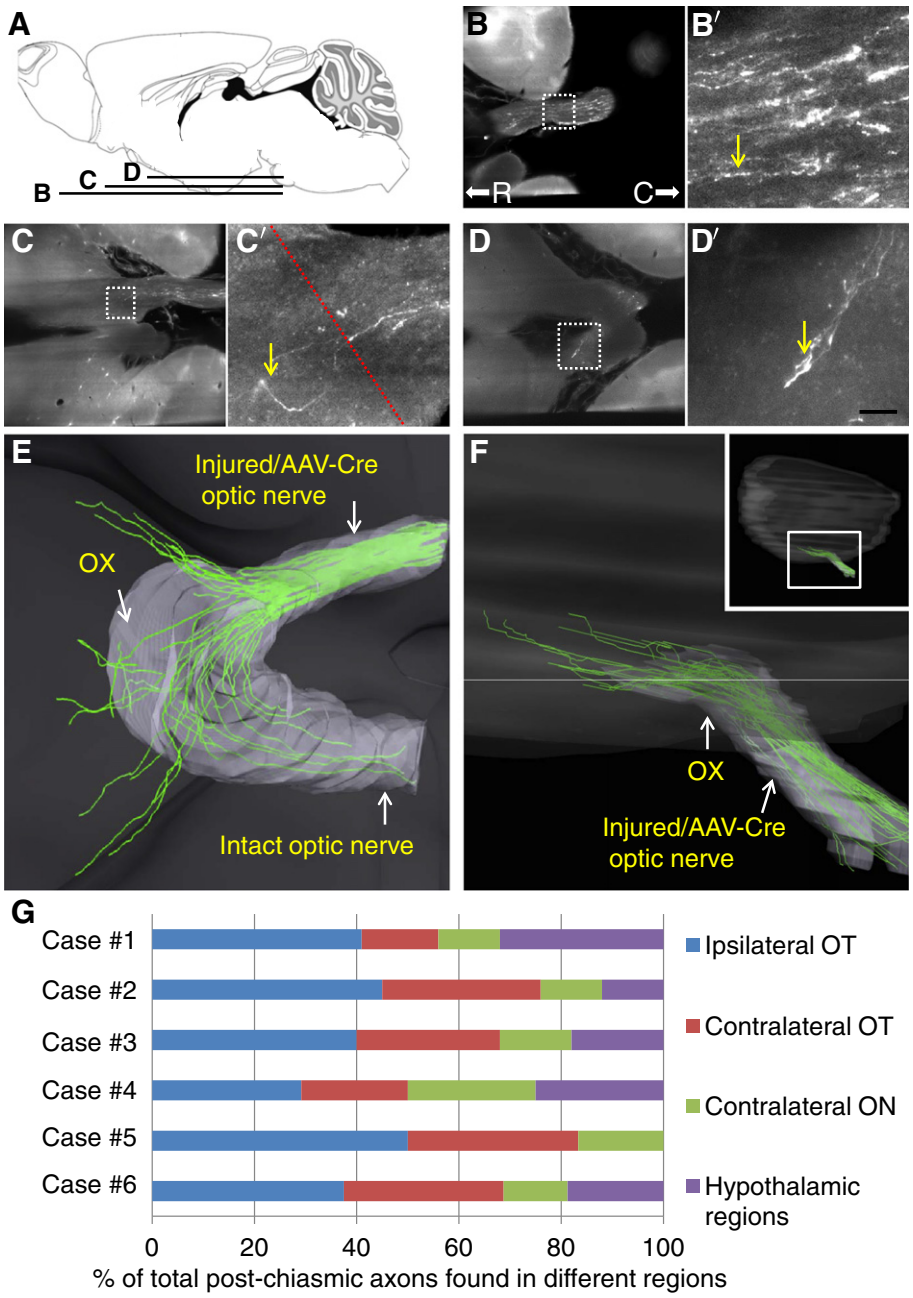

Fig. 4. 3D visualization of axonal projections in the brain of PTEN KO/ZYM/cAMP mice. A, schematic diagram of mouse brain showing horizontal planes at which the images in B–D are derived from. B–D, several representative horizontal optical slices collected from an unsectioned brain of PTEN KO/ZYM/cAMP animal following LSFM. B′–D′, higher magnification of the respective white boxed area in B–D. Yellow arrows indicate CTB-labeled axons. CTB-labeled axons are found in the distal optic nerve near the optic chiasm as shown in B, in the SCN as shown in C and in the optic tract as shown in D. E, ventral view of the 3D reconstruction of traced fibers near the optic chiasm. F, lateral view of the 3D reconstruction of axonal projections into the brain. Inset shows low magnification of the whole brain following 3D reconstruction. G, quantification of axonal trajectory into different regions (i.e. ipsi/contralateral optic tracts, opposite optic nerve or hypothalamic regions). Values are presented as percentages of total axons that have exited the optic chiasm in 6 individual animals (case #1–6). Red dotted line in C′ represents optic nerve-optic chiasm transition zone. C, caudal; ON, optic nerve; OT, optic tract; OX, optic chiasm; R, rostral; SCN, suprachiasmatic nucleus. Scale bar, 100 μm in D.

known to be regulated in part by target-derived trophic factors such as nerve growth factor and brain derived neurotrophic factor (Gibson and Ma, 2011). Although some regenerated axons in our study generated branches prematurely within optic nerve, other axons generated branches in the hypothalamus, raising the possibility that the regenerated axons could, in principle, re-establish connections with multiple synaptic targets in the adults. LSFM also allowed more accurate determination of regenerating fiber numbers. While it was challenging to directly count the axons close to the lesion because of the dense axonal projection, we were able to directly count virtually all axons that regenerated long distances.

To innervate the visual targets in the brain, regenerating RGC axons must travel long distance along the optic nerve and then correctly pathfind through various regions in the brain. While it has been a major challenge to develop strategies that stimulate RGC axons to regenerate long distances in the first place, studies over the past several years have shown that this is feasible, at least for some RGCs. For example, in adult Bcl-2tg mice, virally-induced over-expression of CNTF promotes long distance regeneration to the optic chiasm (Leaver et al., 2006). Very recently, Pernet et al., demonstrated that the expression of CNTF using AAV2 alone induces long distance regeneration of RGC axons in wild type mice (Pernet et al.,

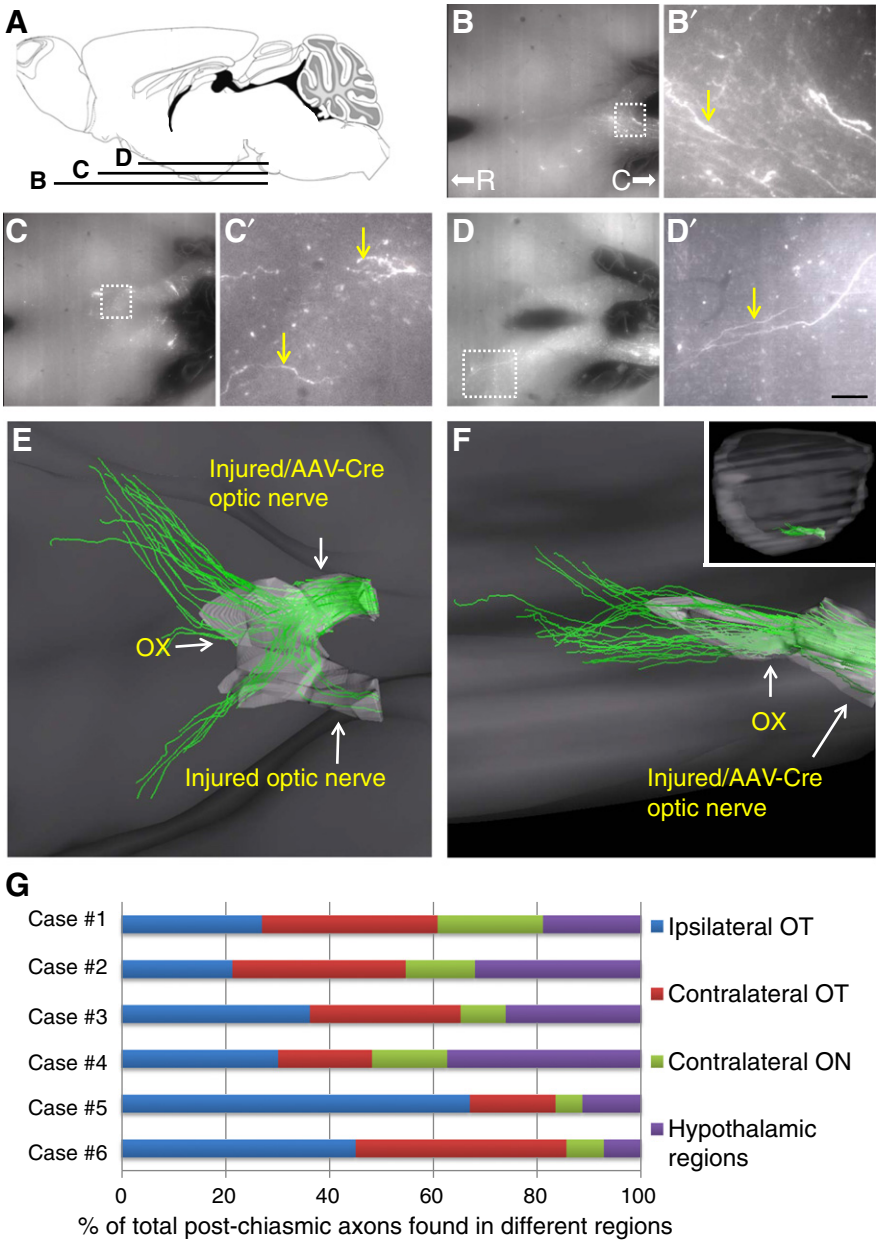

Fig. 5. 3D visualization of axonal projections in the brain following bilateral optic nerve crush. A, schematic diagram of mouse brain showing horizontal planes at which the images in B–D are derived from. B–F, several representative horizontal optical slices collected from an unsectioned brain of PTEN/SOCS3 KO animal following LSFM. B′–D′, higher magnification of the respective white boxed area in B–F. Yellow arrows indicate CTB-labeled axons. CTB-labeled axons extend through the optic chiasm and into the optic tracts and hypothalamus. E, ventral view of the 3D reconstruction of traced fibers near the optic chiasm. F, lateral view of the 3D reconstruction of axonal projections into the brain. Inset shows low magnification of the whole brain following 3D reconstruction. G, quantification of axonal trajectory into different regions (i.e. ipsi/contralateral optic tracts, opposite optic nerve or hypothalamic regions). Values are presented as percentages of total axons that have exited the optic chiasm in 6 individual animals (case #1–6). C, caudal; ON, optic nerve; OT, optic tract; OX, optic chiasm; R, rostral; SCN, suprachiasmatic nucleus. Scale bar, 100 μm in D.

2012). In addition, PTEN deletion in RGCs, combined with SOCS3 deletion/CNTF injection (Sun et al., 2011), or with Zymosan and cAMP analogue (de Lima et al., 2012; Kurimoto et al., 2010) promoted extensive long distance regeneration in the optic nerve, allowing some RGC axons to reach into the brain. Using LSFM, we observed that many axons grew in tortuous paths in the optic nerve, making multiple turns, and often projecting back to the eye. Thus, our data are in agreement with the recent study from Pernet et al., in which extensive axon turning was evident in optic nerves of animals treated with AAV-CNTF (Pernet et al., 2012). Collectively, these studies indicate that there is considerable axon misguidance within the injured optic nerve during regeneration, which may limit some RGC axons extending into the brain and ultimately to their targets.

During development, de novo RGC axons enter the optic nerve and travel in a fasciculated manner towards the brain. This process is tightly regulated by signaling molecules expressed and released by neuronal and non-neuronal cells in the interstitial spaces and the extracellular matrix. For example, Sema5A which is found on neuroepithelial cells surrounding the retinal axons along the optic nerve, was shown to induce growth cone collapse, and antibodies against SemaA5 cause retinal axons to escape from the optic nerve bundle (Oster et al., 2003). Other axon repulsive cues such as myelin associated glycoproteins, semaphorins,

ephrins, chondroitin sulfate proteoglycans (CSPGs) and their respective receptors have also been shown to be expressed in the injured retina and optic nerve (Cai et al., 2012; Du et al., 2007; Goldberg et al., 2004; Hunt et al., 2003; Liu et al., 2006; Park et al., 2008; Selles-Navarro et al., 2001; Shirvan et al., 2002), and could, in principle, contribute to the heterogeneous axon growth patterns seen in the optic nerves. In ALDH1L1-EGFP tg mice in which astrocytes are labeled with EGFP, strong astroglial activation is seen in the nerve regions close to the lesion site. Given that axon turning in PTEN/SOCS3 KO mice was especially prevalent in these regions, it is plausible that high concentration of CSPGs and other repulsive factors (or growth factors) released by reactive astrocytes may contribute to the extensive axon turning. It is currently unclear to what extent these and other growth inhibitory (or attractive) cues present in the injured optic nerve contribute to the aberrant axon trajectories observed in the adult optic nerve.

One major decision point for growing RGC axons en route to their central targets is the optic chiasm where axons must decide whether or not to cross. The majority of animals in our study had similar or higher numbers of axons extending to the ipsilateral side of the brain than the contralateral side. This observation is consistent with the previous report demonstrating large ipsilateral projections of regenerating RGC axons in perinatal Bcl-2 transgenic mice (Cho et al., 2005). Potentially, intact RGC axons from the opposite eye could affect the course of growing axons at the optic chiasm. For instance, previous studies in frogs have demonstrated that the number of axons that regenerate to the opposite nerve is less in animals subjected to a bilateral optic nerve lesion compared to unilaterally lesioned animals (Bohn and Stelzner, 1981). On the other hand, studies using a prechiasmic lesion in adult rats showed no obvious difference in the divergence patterns of regenerating axons at the optic chiasm between animals subjected to bilateral and unilateral crush (Berry et al., 1999). Consistent with this latter study, the overall divergence pattern at the optic chiasm was similar in both of our injury models in mice, supporting the idea that interactions between regenerating axons and the intact axons from the uninjured eye may not be responsible for establishing the aberrant trajectories.

Axonal pathfinding at the optic chiasm during development is regulated by EphB1/ephrinB2 signaling: the Ephb1 receptor is expressed in a small population of RGCs, and axons extending from these RGCs are repelled by ephrinB2 ligand expressed in the chiasm midline, thus giving rise to the ipsilateral projection (Williams et al., 2003). Other guidance cues and receptors involved in pathfinding through the chiasm during nervous system development include Zic2, NrCAM, Islet-1, Plexin-A1 and semaphorin6D (Herrera et al., 2003; Kuwajima et al., 2012; Pak et al., 2004; Petros et al., 2008; Williams et al., 2006). The expression levels of Eph1B and ephrinB2 in the adult mouse retina and optic chiasm, and whether the higher percentage of ipsilaterally projecting axons seen in these studies are due to EphB1/ephrinB2 signaling or other aforementioned guidance factors is not yet known. Nonetheless, our results indicate that the molecular and cellular mechanisms that once guided axons through the optic chiasm during development are not preserved in adult mice.

With the recent progress made in promoting long distance regeneration in the optic nerve, a pressing question is to what extent do these axons navigate correctly to re-innervate their central targets? In both PTEN/SOCS3 KO and PTEN KO/ZYM/cAMP mice, RGC axons projected dorsally into the hypothalamus or short distances laterally to the optic tracts or projected to the uninjured contralateral optic nerve. Centrally, axonal projections were limited primarily to the hypothalamus. Thus, our findings are in contrast to the previous study using PTEN KO/ZYM/cAMP mice in which many regenerating axons were reported to elongate long distances within the brain, correctly navigating and re-innervating all the major visual targets including the SCN, OPT, MTN, LGN and SC (de Lima et al., 2012). The reasons behind these differing results are not clear. Of note, in this present study, similar number of axons regenerated long distances up to the optic chiasm in the PTEN KO/ZYM/cAMP treated mice as reported previously (de Lima et al., 2012), confirming the effectiveness of this combinatorial approach in promoting RGC axon regeneration.

In nearly all animals, regenerating axons were found in the SCN, the master pacemaker of circadian rhythm. In normal mammals, the SCN receives axons predominantly from melanopsin expressing-intrinsically photosensitive RGCs (ipRGCs). These RGCs directly send photic information to the SCN which in turn regulates daily rhythmicity such as sleep, body temperature and food intake (Do and Yau, 2010; Schmidt et al., 2011). This raises questions as to whether or to what extent the regenerated RGC axons found in the SCN originate from the ipRGCs, and whether they form functional synaptic connections with the SCN neurons. In addition, our results demonstrated that some axons generated branches, raising a question as to whether axonal branching during regeneration is a feature unique to a specific RGC subset, or occurs at random in any regenerating RGC axon. The combined use of tissue clearance and 3D visualization together with transgenic mice in which axons from known subtypes of RGCs are GFP-labeled may facilitate addressing these questions. In summary, we demonstrated, for the first time, integration of tissue clearance and LSFM for comprehensive analysis of RGC axon regeneration in mouse models. Our study shows misdirected growth in the optic nerve and brain, indicating that the adult mammalian CNS lacks the signals necessary for proper pathfinding of regenerating RGC axons.

Supplementary data to this article can be found online at http://dx.doi.org/10.1016/j.expneurol.2013.03.001.

Acknowledgments

This work was supported by grants from U.S. Army W81XWH-05-1-0061 (VPL, PT, KKP), NIH HD057521 (VPL), U.S. Army W81XWH-12-1-0319 (KKP), NEI 1R01EY022961-01 (KKP), Ziegler Foundation (KKP), Pew Charitable Trust (KKP) and the Miami Project to Cure Paralysis and Buoniconti Fund (VPL, PT, KKP). VPL holds the Walter G Ross Distinguished Chair in Developmental Neuroscience. We thank the Imaging Core at the Miami Project to Cure Paralysis for the LSFM facility, and Drs. Daniel Liebl, Jae Lee, Jeffrey Rothstein and Wendy Macklin for providing the transgenic mice.

References

Beazley, L.D., Sheard, P.W., Tennant, M., Starac, D., Dunlop, S.A., 1997. Optic nerve regenerates but does not restore topographic projections in the lizard *Ctenophorus ornatus*. J. Comp. Neurol. 377, 105–120.
Becker, C.G., Becker, T., 2007. Growth and pathfinding of regenerating axons in the optic projection of adult fish. J. Neurosci. Res. 85, 2793–2799.
Becker, K., Jahrling, N., Saghafi, S., Weiler, R., Dodt, H.U., 2012. Chemical clearing and dehydration of GFP expressing mouse brains. PLoS One 7, e33916.
Berry, M., Carlile, J., Hunter, A., Tsang, W., Rosenstiel, P., Sievers, J., 1999. Optic nerve regeneration after intravitreal peripheral nerve implants: trajectories of axons regrowing through the optic chiasm into the optic tracts. J. Neurocytol. 28, 721–741.
Bohn, R.C., Stelzner, D.J., 1981. The aberrant retinol–retinal projection during optic nerve regeneration in the frog. III. Effects of crushing both nerves. J. Comp. Neurol. 196, 633–643.
Bunt, S.M., Lund, R.D., Land, P.W., 1983. Prenatal development of the optic projection in albino and hooded rats. Brain Res. 282, 149–168.
Cai, X., Yuan, R., Hu, Z., Chen, C., Yu, J., Zheng, Z., Ye, J., 2012. Expression of PirB protein in intact and injured optic nerve and retina of mice. Neurochem. Res. 37, 647–654.
Cho, K.S., Yang, L., Lu, B., Feng Ma, H., Huang, X., Pekny, M., Chen, D.F., 2005. Re-establishing the regenerative potential of central nervous system axons in postnatal mice. J. Cell Sci. 118, 863–872.
de Lima, S., Koriyama, Y., Kurimoto, T., Oliveira, J.T., Yin, Y., Li, Y., Gilbert, H.Y., Fagiolini, M., Martinez, A.M., Benowitz, L., 2012. Full-length axon regeneration in the adult mouse optic nerve and partial recovery of simple visual behaviors. Proc. Natl. Acad. Sci. U. S. A. 109, 9149–9154.
Do, M.T., Yau, K.W., 2010. Intrinsically photosensitive retinal ganglion cells. Physiol. Rev. 90, 1547–1581.
Doyle, J.P., Dougherty, J.D., Heiman, M., Schmidt, E.F., Stevens, T.R., Ma, G., Bupp, S., Shrestha, P., Shah, R.D., Doughty, M.L., Gong, S., Greengard, P., Heintz, N., 2008. Application of a translational profiling approach for the comparative analysis of CNS cell types. Cell 135, 749–762.
Du, J., Tran, T., Fu, C., Sretavan, D.W., 2007. Upregulation of EphB2 and ephrin-B2 at the optic nerve head of DBA/2J glaucomatous mice coincides with axon loss. Invest. Ophthalmol. Vis. Sci. 48, 5567–5581.

Duffy, P., Wang, X., Seigel, C.S., Tu, N., Henkemeyer, M., Cafferty, W.B., Strittmatter, S.M., 2012. Myelin-derived ephrinB3 restricts axonal regeneration and recovery after adult CNS injury. Proc. Natl. Acad. Sci. U. S. A. 109, 5063–5068.
Erturk, A., Mauch, C.P., Hellal, F., Forstner, F., Keck, T., Becker, K., Jahrling, N., Steffens, H., Richter, M., Hubener, M., Kramer, E., Kirchhoff, F., Dodt, H.U., Bradke, F., 2012. Three-dimensional imaging of the unsectioned adult spinal cord to assess axon regeneration and glial responses after injury. Nat. Med. 18, 166–171.
Gibson, D.A., Ma, L., 2011. Developmental regulation of axon branching in the vertebrate nervous system. Development 138, 183–195.
Goldberg, J.L., Vargas, M.E., Wang, J.T., Mandemakers, W., Oster, S.F., Sretavan, D.W., Barres, B.A., 2004. An oligodendrocyte lineage-specific semaphorin, Sema5A, inhibits axon growth by retinal ganglion cells. J. Neurosci. 24, 4989–4999.
Groszer, M., Erickson, R., Scripture-Adams, D.D., Lesche, R., Trumpp, A., Zack, J.A., Kornblum, H.I., Liu, X., Wu, H., 2001. Negative regulation of neural stem/progenitor cell proliferation by the PTEN tumor suppressor gene in vivo. Science 294, 2186–2189.
Herrera, E., Brown, L., Aruga, J., Rachel, R.A., Dolen, G., Mikoshiba, K., Brown, S., Mason, C.A., 2003. Zic2 patterns binocular vision by specifying the uncrossed retinal projection. Cell 114, 545–557.
Hunt, D., Coffin, R.S., Prinjha, R.K., Campbell, G., Anderson, P.N., 2003. Nogo-A expression in the intact and injured nervous system. Mol. Cell. Neurosci. 24, 1083–1102.
Jung, S., Aliberti, J., Graemmel, P., Sunshine, M.J., Kreutzberg, G.W., Sher, A., Littman, D.R., 2000. Analysis of fractalkine receptor CX(3)CR1 function by targeted deletion and green fluorescent protein reporter gene insertion. Mol. Cell. Biol. 20, 4106–4114.
Kurimoto, T., Yin, Y., Omura, K., Gilbert, H.Y., Kim, D., Cen, L.P., Moko, L., Kugler, S., Benowitz, L.I., 2010. Long-distance axon regeneration in the mature optic nerve: contributions of oncomodulin, cAMP, and PTEN gene deletion. J. Neurosci. 30, 15654–15663.
Kuwajima, T., Yoshida, Y., Takegahara, N., Petros, T.J., Kumanogoh, A., Jessell, T.M., Sakurai, T., Mason, C., 2012. Optic chiasm presentation of Semaphorin6D in the context of Plexin-A1 and Nr-CAM promotes retinal axon midline crossing. Neuron 74, 676–690.
Leaver, S.G., Cui, Q., Plant, G.W., Arulpragasam, A., Hisheh, S., Verhaagen, J., Harvey, A.R., 2006. AAV-mediated expression of CNTF promotes long-term survival and regeneration of adult rat retinal ganglion cells. Gene Ther. 13, 1328–1341.
Lingor, P., Tonges, L., Pieper, N., Bermel, C., Barski, E., Planchamp, V., Bahr, M., 2008. ROCK inhibition and CNTF interact on intrinsic signalling pathways and differentially regulate survival and regeneration in retinal ganglion cells. Brain 131, 250–263.
Liu, X., Hawkes, E., Ishimaru, T., Tran, T., Sretavan, D.W., 2006. EphB3: an endogenous mediator of adult axonal plasticity and regrowth after CNS injury. J. Neurosci. 26, 3087–3101.
Mallon, B.S., Shick, H.E., Kidd, G.J., Macklin, W.B., 2002. Proteolipid promoter activity distinguishes two populations of NG2-positive cells throughout neonatal cortical development. J. Neurosci. 22, 876–885.
Moore, D.L., Blackmore, M.G., Hu, Y., Kaestner, K.H., Bixby, J.L., Lemmon, V.P., Goldberg, J.L., 2009. KLF family members regulate intrinsic axon regeneration ability. Science 326, 298–301.
Muller, A., Hauk, T.G., Fischer, D., 2007. Astrocyte-derived CNTF switches mature RGCs to a regenerative state following inflammatory stimulation. Brain 130, 3308–3320.
Oster, S.F., Bodeker, M.O., He, F., Sretavan, D.W., 2003. Invariant Sema5A inhibition serves an ensheathing function during optic nerve development. Development 130, 775–784.
Pak, W., Hindges, R., Lim, Y.S., Pfaff, S.L., O'Leary, D.D., 2004. Magnitude of binocular vision controlled by islet-2 repression of a genetic program that specifies laterality of retinal axon pathfinding. Cell 119, 567–578.
Park, K.K., Liu, K., Hu, Y., Smith, P.D., Wang, C., Cai, B., Xu, B., Connolly, L., Kramvis, I., Sahin, M., He, Z., 2008. Promoting axon regeneration in the adult CNS by modulation of the PTEN/mTOR pathway. Science 322, 963–966.
Paxinos, G., Franklin, K.B.J., 2004. The Mouse Brain in Stereotaxic Coordinates, Compact2nd edn. Elsevier Academic Press, Amsterdam; Boston.
Pernet, V., Joly, S., Dalkara, D., Jordi, N., Schwarz, O., Christ, F., Schaffer, D.V., Flannery, J.G., Schwab, M.E., 2012. Long-distance axonal regeneration induced by CNTF gene transfer is impaired by axonal misguidance in the injured adult optic nerve. Neurobiol. Dis. 51, 202–213.
Petros, T.J., Rebsam, A., Mason, C.A., 2008. Retinal axon growth at the optic chiasm: to cross or not to cross. Annu. Rev. Neurosci. 31, 295–315.
Qiu, J., Cai, D., Filbin, M.T., 2002. A role for cAMP in regeneration during development and after injury. Prog. Brain Res. 137, 381–387.
Schmidt, T.M., Chen, S.K., Hattar, S., 2011. Intrinsically photosensitive retinal ganglion cells: many subtypes, diverse functions. Trends Neurosci. 34, 572–580.
Selles-Navarro, I., Ellezam, B., Fajardo, R., Latour, M., McKerracher, L., 2001. Retinal ganglion cell and nonneuronal cell responses to a microcrush lesion of adult rat optic nerve. Exp. Neurol. 167, 282–289.
Shirvan, A., Kimron, M., Holdengreber, V., Ziv, I., Ben-Shaul, Y., Melamed, S., Melamed, E., Barzilai, A., Solomon, A.S., 2002. Anti-semaphorin 3A antibodies rescue retinal ganglion cells from cell death following optic nerve axotomy. J. Biol. Chem. 277, 49799–49807.
Smith, P.D., Sun, F., Park, K.K., Cai, B., Wang, C., Kuwako, K., Martinez-Carrasco, I., Connolly, L., He, Z., 2009. SOCS3 deletion promotes optic nerve regeneration in vivo. Neuron 64, 617–623.
Stelzner, D.J., Bohn, R.C., Strauss, J.A., 1986. Regeneration of the frog optic nerve. Comparisons with development. Neurochem. Pathol. 5, 255–288.
Su, Y., Wang, F., Zhao, S.G., Pan, S.H., Liu, P., Teng, Y., Cui, H., 2008. Axonal regeneration after optic nerve crush in Nogo-A/B/C knockout mice. Mol. Vis. 14, 268–273.
Sun, F., Park, K.K., Belin, S., Wang, D., Lu, T., Chen, G., Zhang, K., Yeung, C., Feng, G., Yankner, B.A., He, Z., 2011. Sustained axon regeneration induced by co-deletion of PTEN and SOCS3. Nature 480, 372–375.
Williams, S.E., Grumet, M., Colman, D.R., Henkemeyer, M., Mason, C.A., Sakurai, T., 2006. A role for Nr-CAM in the patterning of binocular visual pathways. Neuron 50, 535–547.
Williams, S.E., Mann, F., Erskine, L., Sakurai, T., Wei, S., Rossi, D.J., Gale, N.W., Holt, C.E., Mason, C.A., Henkemeyer, M., 2003. Ephrin-B2 and EphB1 mediate retinal axon divergence at the optic chiasm. Neuron 39, 919–935.
Winzeler, A.M., Mandemakers, W.J., Sun, M.Z., Stafford, M., Phillips, C.T., Barres, B.A., 2011. The lipid sulfatide is a novel myelin-associated inhibitor of CNS axon outgrowth. J. Neurosci. 31, 6481–6492.
Wong, E.V., David, S., Jacob, M.H., Jay, D.G., 2003. Inactivation of myelin-associated glycoprotein enhances optic nerve regeneration. J. Neurosci. 23, 3112–3117.
Yang, Y., Vidensky, S., Jin, L., Jie, C., Lorenzini, I., Frankl, M., Rothstein, J.D., 2011. Molecular comparison of GLT1 + and ALDH1L1 + astrocytes in vivo in astroglial reporter mice. Glia 59, 200–207.

Development/Plasticity/Repair

Mammalian Target of Rapamycin's Distinct Roles and Effectiveness in Promoting Compensatory Axonal Sprouting in the Injured CNS

Do-Hun Lee, Xueting Luo, Benjamin J. Yungher, Eric Bray, Jae K. Lee, and Kevin K. Park
Miami Project to Cure Paralysis and Department of Neurosurgery, University of Miami Miller School of Medicine, Miami, Florida 33136

Mammalian target of rapamycin (mTOR) functions as a master sensor of nutrients and energy, and controls protein translation and cell growth. Deletion of phosphatase and tensin homolog (PTEN) in adult CNS neurons promotes regeneration of injured axons in an mTOR-dependent manner. However, others have demonstrated mTOR-independent axon regeneration in different cell types, raising the question of how broadly mTOR regulates axonal regrowth across different systems. Here we define the role of mTOR in promoting collateral sprouting of spared axons, a key axonal remodeling mechanism by which functions are recovered after CNS injury. Using pharmacological inhibition, we demonstrate that mTOR is dispensable for the robust spontaneous sprouting of corticospinal tract axons seen after pyramidotomy in postnatal mice. In contrast, moderate spontaneous axonal sprouting and induced-sprouting seen under different conditions in young adult mice (i.e., PTEN deletion or degradation of chondroitin proteoglycans; CSPGs) are both reduced upon mTOR inhibition. In addition, to further determine the potency of mTOR in promoting sprouting responses, we coinactivate PTEN and CSPGs, and demonstrate that this combination leads to an additive increase in axonal sprouting compared with single treatments. Our findings reveal a developmental switch in mTOR dependency for inducing axonal sprouting, and indicate that PTEN deletion in adult neurons neither recapitulates the regrowth program of postnatal animals, nor is sufficient to completely overcome an inhibitory environment. Accordingly, exploiting mTOR levels by targeting PTEN combined with CSPG degradation represents a promising strategy to promote extensive axonal plasticity in adult mammals.

Key words: **axon growth; axon regeneration; axon sprouting; mTOR; PTEN; pyramidotomy**

Introduction

Following injury, axonal remodeling in the form of collateral sprouting of spared axons that compensate for lost circuits represents a key mechanism by which behavioral functions are recovered (Schwab, 2002; Weidner and Tuszynski, 2002; Fouad et al., 2011). For instance, in the case of spinal cord injury (SCI), clinical lesions are often anatomically and functionally incomplete, and thus compensatory sprouting of uninjured axons represents an important mechanism for functional recovery. Such axonal regrowth is robust after injury in postnatal animals but diminishes with age.

Received May 13, 2014; revised Oct. 3, 2014; accepted Oct. 6, 2014.

Author contributions: J.K.L. and K.K.P. designed research; D.-H.L., X.L., B.J.Y., J.K.L., and K.K.P. performed research; E.B. and K.K.P. contributed unpublished reagents/analytic tools; D.-H.L., X.L., J.K.L., and K.K.P. analyzed data; D.-H.L., B.J.Y., J.K.L., and K.K.P. wrote the paper.

This work was supported by grants from U.S Army W81XWH-05-1-0061 (K.K.P., J.K.L.), W81XWH-12-1-0319 (K.K.P.), NIH/NEI (K.K.P.), Ziegler Foundation (K.K.P.), Pew Charitable Trust (K.K.P.), Craig H. Neilsen Foundation (K.K.P., D.H.L., J.K.L.), and the Buoniconti Fund (K.K.P., J.K.L.). We thank the Imaging Core and Viral Vector Core at the Miami Project to Cure Paralysis, Dr Fan Wang (Duke University) for Rosa26 flox-stop-flox tdTomato mice, Dr Veronica J. Tom (Drexel University) for advice on experiment involving CSPGs and chABC, and Yadira Salgueiro for assisting with genotyping and histology.

The authors declare no competing financial interests.

Correspondence should be addressed to either Dr Kevin K. Park or Jae K. Lee, Miami Project to Cure Paralysis, University of Miami, Miller School of Medicine, Miami, FL, 33136, E-mail: kpark@med.miami.edu or JLee22@med.miami.edu.

DOI:10.1523/JNEUROSCI.1935-14.2014

 0270-6474/14/3415347-09$15.00/0

Mammalian target of rapamycin (mTOR) is a protein kinase that controls ribosome biogenesis and protein translation (Laplante and Sabatini, 2012). The level of mTOR activity in CNS neurons declines during development (Park et al., 2008), correlating with the decrease in their regrowth ability. We and others have demonstrated that deletion of phosphatase and tensin homolog (PTEN) or tuberous sclerosis proteins 1/2 in several different types of CNS neurons enhances axonal regeneration, an effect inhibited by mTOR blockade (Park et al., 2008; Abe et al., 2010; Byrne et al., 2014). In contrast, others have reported minimal roles of mTOR in promoting axon regeneration in sensory neurons (Christie et al., 2010), indicating that neurons under different conditions may employ mTOR-dependent or independent mechanisms to trigger axonal regrowth. Overall, although the role of mTOR in regulating regeneration of injured axons has been extensively studied, whether mTOR plays a general role in promoting axonal remodeling by compensatory sprouting of uninjured axons is unclear.

The aims of the present study were twofold. Using a pyramidotomy model in which one side of corticospinal tract (CST) is severed; first, we examined the loss of mTOR function in regulating compensatory sprouting of intact CST axons in postnatal animals and in young adult animals under different growth promoting conditions. Second, we assessed whether coupling PTEN/mTOR modulation with degradation of chondroitin proteoglycans (CSPGs), a

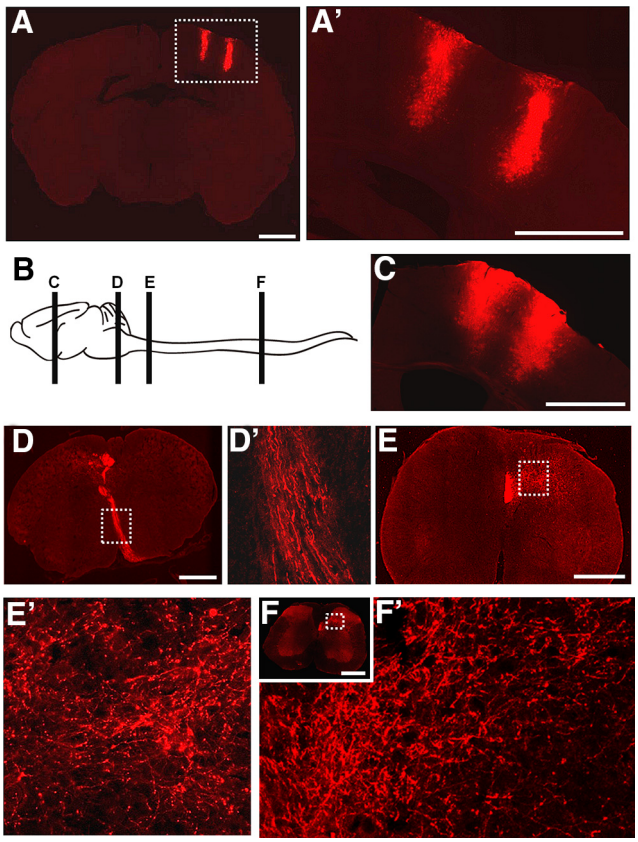

Figure 1. AAV-Cre-mediated labeling of CST axons in *Rosa26-tdTomato* reporter mice. ***A***, Coronal brain section of *Rosa-tdTomato* reporter mouse shows tdTomato $^{+}$ cortical neurons as early as 1 week after AAV-Cre injection ($n = 3$). ***A′***, Higher-magnification of the boxed areas in ***A***. Schematic representation showing the transverse planes at which the images (***C–F***) are found in mouse brain and spinal cord. At 2 weeks following intracortical AAV-Cre injection in the Rosa26 reporter mice, tdTomato-labeled axons are seen in (***C***) motor cortex, (***D***) brainstem at the level of CST decussation, (***E***) cervical spinal cord, and (***F***) lumbar spinal cord. ***D′***, Higher-magnification of the boxed areas in ***D***. ***F***, Low-magnification image of the coronal section at the lumbar level. ***F′***, Higher-magnification of the boxed areas in ***F***. Scale bars: ***A***, ***C***, 1000 μm; ***D–F***, 500 μm.

potent extrinsic inhibitor of axon regrowth (Davies et al., 1997; Bradbury et al., 2002; Barritt et al., 2006; Crespo et al., 2007; Kwok et al., 2008; Harris et al., 2010; Lee et al., 2010a; Jefferson et al., 2011; Zhao et al., 2011; Takeuchi et al., 2013) enhances sprouting in an additive or synergistic manner.

Materials and Methods

Animals. All experimental procedures were performed in compliance with protocols approved by the IACUC at University of Miami. Animals used were C57BL/6, *PTEN$^{f/f}$* mice (The Jackson Laboratory; 006440), Rosa26 loxP-stop-loxP-tdTomato (*Rosa-tdTomato;* a generous gift from Dr Fan Wang, Duke University) and *PTEN$^{f/f}$;Rosa-tdTomato*.

AAV preparation. For making adeno-associated viruses (AAVs), the cDNA of Cre was inserted downstream of the CMV promoter/β-globin intron enhancer in the plasmid pAAV-MCS (Stratagene), containing the AAV serotype-2 (AAV2) inverted terminal repeats and a human growth hormone polyA signal. pAAV-RC (Stratagene) that encodes the AAV2 genes (rep and cap) and the helper plasmid (Stratagene) that encodes E2A, E4, and VA were used for cotransfection in 293T cells to generate recombinant AAV. Plasmids were then used to produce AAV2 ($1–4 \times 10^{13}$ particles/ml) at the University of Miami Viral Vector Core.

AAV injection and BDA labeling. Female *PTEN$^{f/f}$;Rosa-tdTomato* or *Rosa-tdTomato* mice aged 4–5 weeks were anesthetized with ketamine/xylazine (100 mg/15 mg/kg, i.p) and injected with a total of 1–2 μl AAV into the left sensorimotor cortex at the following six sites: 0.5 and 0.1 mm anterior, and 0.3 mm posterior; 1.2 and 2.2 mm lateral (in reference to bregma). To label CST axons using biotinylated dextran amines (BDA), 1–2 μl of BDA (10%, Invitrogen) was injected into sensorimotor cortex 2 weeks before euthanasia (Lee et al., 2010b).

Pyramidotomy. For pyramidotomy, mice were anesthetized with ketamine/xylazine. The procedure is similar to that described previously (Lee et al., 2010b; Liu et al., 2010). Following craniotomy of the occipital bone using laminectomy forceps to expose the underlying pyramidal tract of mice (Starkey et al., 2005), a micro feather scalpel was used to puncture the dura and lesion the entire right pyramidal tract.

ChABC delivery. Immediately after pyramidotomy, mice received either 6 μl protease-free Chondroitinase ABC(ChABC; Sigma-Aldrich; 10 U/ml in saline) followed by a 3 μl saline flush, delivered as a bolus injection via the intracerebroventricular cannula tubing as described previously (Starkey et al., 2012). Control-treated mice were treated with vehicle (9 μl of saline). Further injections were performed on days 2, 4, 6, 8, and 10 following pyramidotomy. Briefly, the skull was exposed and a hole made with a 25 gauge needle at the following coordinates: −0.5 from bregma, 1 mm lateral to the midline. An intracerebroventricular cannula (Alzet) was inserted into the hole and secured into place using super glue (Loctite). The skin was then sutured over the cannula leaving the tubing exposed.

Rapamycin administration. Rapamycin was obtained from LC Laboratories, dissolved at 20 mg/ml in ethanol. Before each administration, rapamycin was diluted in 5% Tween 80, 5% polyethylene glycol 400 (0.5–1.5 mg/ml). Rapamycin at 6 mg/kg or the vehicle was given intraperitoneally on the day of pyramidotomy and every third day until euthanasia.

Tissue processing and immunohistochemistry. Tissue processing and immunohistochemical procedures were performed as described previously (Liu et al., 2010; Sun et al., 2011). Mice were killed and transcardially perfused with 4% paraformaldehyde. Tissues were isolated and postfixed in the same fixative overnight at 4°C. Tissues were cryoprotected in 30% sucrose and serial sections (16–25 μm) were collected. To detect BDA labeled fibers, coronal sections were washed in PBS and detected with streptavidin-AlexaFluor 594 (Invitrogen). To detect tdTomato signal, sections were immunostained overnight at 4°C with rabbit red fluorescent protein antibody (RFP; 1:200 dilution; Rockland). Other antibodies used were rabbit p-S6 (1:200 dilution; S235–236; Cell Signaling Technology), Mouse NeuN (1:500 dilution; Millipore), and rabbit PTEN (1:200 dilution; CST).

Assessment of lesion and CSPG degradation. Cryosections from spinal cord 10 d after pyramidotomy were incubated with anti-C-4-S (ICN) followed by incubation with secondary antibody (Jackson ImmunoResearch; Starkey et al., 2012). To determine the degree of unilateral pyramidotomy, sections from spinal cord at 4 weeks after injury was immunostained with an antibody against PKC-γ (1:50 dilution; Santa Cruz Biotechnology; Starkey et al., 2012).

Axon counting. For quantifying total labeled CST axons, axons were manually counted at the level of medulla oblongata proximal to the pyramidal decussation. Axons were counted in four rectangular areas randomly placed in the pyramidal tract and this axon density was multiplied by the total area of the tract to obtain the total number of labeled axons. This was done for two sections placed 160 μm apart and then the two counts were averaged to obtain the final number for each animal. To count the sprouted axons, two vertical lines, adjacent and 500 μm lateral to the central canal were drawn, and fibers crossing each line were manually counted in each section. The results were presented after normalization with the number of counted CST fibers at the medulla level: sprouting axon number index is represented as the ratio of the total number of sprouted axons in the denervated spinal cord over the number of labeled axons at the level of medulla. At least three sections were counted for each animal and averaged together.

The numbers of animals used for quantifying the degree of axonal sprouting. Animals with profound lack of tdTomato labeling in the cortex and medulla (1–2 animals per group), most likely due to injection errors were excluded from analysis. For the final quantification in Figure 4, the numbers of animals used per group are as follows: 8 (for "sham," "Px+rapamycin," "Px+PTEN KO+rapamycin" and

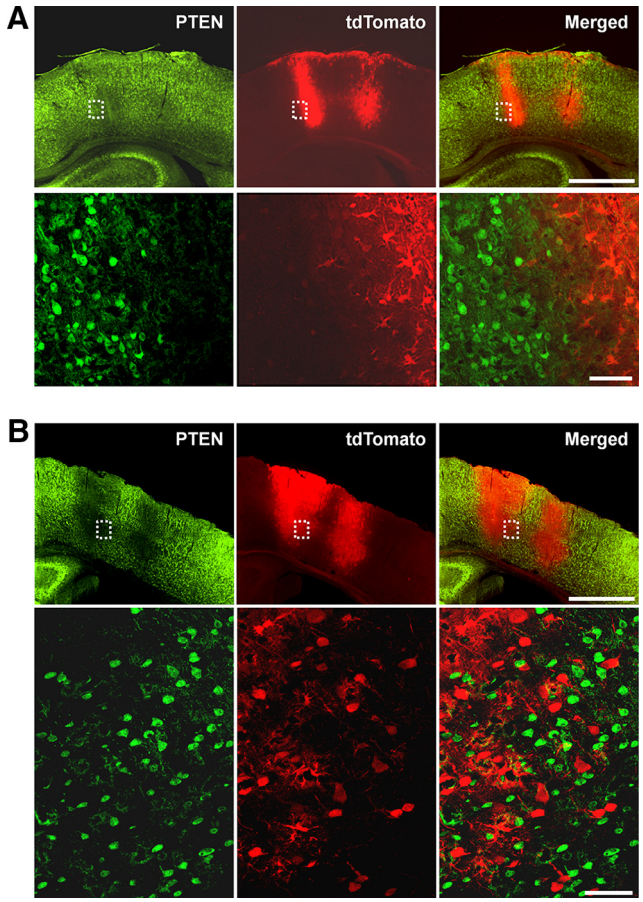

Figure 2. Concomitant PTEN deletion and axonal labeling in *PTEN$^{f/f}$;Rosa26-tdTomato* mice. Sensorimotor cortex of *PTEN$^{f/f}$;Rosa-tdTomato* mice, at 1 (***A***) and 2 (***B***) weeks after AAV-Cre injection. PTEN is depleted in tdTomato-expressing neurons as early as 1 week after AAV-Cre injection ($n = 3$). Coronal sections were immunostained with antibodies against PTEN (green) and RFP (red). ***A***, Bottom, Higher-magnification of the boxed areas above. ***B***, Bottom, Higher-magnification of the boxed areas above. Scale bars: (top) ***A***, ***B***, 1000 μm; (bottom) ***A***, ***B***, 100 μm.

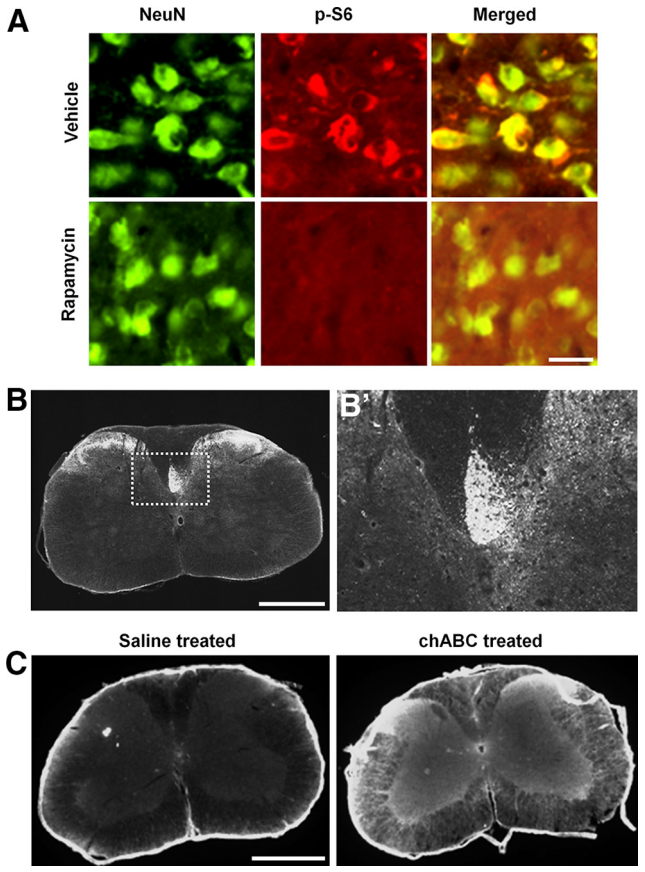

Figure 3. Validation of the lesion, levels of mTOR activity and CSPG degradation in pyramidotomy model. ***A***, Representative coronal sections of *PTEN$^{f/f}$;Rosa-tdTomato* motor cortex stained with p-S6 and NeuN antibodies show depletion of p-S6 immunoreactivity in cortical neurons following rapamycin treatment. Rapamycin or vehicle was administered every third day, starting from the day of pyramidotomy and animals were perfused 4 weeks after injury. ***B***, Representative coronal section of cervical spinal cord showing absence of PKC-γ immunoreactivity in the transected CST tract ($n = 8$). ***B'***, Higher-magnification of the boxed area in ***B***. ***C***, C-4-S immunostaining to validate CSPG digestion in the cervical spinal cord ($n = 3$). Scale bars: ***A***, 25 μm; ***B***, ***C***, 500 μm.

"Px+ChABC+rapamycin"), 10 (for "Px only"), and 13 (for "Px+PTEN KO+rapamycin). For the quantification in Figure 7, the numbers of animals used per group are as follows: 7 (for "sham" and "Px only"), 8 (for "Px+rapamycin"), and 9 (for "sham+rapamycin). For the quantification in Figure 8, the numbers of animals used per group are as follows: 8 (for "Px+PTEN KO"), 10 (for "Px only" and "Px+ChABC"), and 12 (for "Px+PTEN KO+ChABC").

Statistics. GraphPad Prism software was used for statistical analyses. Values were calculated as mean + SEM. For sprouting axon number index, two-way repeated-measures ANOVA was used, followed by Bonferroni *post hoc* test. Values of $p < 0.05$ were considered significant.

Results

Assessment of PTEN deletion-induced axonal regrowth in Rosa26-tdTomato reporter mice

Recent studies have identified several neuron intrinsic factors that limit axon regeneration. For instance, AAV-Cre-mediated PTEN deletion in neonatal animals followed by pyramidotomy in young adults resulted in enhanced axonal sprouting (Liu et al., 2010). We sought to further define the effects of PTEN deletion and the role of its key downstream effector mTOR in axonal sprouting responses. In the previous study, *PTEN$^{f/f}$* mice received AAV-Cre injection into sensorimotor cortex, followed by BDA injections several weeks later (Liu et al., 2010). However, even multiple BDA injections were only able to label axons in 20–50% of PTEN deleted-neurons (data not shown), thus limiting faithful assessment of PTEN-deletion effects. To study axonal phenotype specifically in PTEN-deleted neurons, we tested AAV-Cre that also expresses enhanced green florescent protein (EGFP), which can be used to label axons in place of dye tracers. However, EGFP labeling was weak in terms of both the number of labeled axons and signal intensity (data not shown). Alternatively, we crossed *PTEN$^{f/f}$* mice with *Rosa-tdTomato* to generate *PTEN$^{f/f}$;Rosa-tdTomato* mice, allowing simultaneous gene deletion and axon labeling via Cre-mediated recombination. Because even very low expression of Cre is sufficient to recombine *lox* sites, AAV-Cre should yield efficient axon labeling. Indeed, injections of AAV-Cre into the cortex of *Rosa-tdTomato* or *PTEN$^{f/f}$;Rosa-tdTomato* mice led to transduction of cortical cells as revealed by Tdtomato immunostaining as early as 7 d after injection (Fig. 1*A*) and, importantly, efficient labeling of the CST in the brain and spinal cord by 2 weeks (Fig. 1*B–F*). In *PTEN$^{f/f}$;Rosa-tdTomato* mice, immunohistochemistry performed at 7 and 14 d after AAV-Cre injection shows deletion of PTEN in tdTomato-expressing cells in the cortex (Figs. 2*A*,*B*).

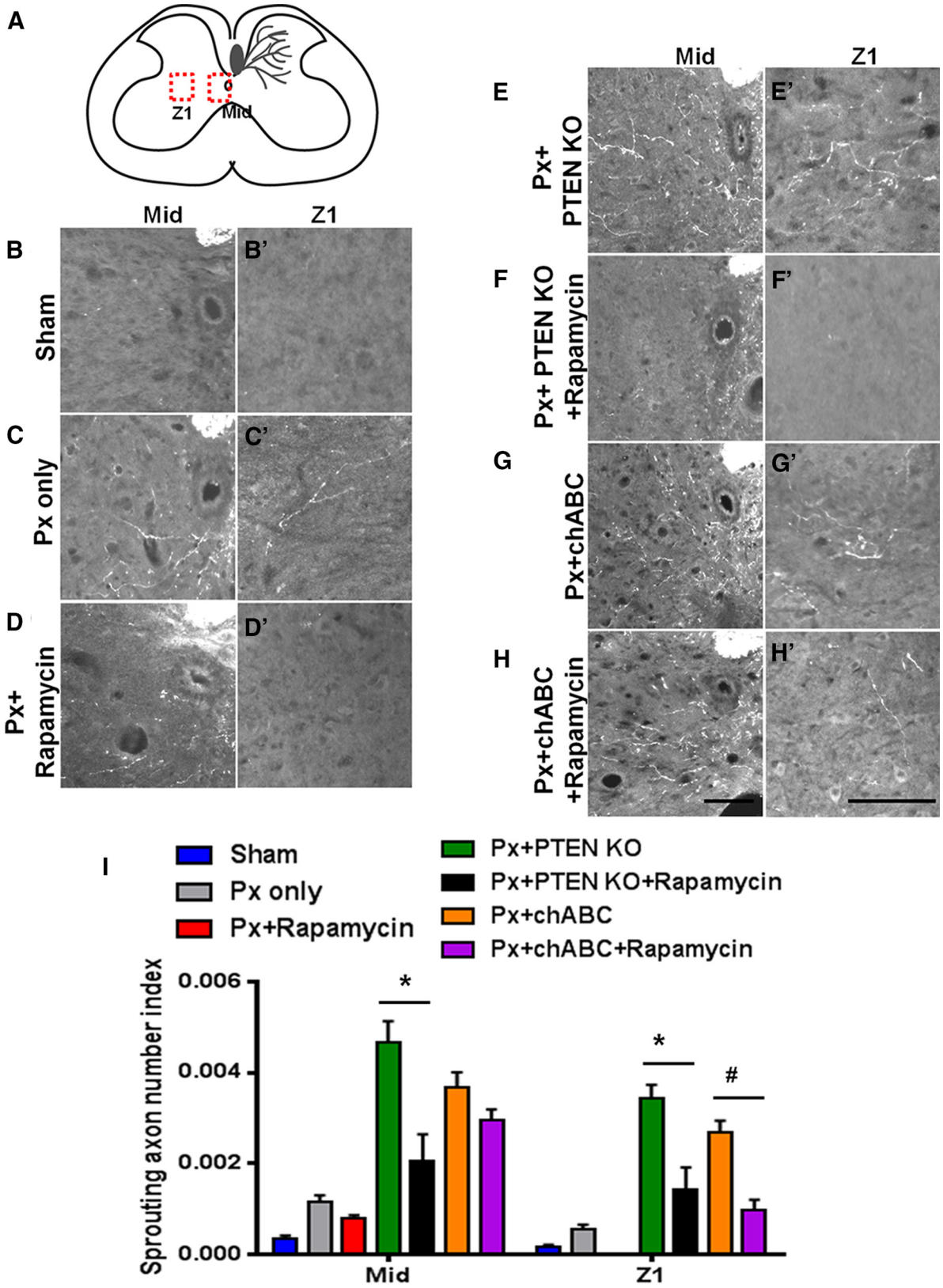

Figure 4. Axonal sprouting and mTOR dependency in young adult mice. ***A***, Schematic representation of spinal cord section showing two areas (Mid and Z1) where vertical lines were drawn, and crossing axons were counted. ***B***–***H***, Representative of C5 coronal sections, enlarged midline (***B***–***H***) or Z1 (***B′***–***H′***) regions from sham-operated *Rosa-tdTomato* (sham), pyramidotomized *Rosa-tdTomato* (Px only), pyramidotomized *PTEN*$^{f/f}$*Rosa-tdTomato* with vehicle (Px+PTEN KO), or with rapamycin (Px+PTEN KO+Rap), and pyramidotomized *Rosa-tdTomato-ChABC* mice with vehicle (Px+ChABC) or rapamycin (Px+ChABC+Rapamycin); $n = 8–13$/group. ***I***, Quantifications of crossing axons counted in different regions normalized against the numbers of labeled CST axons in sham-operated *Rosa-tdTomato* (sham), pyramidotomized *Rosa-tdTomato* (Px only), pyramidotomized *PTEN*$^{f/f}$*Rosa-tdTomato* with vehicle (Px+PTEN KO) or with rapamycin (Px+PTEN KO+Rap), and pyramidotomized *Rosa-tdTomato-ChABC* mice with vehicle (Px+ChABC) or rapamycin (Px+ChAB + Rapamycin); *$p < 0.001$; #$p < 0.05$, two-way repeat measures ANOVA followed by Bonferroni post-test. Error bars indicate SEM; $n = 8–13$/group. Scale bar, 100 μm.

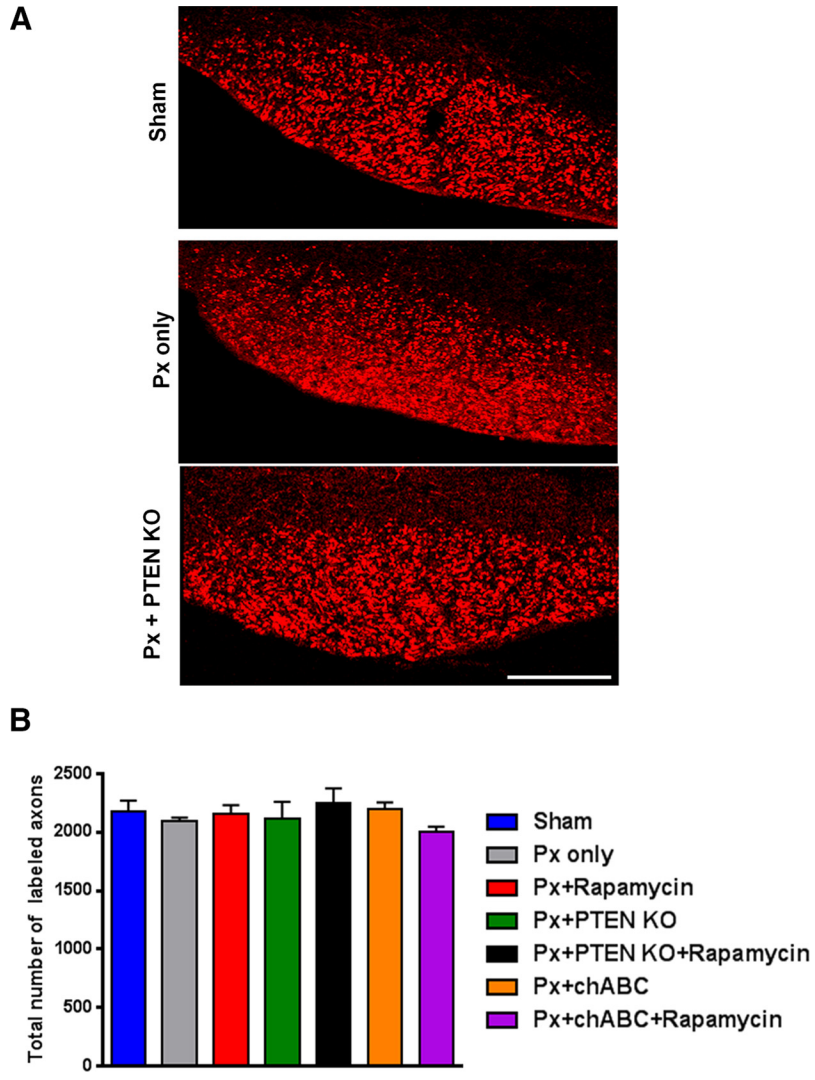

Figure 5. Degree of tdTomato labeling at the level of medulla in various animal groups. ***A***, Representative coronal sections of the medullary pyramid showing tdTomato labeled-CST axons 5 weeks after AAV-Cre injection (i.e., 4 weeks after pyramidotomy) in sham-operated *Rosa-tdTomato* (sham), pyramidotomized *Rosa-tdTomato* (Px only), and pyramidotomized *PTEN*$^{f/f;}$*Rosa-tdTomato* (Px + PTEN KO) mice. ***B***, Quantification of total tdTomato labeled-CST axons at the medullary pyramid in each animal groups. Error bars indicate SEM. Px, Pyramidotomy. Scale bars, 100 μm.

Axonal sprouting and mTOR-dependency in young adult mice

We set out to determine whether PTEN deletion in CST neurons of young adult mice (4–5 weeks of age) enhances compensatory sprouting, and if so, whether mTOR is required. *PTEN*$^{f/f}$*;Rosa-tdTomato*, or *Rosa-tdTomato* mice received AAV-Cre injection, followed by unilateral pyramidotomy 1 week later. Some of these animals also received rapamycin treatment to block mTOR activity. Rapamycin's efficacy in inhibiting mTOR in cortical neurons was validated by the decrease in p-S6 immunoreactivity, a commonly used marker of mTOR activity (Fig. 3*A*). The completeness of lesion was assessed by the degree of loss of PKCγ immunostaining in the lesioned CST tract (Lee et al., 2010b; Starkey et al., 2012). We find that the lesion results in drastic loss of PKCγ, confirming the severity of pyramidotomy (Fig. 3*B*). As assessed by immunofluorescent visualization of tdTomato labeled-axons 4 weeks after injury, PTEN deletion elicited significant increase in *trans*-midline sprouting of CST axons from the intact side into the denervated side compared with the wild-type injured mice (Figs. 4*A–I*). Thus, these results extend the previous study (Liu et al., 2010; in which PTEN was deleted in neonatal animals) to show that PTEN deletion in young adult mice is also sufficient to enhance axonal sprouting. Furthermore, we found that inhibition of mTOR in cortical neurons via rapamycin treatment significantly inhibited sprouting in PTEN KO mice; at two different distances (i.e., Mid and Z1) away from the central canal, sprouting was markedly reduced in mTOR-inhibited animals (Figs. 4*A–I*). The total numbers of tdTomato-labeled axons in the brainstem at the level of medullar oblongata were similar among the different animal groups (Figs. 5*A*,*B*), indicating that rapamycin treatment *per se* does not affect the degree of axonal labeling, and that differences in sprouting axon number was not due to differences in axon labeling efficiency. Overall, these data indicate that mTOR is critically involved in promoting axonal sprouting in PTEN KO animals.

We observed that pyramidotomy *per se* in young adult mice also increases sprouting compared with sham-operated animals (Figs. 4*A–I*), indicating that CST neurons at this age possess some degree of sprouting capacity Baseline mTOR activity is detected in the young adult CST neurons (Fig. 6*A*). Thus, we examined whether endogenous mTOR is required for the spontaneous sprouting. Indeed, mTOR inhibition reduced the spontaneous sprouting in the young adults; the extent of reduction was more drastic in the areas distant (i.e., Z1) to the midline (Figs. 4*A–I*).

Inactivation of CSPGs has been shown to enhance axonal regrowth after SCI (Cafferty et al., 2007; Tom et al., 2009; Lee et al., 2010a; Alilain et al., 2011; Zhao et al., 2011; Starkey et al., 2012; Takeuchi et al., 2013). We also examined whether mTOR is required for enhanced sprouting in CSPG-inactivated animals, without PTEN deletion. To this end, *Rosa-tdTomato* mice received AAV-Cre injection and intracerebroventricular delivery of ChABC, an enzyme that degrades the inhibitory glycosaminoglycan side-chains. To validate CSPG digestion, tissues were immunostained with anti-C-4-S antibody, which detects digested disaccharide "stubs" but not the intact chondroitin sulfate. ChABC led to intense C-4-S immunofluorescence in the cervical spinal cord of animals with unilateral lesion while no obvious signal was evident in animals with saline treatment (Fig. 3*C*), confirming CSPG degradation. Consistent with the previous report (Starkey et al., 2012), ChABC enhanced sprouting of intact CST axons after pyramidotomy compared with the animals receiving pyramidotomy and intracerebroventricular delivery of saline (Figs. 4*A–I*). Inhibition of mTOR led to a small reduction in the number of sprouting axons at the "Mid" area close to the midline in ChABC animals. A more drastic re-

duction was found at the "Z1" area distal to the midline (Figs. 4*A–I*).

mTOR is dispensable for compensatory sprouting of CST axons in postnatal mice

Consistent with the idea that mTOR correlates with neurons' capacity to regrow axons, mTOR activity is high in postnatal day (P)7 cortical neurons compared with young adult mice (Fig. 6*A*). A previous study has reported that a unilateral pyramidotomy given at P7 mice results in extensive spontaneous sprouting of CST axons (Liu et al., 2010). Next, we examined whether mTOR is also involved in this form of sprouting in postnatal animals. Similar to that seen in young adult mice, phospho-S6 immunoreactivity shows effective blockade of mTOR after rapamycin treatment in the layer V neurons (Fig. 6*B*). Importantly, the total numbers of labeled axons in the brainstem at the level of medullar oblongata were similar among the different animal groups (data not shown). Consistent with the previous report (Liu et al., 2010), we observed extensive axonal spouting 4 weeks after injury in animals receiving pyramidotomy at P7, (Figs. 7*A–E*). Interestingly, despite mTOR inhibition, the degree of sprouting was not affected compared with pyramidotomy-only animals. In fact, we observed more sprouting in rapamycin-treated animals, though this increase was not statistically significant (Figs. 7*A–E*). Together, these data indicate that mTOR is not required for extensive compensatory axonal sprouting in postnatal animals.

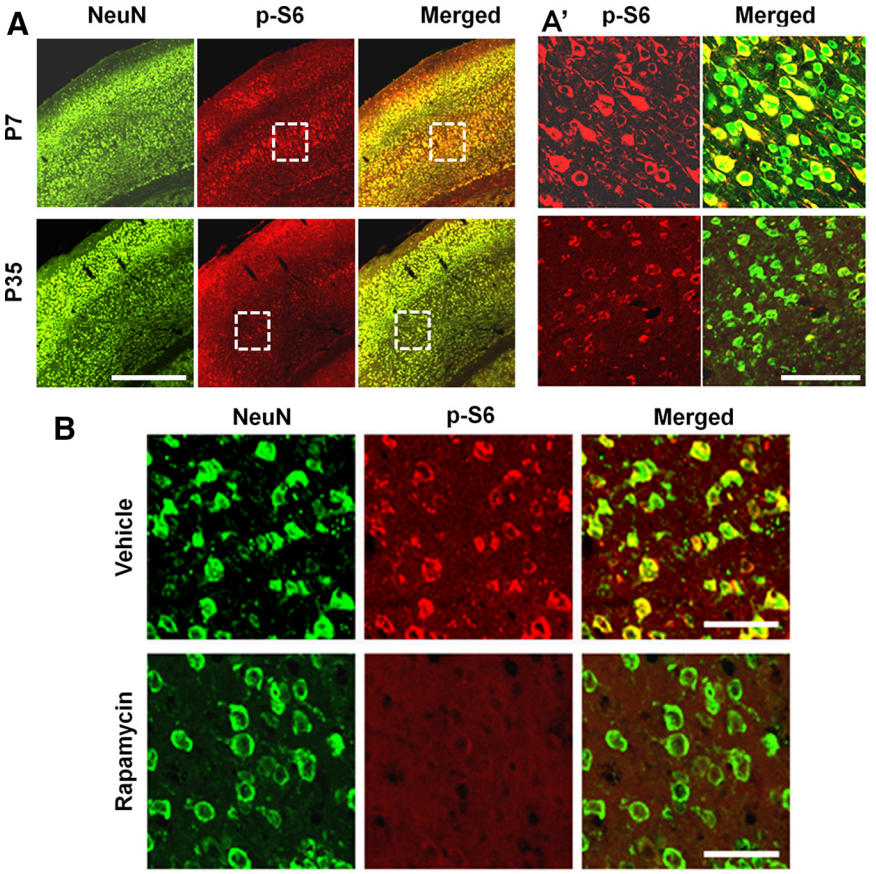

Figure 6. The level of cortical mTOR activity in postnatal, young adult mice and after postnatal rapamycin treatment. ***A***, Representative coronal sections of motor cortex from P7 and P35 mice stained with p-S6 and NeuN antibodies. ***A′***, Higher-magnification of the boxed areas in ***A***. ***B***, Coronal sections of motor cortex from mice subjected to P7 pyramidotomy stained with p-S6 and NeuN antibodies. Animals received either vehicle or rapamycin treatment and were perfused at 4 weeks after pyramidotomy. Scale bars: ***A***, 500 μm; ***A′***, 100 μm; ***B***, 50 μm.

Coinactivation of PTEN and CSPGs additively enhances axonal sprouting

Our results show that immature neurons spontaneously mount robust sprouting responses regardless of mTOR level. In adult animals however, robust sprouting likely require comodulating multiple neuron intrinsic pathways (i.e., PTEN/mTOR and others). Alternatively, comodulating PTEN/mTOR and environmental inhibitors may yield greater effects. To examine the effects of coinactivating PTEN and CSPGs, we generated *PTEN$^{f/f}$;Rosa-tdTomato* mice receiving both AAV-Cre and ChABC. This cotreatment (i.e., PTEN KO/ChABC) led to marked increases in the number of sprouting axons compared with either treatment alone; at 4 weeks after pyramidotomy, there was ~2-fold increase in the number of Tdtomato-labeled sprouting axons in the PTEN KO/ChABC group compared with either single treatment groups, indicating additive effects by targeting both PTEN and CSPGs (Figs. 8*A–E*). Furthermore, we observed that many of the tdTomato-labeled sprouting axons in the PTEN KO/ChABC animals that are in close contact with the motor neurons colocalize with presynaptic marker, Vglut1 (Figs. 8*F*, *G*), suggesting that newly formed collaterals in PTEN KO/ChABC animals are capable of forming synapses in the denervated spinal cord.

Discussion

Due to its function as a master sensor that integrates extracellular signal to regulate protein synthesis, enhanced regeneration seen after neuronal overactivation of mTOR has been attributed partly to enhanced protein translation and efficient provision of building materials required for new axons. While several studies have elicited the function of mTOR in promoting long distance regeneration of transected axons, whether mTOR is also involved in compensatory axonal rearrangement after injury remained unclear. Overall, we observed that young adult mice are more dependent on mTOR than postnatal animals. In postnatal stage, neurons may be capable of compensating for the loss of mTOR by triggering multiple signaling pathways relevant to axonal growth, and in promoting axonal sprouting. Both mTOR-dependent and -independent mechanisms of axon regeneration have been demonstrated in previous studies (Christie et al., 2010) where regeneration induced by cytokines relied on JAK/STAT3 but not on mTOR pathway (Sun et al., 2011). Therefore, mTOR, STAT3, and other signaling pathways relevant to axonal growth may be highly active in immature neurons, but not in the adult neurons (Lang et al., 2013) and facilitate sprouting. Of note, whereas short distance sprouting close to the midline is modestly reduced by mTOR inhibition, the lengthy sprouted axons normally seen in areas distant to the midline are eliminated in many animals, indicating that mTOR may play a partial role in initiating early growth responses but a more central role in sustained

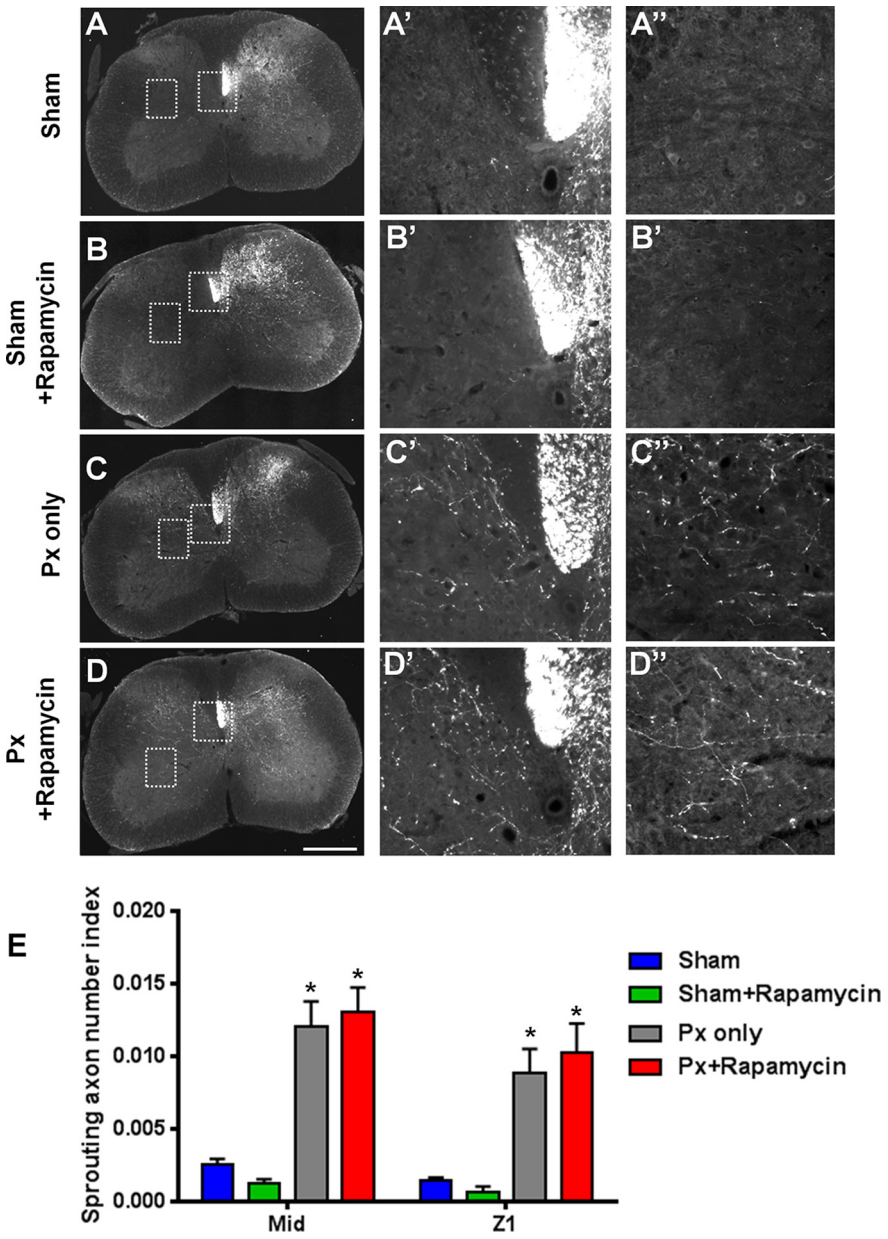

Figure 7. mTOR is dispensable for collateral axonal sprouting following CNS injury in postnatal mice. ***A–D***, Representative C5 coronal sections, enlarged midline (***A′–D′***) or Z1 (***A″–D″***) from sham and P7 pyramidotomy groups with vehicle or rapamycin treatment. BDA was injected into motor cortex 2 weeks before euthanasia. ***E***, Quantifications of crossing axons counted in different regions normalized against the numbers of labeled CST axons ($n = 7–9$/group). Asterisk indicates significantly different to the "sham" group; $p < 0.0001$, two-way repeated-measures ANOVA followed by Bonferroni post-test. Error bars indicate SEM. Px, Pyramidotomy. Scale bar, 500 μm.

axonal elongation. Such distinct requirements for mTOR in different stages of axonal growth (axonal initiation vs elongation) has been reported previously in retinal neurons (Leibinger et al., 2012). There is also the possibility that the uncrossed CST running in the ipsilateral white matter may contribute to the axonal sprouting in the Z1 area. Thus, an alternative explanation is that the effect of rapamycin on reducing sprouting in the Z1 region after pyramidotomy and ChABC treatment may be due to its effect on the uncrossed dorsolateral CST axons innervating this region.

We note that systemic rapamycin treatment would have had global effects and inhibit mTOR activity in cell types other than CST neurons including other CNS neurons, as well as glial cells and therefore, the impact on sprouting could be attributed to non-cell autonomous effects. Interestingly, systemic rapamycin treatment has shown previously to induce neuroprotection and improved functional recovery after contusive SCI (Kanno et al., 2012; Chen et al., 2013). Thus, mTOR may mediate different biological functions in different cell types to influence pathophysiology after SCI. In the context of axonal plasticity, we find that mTOR inhibition in young adults has an adverse impact on sprouting responses. Given that systemic administration of rapamycin could potentially exert cytotoxic effects (Law, 2005), there is a possibility that the reduction in axonal sprouting seen in young adult mice may be due to reduced cell viability and axonal transport of tdTomato. However, this is unlikely because we observed no obvious neuronal death in the motor cortex of rapamycin-treated animals. Furthermore, the total numbers of labeled axons in rapamycin-treated animals were similar to that of vehicle-treated animals, indicating that the rapamycin treatment does not diminish axonal labeling. Importantly, in postnatal animals, rapamycin treatment did not reduce the degree of axonal sprouting, further indicating that rapamycin's potential toxicity does not contribute to reduction seen in the young adult animals.

Studies in the past have used AAV vectors to label regrowing axons in place of dyes (Yip et al., 2010; Blackmore et al., 2012). In this present study, we took advantage of AAV-Cre-mediated recombination in Rosa26 reporter mice for labeling axons, thus obviating the need for subsequent labeling with anterograde dyes. Given that injections of dyes can only label a portion of CST neurons that are infected previously with AAV vectors, and the sensitive nature of Cre recombination, the use of reporter mice should allow more precise assessment of PTEN deletion effects than dye tracers. However, we observed that the tdTomato signal in axons made them appear much thinner compared with what we have typically observed using BDA, and the number of axons detected in at the level of cervical spinal cord to be generally lower than that reported in our previous study using BDA (Liu et al., 2010). This difference could be attributed to bona fide difference in the number of axons in the cervical spinal cord, but a more likely reason is a technical one where BDA signal was detected with a much more sensitive method (using tyramide signal amplification).

Previous studies targeting various molecules to promote axonal growth have demonstrated that a combinatorial approach with CSPGs has synergistic/additive effects (Steinmetz et al., 2005; Tom et al., 2009; Karimi-Abdolrezaee et al., 2010; Alilain et

al., 2011; García-Alías et al., 2011; Zhao and Fawcett, 2013; Zhao et al., 2013; Kanno et al., 2014). However, whether combined targeting of neuron intrinsic (PTEN) and extrinsic (CSPG) can have additive effects on supraspinal axonal growth has not been directly addressed. We observed significant enhancement in the degree of sprouting when both PTEN and CSPGs were inactivated simultaneously. This effect was close to the sum of the effects of each treatment alone, indicating an additive action of the two manipulations. Consistently, we previously observed that the onset of robust axonal regeneration in the injured mice optic nerve after PTEN deletion in adult retinal ganglion cells coincide with the onset of spontaneous decrease of CSPG level in the lesion, indicating the potent growth-inhibitory effect of CSPGs on the axons of PTEN deleted-neurons (Park et al., 2008).

Although our data indicate that mTOR is involved in promoting sprouting induced by PTEN deletion or CSPG digestion, the extent to which these mechanisms are shared between these two cases is not clear and mTOR likely represents one of many different intracellular factors that could regulate axonal sprouting. In our study, we show that axon sprouting after ChABC treatment is reduced by rapamycin. This was unexpected because rapamycin was supposed to target neuron intrinsic mechanisms, whereas ChABC was supposed to target extrinsic mechanisms. However, we do not believe that ChABC is directly triggering increased mTOR activity in neurons. Rather, it seems that certain neurons have a basal level of mTOR-dependent growth capacity that enables them to sprout in response to CNS injury. This sprouting is enhanced further once extracellular inhibitory factors, such as CSPG, are removed. However, in the absence of this basal level of growth capacity, such as after rapamycin treatment, neurons are no longer capable of sprouting and thus do not respond to the removal of inhibitory molecules in the extracellular environment.

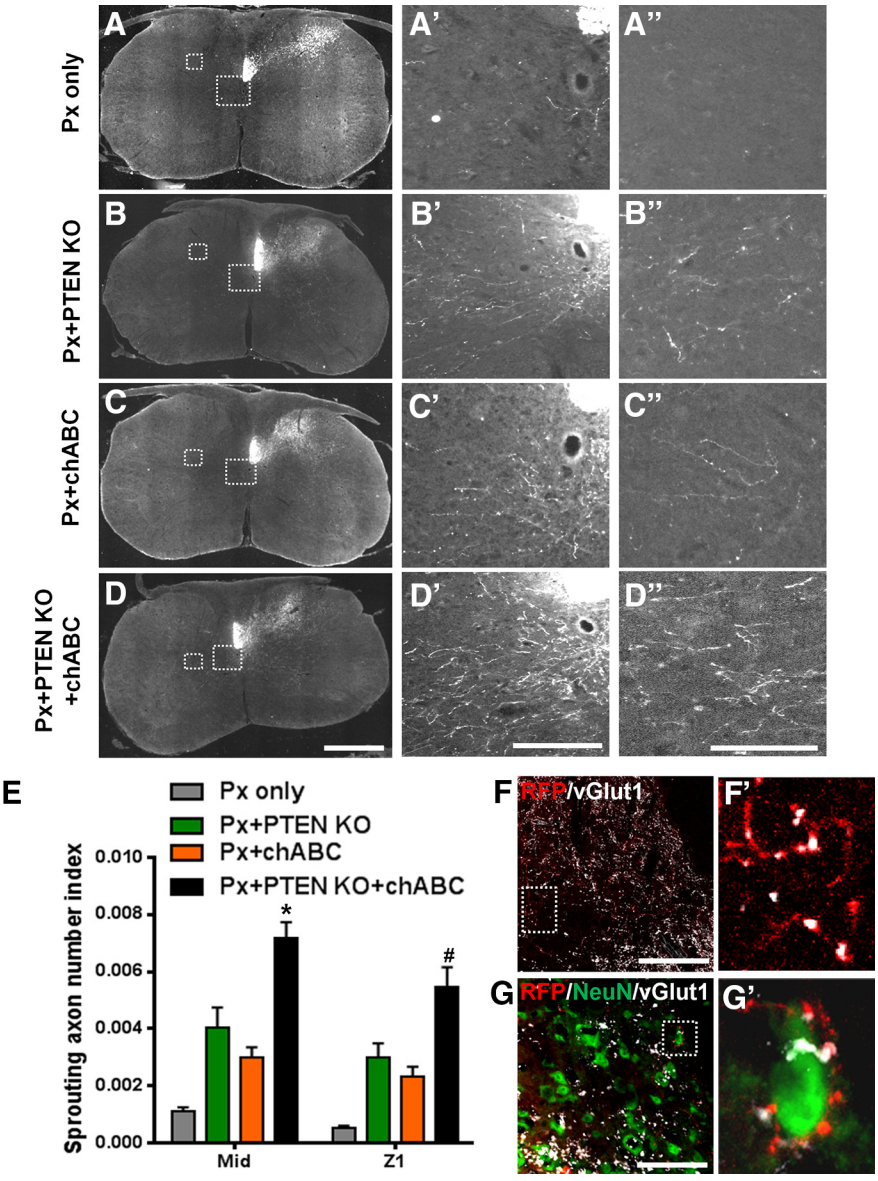

Figure 8. Combined modulation of PTEN/mTOR and CSPGs additively improves axonal sprouting. ***A–D***, Representative C5 spinal cord coronal sections from animals receiving pyramidotomy only (Px only) and pyramidotomized animals receiving PTEN deletion (Px+PTEN KO), ChABC treatment (Px+ChABC), and PTEN deletion/ChABC treatment (PTEN KO/ChABC). In "Px only" and "Px+ChABC" animal groups, AAV-Cre was injected into *Rosa-tdTomato* mice, whereas in "Px+PTEN KO" and "Px+PTEN KO/ChABC" groups, AAV-Cre was injected into *PTEN*$^{f/f}$*Rosa-tdTomato* mice. "Px only" and "Px+PTEN KO"groups received intracerebroventricular delivery of saline. ***E***, Quantifications of crossing axons counted in different regions normalized against the numbers of tdTomato-labeled CST axons ($n = 8–12$/group). ***F***, ***G***, Low-magnification coronal sections of the C5 spinal cord showing gray matter of a pyramidotomized PTEN KO/ChABC mouse at 4 weeks after injury, stained for CST axons (RFP, red), vGlut1(white), and neurons (NeuN, green). ***F'***, Enlargement of box in ***F*** showing Vglut1$^+$ RFP$^+$ (tdTomato$^+$) axons. ***G''***, Enlargement of box in ***G'*** showing Vglut1$^+$ RFP$^+$ terminals around a neuron. Asterisk indicates significantly different to "Px+PTEN KO" and "Px+ChABC" groups; $p < 0.0001$. #Indicates significantly different to "Px+PTEN KO" ($p < 0.01$) and "Px+ChABC" ($p < 0.0001$) groups; $n = 8–12$/group; two-way repeated-measures ANOVA followed by Bonferroni post-test. Error bars indicate SEM. Scale bars: ***A–D***, 500 μm; ***A'–D'***, ***A''–D''***, ***F***, ***G***, 100 μm.

Collectively, our findings specify distinct mTOR requirement in postnatal and young adult CNS neurons for inducing axonal sprouting. Although the mechanisms underlying this disparity await future elucidation, our findings raise the possibility that the mechanisms allowing extensive sprouting in postnatal CNS neurons are rather distinct and more versatile compared with their young adult counterparts. We also demonstrate, for the time, that coinactivation of PTEN and CSPGs further improves collateral sprouting of CNS axons, indicating that mature neurons receiving PTEN deletion possess confined ability to fully overcome environmental inhibition, and require simultaneous CSPG inactivation for a more robust effect. This requirement to target both neuron intrinsic and extrinsic mechanisms will be especially important in promoting functional recovery after more complex injuries, such as those to the spinal cord where there are multiple inhibitory barriers against axon regeneration.

References

Abe N, Borson SH, Gambello MJ, Wang F, Cavalli V (2010) Mammalian target of rapamycin (mTOR) activation increases axonal growth capacity of injured peripheral nerves. J Biol Chem 285:28034–28043. CrossRef Medline

Alilain WJ, Horn KP, Hu H, Dick TE, Silver J (2011) Functional regeneration of respiratory pathways after spinal cord injury. Nature 475:196–200. CrossRef Medline

Barritt AW, Davies M, Marchand F, Hartley R, Grist J, Yip P, McMahon SB, Bradbury EJ (2006) Chondroitinase ABC promotes sprouting of intact and injured spinal systems after spinal cord injury. J Neurosci 26:10856–10867. CrossRef Medline

Blackmore MG, Wang Z, Lerch JK, Motti D, Zhang YP, Shields CB, Lee JK, Goldberg JL, Lemmon VP, Bixby JL (2012) Kruppel-like Factor 7 engineered for transcriptional activation promotes axon regeneration in the adult corticospinal tract. Proc Natl Acad Sci U S A 109:7517–7522. CrossRef Medline

Bradbury EJ, Moon LD, Popat RJ, King VR, Bennett GS, Patel PN, Fawcett JW, McMahon SB (2002) Chondroitinase ABC promotes functional recovery after spinal cord injury. Nature 416:636–640. CrossRef Medline

Byrne AB, Walradt T, Gardner KE, Hubbert A, Reinke V, Hammarlund M (2014) Insulin/IGF1 signaling inhibits age-dependent axon regeneration. Neuron 81:561–573. CrossRef Medline

Cafferty WB, Yang SH, Duffy PJ, Li S, Strittmatter SM (2007) Functional axonal regeneration through astrocytic scar genetically modified to digest chondroitin sulfate proteoglycans. J Neurosci 27:2176–2185. CrossRef Medline

Chen HC, Fong TH, Hsu PW, Chiu WT (2013) Multifaceted effects of rapamycin on functional recovery after spinal cord injury in rats through autophagy promotion, anti-inflammation, and neuroprotection. J Surg Res 179:e203–210. CrossRef Medline

Christie KJ, Webber CA, Martinez JA, Singh B, Zochodne DW (2010) PTEN inhibition to facilitate intrinsic regenerative outgrowth of adult peripheral axons. J Neurosci 30:9306–9315. CrossRef Medline

Crespo D, Asher RA, Lin R, Rhodes KE, Fawcett JW (2007) How does chondroitinase promote functional recovery in the damaged CNS? Exp Neurol 206:159–171. CrossRef Medline

Davies SJ, Fitch MT, Memberg SP, Hall AK, Raisman G, Silver J (1997) Regeneration of adult axons in white matter tracts of the central nervous system. Nature 390:680–683. CrossRef Medline

Fouad K, Krajacic A, Tetzlaff W (2011) Spinal cord injury and plasticity: opportunities and challenges. Brain Res Bull 84:337–342. CrossRef Medline

García-Alías G, Petrosyan HA, Schnell L, Horner PJ, Bowers WJ, Mendell LM, Fawcett JW, Arvanian VL (2011) Chondroitinase ABC combined with neurotrophin NT-3 secretion and NR2D expression promotes axonal plasticity and functional recovery in rats with lateral hemisection of the spinal cord. J Neurosci 31:17788–17799. CrossRef Medline

Harris NG, Mironova YA, Hovda DA, Sutton RL (2010) Chondroitinase ABC enhances pericontusion axonal sprouting but does not confer robust improvements in behavioral recovery. J Neurotrauma 27:1971–1982. CrossRef Medline

Jefferson SC, Tester NJ, Howland DR (2011) Chondroitinase ABC promotes recovery of adaptive limb movements and enhances axonal growth caudal to a spinal hemisection. J Neurosci 31:5710–5720. CrossRef Medline

Kanno H, Ozawa H, Sekiguchi A, Yamaya S, Tateda S, Yahata K, Itoi E (2012) The role of mTOR signaling pathway in spinal cord injury. Cell Cycle 11:3175–3179. CrossRef Medline

Kanno H, Pressman Y, Moody A, Berg R, Muir EM, Rogers JH, Ozawa H, Itoi E, Pearse DD, Bunge MB (2014) Combination of engineered Schwann cell grafts to secrete neurotrophin and chondroitinase promotes axonal regeneration and locomotion after spinal cord injury. J Neurosci 34:1838–1855. CrossRef Medline

Karimi-Abdolrezaee S, Eftekharpour E, Wang J, Schut D, Fehlings MG (2010) Synergistic effects of transplanted adult neural stem/progenitor cells, chondroitinase, and growth factors promote functional repair and plasticity of the chronically injured spinal cord. J Neurosci 30:1657–1676. CrossRef Medline

Kwok JC, Afshari F, García-Alías G, Fawcett JW (2008) Proteoglycans in the central nervous system: plasticity, regeneration and their stimulation with chondroitinase ABC. Restor Neurol Neurosci 26:131–145. Medline

Lang C, Bradley PM, Jacobi A, Kerschensteiner M, Bareyre FM (2013) STAT3 promotes corticospinal remodelling and functional recovery after spinal cord injury. EMBO Rep 14:931–937. CrossRef Medline

Laplante M, Sabatini DM (2012) mTOR signaling in growth control and disease. Cell 149:274–293. CrossRef Medline

Law BK (2005) Rapamycin: an anti-cancer immunosuppressant? Crit Rev Oncol Hematol 56:47–60. CrossRef Medline

Lee H, McKeon RJ, Bellamkonda RV (2010a) Sustained delivery of thermostabilized chABC enhances axonal sprouting and functional recovery after spinal cord injury. Proc Natl Acad Sci U S A 107:3340–3345. CrossRef Medline

Lee JK, Geoffroy CG, Chan AF, Tolentino KE, Crawford MJ, Leal MA, Kang B, Zheng B (2010b) Assessing spinal axon regeneration and sprouting in Nogo-, MAG-, and OMgp-deficient mice. Neuron 66:663–670. CrossRef Medline

Leibinger M, Andreadaki A, Fischer D (2012) Role of mTOR in neuroprotection and axon regeneration after inflammatory stimulation. Neurobiol Dis 46:314–324. CrossRef Medline

Liu K, Lu Y, Lee JK, Samara R, Willenberg R, Sears-Kraxberger I, Tedeschi A, Park KK, Jin D, Cai B, Xu B, Connolly L, Steward O, Zheng B, He Z (2010) PTEN deletion enhances the regenerative ability of adult corticospinal neurons. Nat Neurosci 13:1075–1081. CrossRef Medline

Park KK, Liu K, Hu Y, Smith PD, Wang C, Cai B, Xu B, Connolly L, Kramvis I, Sahin M, He Z (2008) Promoting axon regeneration in the adult CNS by modulation of the PTEN/mTOR pathway. Science 322:963–966. CrossRef Medline

Schwab ME (2002) Increasing plasticity and functional recovery of the lesioned spinal cord. Prog Brain Res 137:351–359. CrossRef Medline

Starkey ML, Barritt AW, Yip PK, Davies M, Hamers FP, McMahon SB, Bradbury EJ (2005) Assessing behavioural function following a pyramidotomy lesion of the corticospinal tract in adult mice. Exp Neurol 195:524–539. CrossRef Medline

Starkey ML, Bartus K, Barritt AW, Bradbury EJ (2012) Chondroitinase ABC promotes compensatory sprouting of the intact corticospinal tract and recovery of forelimb function following unilateral pyramidotomy in adult mice. Eur J Neurosci 36:3665–3678. CrossRef Medline

Steinmetz MP, Horn KP, Tom VJ, Miller JH, Busch SA, Nair D, Silver DJ, Silver J (2005) Chronic enhancement of the intrinsic growth capacity of sensory neurons combined with the degradation of inhibitory proteoglycans allows functional regeneration of sensory axons through the dorsal root entry zone in the mammalian spinal cord. J Neurosci 25:8066–8076. CrossRef Medline

Sun F, Park KK, Belin S, Wang D, Lu T, Chen G, Zhang K, Yeung C, Feng G, Yankner BA, He Z (2011) Sustained axon regeneration induced by co-deletion of PTEN and SOCS3. Nature 480:372–375. CrossRef Medline

Takeuchi K, Yoshioka N, Higa Onaga S, Watanabe Y, Miyata S, Wada Y, Kudo C, Okada M, Ohko K, Oda K, Sato T, Yokoyama M, Matsushita N, Nakamura M, Okano H, Sakimura K, Kawano H, Kitagawa H, Igarashi M (2013) Chondroitin sulphate *N*-acetylgalactosaminyl-transferase-1 inhibits recovery from neural injury. Nat Commun 4:2740. CrossRef Medline

Tom VJ, Sandrow-Feinberg HR, Miller K, Santi L, Connors T, Lemay MA, Houlé JD (2009) Combining peripheral nerve grafts and chondroitinase promotes functional axonal regeneration in the chronically injured spinal cord. J Neurosci 29:14881–14890. CrossRef Medline

Weidner N, Tuszynski MH (2002) Spontaneous plasticity in the injured spinal cord-implications for repair strategies. Mol Psychiatry 7:9–11. CrossRef Medline

Yip PK, Wong LF, Sears TA, Yáñez-Muñoz RJ, McMahon SB (2010) Cortical overexpression of neuronal calcium sensor-1 induces functional plasticity in spinal cord following unilateral pyramidal tract injury in rat. PLoS Biol 8:e1000399. CrossRef Medline

Zhao RR, Fawcett JW (2013) Combination treatment with chondroitinase ABC in spinal cord injury: breaking the barrier. Neurosci Bull 29:477–483. CrossRef Medline

Zhao RR, Muir EM, Alves JN, Rickman H, Allan AY, Kwok JC, Roet KC, Verhaagen J, Schneider BL, Bensadoun JC, Ahmed SG, Yáñez-Muñoz RJ, Keynes RJ, Fawcett JW, Rogers JH (2011) Lentiviral vectors express chondroitinase ABC in cortical projections and promote sprouting of injured corticospinal axons. J Neurosci Methods 201:228–238. CrossRef Medline

Zhao RR, Andrews MR, Wang D, Warren P, Gullo M, Schnell L, Schwab ME, Fawcett JW (2013) Combination treatment with anti-Nogo-A and chondroitinase ABC is more effective than single treatments at enhancing functional recovery after spinal cord injury. Eur J Neurosci 38:2946–2961. CrossRef Medline

Viral vector based improvement of optic nerve regeneration: characterization of individual axons' growth patterns and synaptogenesis in a visual target

B J Yungher, X Luo, Y Salgueiro, M G Blackmore, K K Park

Cite this article as: B J Yungher, X Luo, Y Salgueiro, M G Blackmore, K K Park, Viral vector based improvement of optic nerve regeneration: characterization of individual axons' growth patterns and synaptogenesis in a visual target, *Gene Therapy* accepted article preview 25 May 2015; doi: 10.1038/gt.2015.51.

Received 5 February 2015; revised 10 April 2015; accepted 5 May 2015; Accepted article preview online 25 May 2015

Title: Viral Vector Based Improvement of Optic Nerve Regeneration: Characterization of Individual Axons' Growth Patterns and Synaptogenesis in a Visual Target

Authors: Benjamin J. Yungher, Xueting Luo, Yadira Salgueiro, Murray G. Blackmore, Kevin K. Park

Benjamin J. Yungher, B.A, Miami Project to Cure Paralysis and Department of Neurosurgery, University of Miami Miller School of Medicine
Mailing address: Miami Project to Cure Paralysis, 1094 NW 14th Ter. RM 3-01, Miami, FL, 33136. Phone: (1) 305 243 2599, Fax: (1) 305 243 3921, Email address: byunger@med.miami.edu

Xueting Luo, Ph.D., Miami Project to Cure Paralysis and Department of Neurosurgery, University of Miami Miller School of Medicine
Mailing address: Miami Project to Cure Paralysis, 1094 NW 14th Ter. RM 3-01, Miami, FL, 33136. Phone: (1) 305 243 2599, Fax: (1) 305 243 3921, Email address: xluo@med.miami.edu

Yadira Salgueiro, Miami Project to Cure Paralysis and Department of Neurosurgery, University of Miami Miller School of Medicine
Mailing address: Miami Project to Cure Paralysis, 1094 NW 14th Ter. RM 3-01, Miami, FL, 33136. Phone: (1) 305 243 2599, Fax: (1) 305 243 3921, Email address: ysalgueiro@med.miami.edu

Murray G. Blackmore, Ph.D., Department of Biomedical Sciences, Marquette University

Mailing address: Department of Biomedical Sciences, College of Health Sciences, Schroeder Complex, 429, Milwaukee, WI 53201-1881. Phone: 1 (414) 288-4532 Email address: murray.blackmore@marquette.edu

Kevin K. Park, Ph.D., Miami Project to Cure Paralysis and Department of Neurosurgery, University of Miami Miller School of Medicine

Mailing address: Miami Project to Cure Paralysis, 1094 NW 14th Ter. RM 4-20, Miami, FL, 33136. Phone: (1) 305 243 2493, Fax: (1) 305 243 3921, Email address: kpark@med.miami.edu

Correspondence should be addressed to Kevin K. Park

Miami Project to Cure Paralysis, University of Miami, Miller School of Medicine, Miami, FL, 33136, USA. Phone: (1) 305 243 2493, Email Address: kpark@med.miami.edu

Running title: Viral based optic nerve regrowth

Key words: Axon regeneration, Retinal ganglion cell, PTEN, Axon injury, Axon guidance

Authors declare no conflict of interest

ABSTRACT

Lack of axon growth ability in the central nervous system poses a major barrier to achieving functional connectivity after injury. Thus, a non-transgenic regenerative approach to reinnervating targets has important implications in clinical and research settings. Previous studies using knockout (KO) mice have demonstrated long distance axon regeneration. Using an optic nerve injury model, here we evaluate the efficacy of viral, RNAi and pharmacological approaches that target the PTEN and STAT3 pathways to improve long distance axon regeneration in wild type (WT) mice. Our data show that adeno-associated virus (AAV) expressing short hairpin RNA (shRNA) against PTEN (shPTEN) enhances retinal ganglion cell axon regeneration after crush injury. However, compared to the previous data in PTEN KO mice, AAV-shRNA results in a lesser degree of regeneration, likely due to incomplete gene silencing inherent to RNAi. In comparison, an extensive enhancement in regeneration is seen when AAV-shPTEN is coupled to AAV encoding ciliary neurotrophic factor (CNTF) and to a cyclic adenosine monophosphate (cAMP) analogue, allowing axons to travel long distances and reach their target. We apply whole tissue imaging that facilitates three-dimensional visualization of single regenerating axons and document heterogeneous terminal patterns in the targets. This shows that some axonal populations generate extensive arbors and make synapses with the target neurons. Collectively, we show a combinatorial viral RNAi and pharmacological strategy that improves long distance regeneration in WT animals and provide single fiber projection data that indicates a degree of preservation of target recognition.

Introduction

Following injury, axons in the adult central nervous system (CNS) generally fail to regenerate long distances and reinnervate their target. Using optic nerve injury and conditional knockout (KO) mice, we and others have previously demonstrated that deleting phosphatase and tensin homologue (PTEN) and suppressor of cytokine signaling 3 (SOCS3) in adult retinal ganglion cells (RGC) allows long distance optic nerve regeneration and target reinnervation to some degree [1-3]. Moreover, it was reported that PTEN KO combined with zymosan and cAMP analogue induces long distance regeneration and partial recovery of visual functions [4], providing a framework for developing reparative therapy. However, whether non-transgenic approaches that modulate PTEN alone or with other growth regulating factors can promote a similar level of RGC axon regeneration in wild type animals has not been directly addressed. Adeno-associated virus (AAV) lacks significant pathogenicity and has been used safely in clinical trials for a number of ocular and non-ocular diseases [5]. Therefore, the first aim of this present study was to evaluate whether AAV vectors that incorporate RNA interference (RNAi) can suppress endogenous PTEN in adult RGCs and promote RGC axon regeneration in the adult mouse. Next, we examined whether combined viral RNAi and pharmacotherapy approaches that modulate PTEN and other growth promoters will further improve long distance regeneration of axons to their brain targets.

On arriving at the final targets, the growth cones of long projecting axons switch from an extension program to one that facilitates target recognition and reconnection. One key feature during this process is the formation of axon arbors that facilitates connection with their proper

target neurons. To visualize single axon and their entire arbors and to unequivocally assess axon terminals, several studies in model organisms including zebrafish have used single cell labeling and whole tissue imaging [6, 7]. However, such techniques have not yet been established for the study of axon targeting in mammals. In our previous studies, we have described the use of optical clearance and whole tissue imaging to assess RGC axon regeneration *in vivo*. In this present study, we expand the application of these imaging techniques, establish single axon visualization and determine terminal morphology of regenerating axons within a visual target in mice.

RESULTS

Evaluation of AAV2-shRNA mediated PTEN knockdown and RGC axon regeneration

Here we sought to examine the degree of RGC axon regeneration after AAV-shRNA mediated PTEN knockdown. To this end, we first tested a shRNA strategy, based on SIBR vector system [8]. In a SIBR vector, shRNA is located in an intron and flanked by sequences derived from mir155, an endogenous intronic shRNA. This design allows a single primary transcript to produce shRNA from intronic sequences, as well as an intact exon that encodes an enhanced green fluorescent protein (EGFP) reporter (Figure 1a). Furthermore, this design allows insertion of four separate shRNA sequences, concatenated in a single plasmid, each targeting a different region of PTEN (referred hereafter as "shPTEN4"), thereby increasing the probability of effectively silencing the gene of interest. Alternatively, we used a previously tested PTEN targeting sequence [9, 10] shown to be highly specific to PTEN (referred hereafter as shPTEN1)[10]. Since AAV serotype 2 has been shown to effectively transduce postmitotic neurons including the

RGCs [11], these plasmids were then used to produce adeno-associated virus serotype 2 (AAV-shPTEN4 or shPTEN1). To evaluate the knockdown efficiency of PTEN, we initially incubated rat cortical neurons with either AAV-anti-luciferase-EGFP (AAV-EGFP) or AAV-shPTEN4. Seven days after treatment AAV-shPTEN4 markedly suppresses the endogenous expression of PTEN as shown by immunocytochemistry (Figure 1b; n=2 biological replicates). To evaluate the gene knockdown efficiency in mouse RGCs, we injected AAV-shPTEN4 into the vitreous body of young adult C57BL/6 mouse eyes. In cross-section immunohistochemistry performed two weeks after injection, transduced RGCs show a significant reduction of PTEN expression compared to control RGCs transduced with AAV-EGFP (Figure 1c). Flat-mounted retinae show over 90% transduction of RGCs by the AAV vector (Figure 1d; n=4). Quantification using western blot in cortical neurons (Figure 1e, f), and PTEN intensity analysis in retina sections (Figure 1g), we observe about 70% reduction in PTEN level after AAV-shPTEN4. Consistent with the previous study [9, 10], AAV-shPTEN containing a single targeting sequence (AAV-shPTEN1) led to approximately 70% reduction in PTEN expression in adult RGCs (data not shown). As an initial test to examine the effect of PTEN knockdown on RGC axon regeneration, we injected AAV-shPTEN4, AAV-shPTEN1 or AAV-EGFP two weeks before an optic nerve crush. Anterograde labeling of regenerating axons by CTB injection occurred two days prior to sacrifice. As expected, we observed significant increases in the number of axons growing beyond the lesion site in mice receiving either AAV-shPTEN4 (6-fold increase) or AAV-shPTEN1 (4-fold increase) compared to AAV-EGFP treatment at 0.2 mm from the lesion 4 weeks after injury (Figure 2a, b; n=5/group). We noticed however that the degree of regeneration in the AAV-shPTEN animals is less extensive than that of the PTEN KO mice (i.e. $PTEN^{f/f}$ mice subjected to AAV-Cre injection) [1]. At 4 mm distal to the lesion (i.e. near the chiasm), we did not observe

regenerating axons in the AAV-shPTEN animals. On the other hand, more than 20 axons per one optic nerve section were seen at this distance in the PTEN KO animals treated with AAV-Cre [1]. Since we have previously shown that the level of axotomy-induced cell death is reduced by PTEN deletion in RGCs [1], we also assessed whether AAV-mediated PTEN knockdown will similarly enhance RGC survival. By using an antibody against βIII tubulin (TUJ1) to immunostain viable RGCs, we observed that AAV-shPTEN4 treatment results in a 2-fold increase in RGC survival rates compared to control mice (Figure 2c, d). Unlike the difference seen in regeneration rate, this increase in survival is similar to that seen in the PTEN KO mice [1]. Overall, these data demonstrate that PTEN knockdown, albeit at a lower level than the PTEN KO mice, increases RGC axon regeneration in adult mice.

Assessment of combinatorial AAV and RNAi strategy to enhance long distance axon regeneration

PTEN is one of many factors known to regulate RGC axon regeneration. Other strategies that were shown to facilitate long distance RGC axon regeneration include deletion of SOCS3 or Klf4, and elevation of CNTF [2, 12-18]. Given the synergistic effects induced by combining PTEN KO mice with modulation of the CNTF/STAT3 pathway, we sought to test combining RNAi and AAV approach to target these factors and further improve regeneration. First, we generated AAV expressing shRNA against SOCS3 using the SIBR vector system, but this failed to drastically knockdown SOCS3 expression (data not shown). Given that elevation of CNTF using AAV vector allows significant increase in long distance regeneration in the injured optic nerve [12-15, 19], we then tested combining AAV-CNTF with AAV-shPTEN. To mimic clinical situations, all animals in subsequent experiments received intravitreal injection immediately after an optic

nerve crush. Consistent with the previous studies, we observed that animals receiving the AAV expressing a secretable form of CNTF alone show significant increase in regeneration (Figure 3a, b). Double combination of AAV-shPTEN with AAV-CNTF did not result in a significant increase compared to AAV-CNTF alone (Figure 3a, b). Next we tested the effect of biweekly application of cell permeant cAMP analogue, cpt-cAMP in improving axon regeneration in the background of AAV-shPTEN and AAV-CNTF. Previous studies have shown that cpt-cAMP can facilitate CNS axon regeneration by recruiting multiple mechanisms including down-regulation of SOCS3 as well as activating mitogen activated protein kinase (MAPK) and protein kinase A (PKA) pathways [17, 20]. Indeed, this three-way combination of AAV-shPTEN4, AAV-CNTF and cpt-cAMP (hereafter referred as "PCC" treatment) led to a marked increase in the number of regenerating axons; there is more than 3-fold increase in the number of axons regenerating up to 2 mm distal to the lesion compared to AAV-CNTF alone (Figure 3a, b; n=6-8/group). Of note, double combination of shPTEN and cpt-cAMP does not result in an obvious increase in axon regeneration compared to shPTEN treatment alone (Figure 3b). We also assessed RGC survival rates in the combinatorial paradigm using TUJ1 immunostaining, and observed that mice receiving PCC treatment have similar RGC survival (i.e. over 20% survival compared to the contralateral uninjured retina) compared to AAV-shPTEN4 and AAV-CNTF/cpt-cAMP-treated groups in this post-injury treatment paradigm (Figure 3c, d). Overall, these results show that concomitant modulation of PTEN, CNTF and cAMP using a combination of viral, RNAi and pharmacotherapy approaches greatly enhances long distance axon regeneration.

Assessment of RGC axon regeneration in PCC-treated mouse brains

Next we examined the extent to which the regenerate RGC axons in PCC-treated animals extend beyond the optic chiasm and reach their visual targets. To this end, we used tissue clearing and LSFM to image regenerating axons in whole mouse optic nerves and brains without the data loss that results from tissue sectioning [21, 22]. This protocol uses THF and BABB to turn optic nerves and brains relatively transparent (Figure. 4a), allowing visualization of the entire optic projection in whole tissues (Figure 4b). Animals received crush injury followed immediately by PCC treatment or AAV-EGFP injection. By 4 to 6 weeks post-injury, regenerating axons reach the optic chiasm. About 20% of these axons extend into the opposite, uninjured optic nerve (Figure. 4c-e). Similar or higher numbers of regenerating axons are found in the ipsilateral compared to the contralateral optic tract (Figure 4c-e) en route to more distal visual targets. Similar to the previous studies [14, 22, 23], at 10-14 weeks post-injury (n=13), path-finding errors are evident in the brain as most axons extend dorsally, parallel to the third ventricle and do not find the distant brain targets (i.e. superior colliculus (SC) and lateral geniculate nucleus(LGN)) (data not shown).

Characterizing individual axons' morphologies in a visual target

Importantly, regenerating axons are found in and around RGCs' first brain target the suprachiasmatic nucleus (SCN), located directly above the optic chiasm (Figure 5a). In control animals treated with AAV-EGFP (n=14), we do not detect any CTB-labeled axons in the brain (Figure 5b). The growing tips of elongating axons sense their post-synaptic partners within the target to begin to form arbors and to establish synaptic connection. Do the adult RGC axons regenerating long distances through the optic nerve have the ability to sense their target and arborize? Traditionally, morphological analysis of axon terminals and arborization is carried out in histological sections. However, tissue sections provide limited spatial information, making it

difficult to determine unequivocally whether the axon terminals are in fact located within a correct region. It is also difficult to ascertain the extent of arborization, a key step toward establishing a proper target reconnection. Here, we sought to expand the application of whole tissue imaging techniques and to evaluate qualitatively the growth behavior as axons reach a correct visual target, the SCN. To this end, we scanned individual 2D LSFM images of mouse brains to visualize CTB-labeled axons. We took advantage of the fact that the number of axons that reach the SCN is small (ranging between 5 and 40 axons per animal), allowing us to visualize, trace, and sample single axons and their entire arbors. The vast majority of PCC treated animals (11 out of 13 mice) had regenerating axons in the SCN. Figure 5 shows examples of two different animals with regenerating RGC axons reaching the SCN (Figure 5c, d). We were able to trace all visibly distinct axons in 2D optical slices and then compile these slices into a 3D reconstruction (Figure 5e-j). In total, we traced 18 axons that reach the SCN. Overall, we observe at least four different re-growth patterns in and around the SCN. First, some axons approach the SCN but turn and bypass the region. Figure 5e shows an example of such behavior where an axon bifurcates outside the SCN and its branches extend and wrap around the SCN, suggesting that these axons may be repelled and actively prevented from entering this nucleus. Second, some axons enter the SCN, but they traverse and their terminals are found outside the region (Figure 5f). In this category, axons often branch within the SCN but the arbors exit and continue to extend outside the SCN (Figure 5g). Thus, these axons appear to lack signals that facilitate target recognition. Third, terminals of some axons are found inside the SCN (Figure 5h). Fourth, there are axons that generate complex arbors within the target (Figure 5i, j). Figure 5i shows tracing of such fiber entering the SCN and generating complex arbors. Immediately after entering the contralateral SCN, this axon bifurcates and its branches subsequently generate

multiple arbors. The branches stemming from this individual axon extend and cover a large field area within the SCN, suggesting the possibility that they may have made synapses with multiple SCN neurons.

Synaptogenesis

To find evidence of re-synaptogenesis by regenerated axons, we performed immunohistochemistry using an antibody against vesicular glutamate transporter 2 (Vglut2), a major presynaptic protein of RGCs. We observe that some CTB-labeled axons in the SCN (the anatomical location depicted in Figure 6a) have Vglut2-positive patches at bouton-like structures and along the axonal length (Figure 6b), suggesting an accumulation of the molecular machinery characteristic of a presynaptic terminal. To further confirm the ability of regenerating axons to make reconnection with the target neurons, we used the trans-synaptic reporter mouse line, iZ/WAP [24]. These transgenic mice express a Cre recombinase-inducible WGA under the direction of the CMV, cytomegalovirus, promoter and serves as a reporter strain, with successful Cre excision being indicated by WGA expression in Cre-expressing neurons. WGA acts as a trans-synaptic tracer, allowing identification of the synaptic contacts of Cre-expressing neurons [24]. In normal animals, between 40-80% of RGCs expressed WGA at 2 weeks following intravitreal AAV2-Cre injection as shown by immunohistochemistry (Figure 6c). In accordance, many WGA^+ cells (i.e. cells that are post-synaptically connected with RGCs) are visible in the SCN of uninjured animals (Figure 6d). Similarly, WGA^+ cells are present in the LGN in uninjured animals (Figure 6e). In contrast, no WGA^+ cells are detected in injured animals receiving control AAV2-EGFP injection (n=5; Figure 6f). In some PCC animals (3 out of 10 animals), we observe WGA^+ cells in the SCN in close proximity to CTB^+ axons, indicating that

these regenerate RGCs reform synapses with the target (Figure 6g, h). Overall, these data suggest that following the combinatorial treatment, individual regenerating axons possess varying capacity to recognize the target, and are able to form synapses and reconnect with the target neurons.

DISCUSSION

Previous studies have demonstrated that RGCs induced to regenerate in PTEN KO mice travel the entire length of the optic nerve [1] or, in combination with other factors, reach the targets [3, 25] and induce partial recovery of visual functions [4]. While these KO mouse studies have revealed some key molecular mechanisms underlying axon regeneration, it remained to be seen whether a non-transgenic approach that targets PTEN alone or in combination can also promote a similar degree of optic nerve regeneration and target re-innervation. Since axonal damage in the optic nerve causes irreversible loss of visual functions in glaucoma and after trauma, therapeutically relevant strategies that promote regeneration through the optic nerve and reconnection have important clinical implications. More broadly, therapeutic strategies designed to improve RGC axon regeneration may provide ideas to treat injuries in other long CNS tracts including the spinal cord.

Previous studies have reported successful uses of non-transgenic PTEN blockers to promote axon regeneration after nerve injury. Following a spinal cord injury, PTEN antagonist peptide or AAV-shPTEN were shown to improve axon regeneration in the spinal cord [9, 26, 27]. Others have

demonstrated that PTEN inhibitor bisperoxovanadium enhances regeneration of sensory axons [28]. However, it has not been established whether AAV-shRNA that suppresses PTEN would induce regeneration in RGC axons. More importantly, whether combining RNAi knockdown of PTEN with other non-transgenic strategies known to increase neuron's growth ability could further enhance long distance axon regeneration has not been directly addressed.

Here we compare rates of RGC axon regeneration following PTEN knockdown using two AAV vectors each carrying different PTEN target sequences. Despite protein knockdown efficacy as high as 70-90%, the effect on axon regeneration is far less robust than that seen after PTEN deletion in transgenic mice. This difference could be attributed to potential off-target effects associated with RNAi (i.e. silencing of pro-regenerative genes); however, this is unlikely since the two AAV-shPTEN vectors target different sequences within PTEN. Furthermore, the shPTEN1 used in this study was previously shown to cause no detectable off-target effects when the closest potential off-target genes were examined [10]. Thus it is more likely that the weaker regeneration seen with RNAi is due to incomplete PTEN silencing, a common limitation in the use of shRNA technology [29]. In many instances, a low level of residual expression may still be sufficient for gene function. For example, conditional PTEN heterozygote mice typically display less severe phenotypes than null-homozygotes [30]. In accordance, we observe no obvious increase in axon regeneration after heterozygous PTEN ablation (i.e. $PTEN^{f/+}$ mice subjected to intravitreal AAV-Cre injection) (data not shown).

Virally expressed CNTF represents a potent way to induce long distance RGC axon regeneration. Consistent with the previous studies [12-15, 19], AAV-CNTF alone results in a significant induction of long distance regeneration, and cAMP analogue did not significantly enhance axon regeneration in the background of AAV-CNTF [20, 31] . However, combined treatment of cAMP analogue, AAV-shPTEN, and AAV-CNTF greatly enhanced regeneration and allowed more axons to reach the brain. Interestingly, similar enhancement in regeneration has been reported when PTEN depletion and cAMP analogue are combined with zymosan [25]. Mechanistically, previous studies have demonstrated that axon regeneration induced by PTEN depletion relies on downstream activation of Akt/mammalian target of rapamycin (mTOR). On the other hand, axon regeneration induced by SOCS3 deletion or CNTF elevation is dependent on activation of the signal transducer and activator of transcription-3 (STAT3) pathway [1-3]. Multiple signaling pathways and molecules have been suggested to mediate the pro-regenerative effect of cAMP, including activation of MAPK, PKA and cAMP response element-binding protein (CREB) [17, 20, 32]. It has also been shown that cAMP can reduce CNTF-induced SOCS3 expression, diminishing the effect of this negative feedback system [33]. Thus, it is likely that PCC treatment activates multiple pathways and mounts complementary growth programs that ultimately lead to more robust regeneration. However, the intricate mechanisms underlying the crosstalk between these molecules are unknown and await future elucidation.

While mammalian RGCs can be induced to regenerate along the optic nerve, axons fail to correctly pathfind to their distant targets, the LGN and SC. These observations are consistent with the notion that axons do not simply re-use degenerating optic tracts [34]. Nonetheless, some

regenerating axons successfully reach a target that is located much closer to the eye, the SCN. Using whole tissue imaging, we provide single fiber projection data that unequivocally reveal the behaviors of regenerating RGC axons as they reach this target. During development, growing RGC axons navigate towards their targets where they arborize and form synapses [7, 35, 36]. The transition from axon extension to target recognition and axon branch initiation is regulated by spatiotemporal expression of receptors and respective ligands in the axons and target regions. In particular, local expression of growth factors such as brain derived neurotrophic factor (BDNF) and fibroblast growth factor 2 (FGF2) have been shown to play critical roles in modulating axon arborization and synaptic formation in the visual targets [6, 36, 37]. Do adult mammalian brains express relevant target cues, and do the regenerate RGC axons retain the capacity to recognize correct targets? These questions have been addressed extensively using peripheral nerve graft experiments, in which transected RGC axons are permitted to regenerate through a segment of peripheral nerve and reinnervate their targets [38-44]. These studies have indicated the presence of considerable axon arborization and synaptic connection in the SC and concluded that both optic axons and target neurons in adult mammals retain recognition ability.

In this study, use of single fiber tracing decisively shows extensive axon arborization, thereby providing morphological evidence of some axons' ability to recognize and reconnect with a visual target, while other axons seem to be repelled from entering this site. Of note, we observed the presence of synaptic marker (i.e. Vglut2) in a variety of cases that include animals with relatively high number of axons in the SCN as well as animals with relatively low axon numbers. Thus, it is likely that regenerated axons with or without extensive arborization may make

synapses in the SCN. This is further supported in trans-synaptic reporter mouse line in which WGA labeled cells were observed in SCN, indicating that the axons indeed made connection with the target. Recently, it was reported that axons of *pten/socs3* KO animals make synaptic connections with SCN neurons following pre-chiasmic lesion [45]. However, it is not established whether the PCC in this study or the *pten/socs3* KO allows restoration of visual functions. Our lab is currently investigating this question. Since the SCN is normally innervated by a small population intrinsically photosensitive RGCs (ipRGCs), a question rises as to whether there is any degree of neuron-target selectivity in adult animals. While several studies have used single cell labeling to characterize axon targeting and branching patterns of different RGC types in lower species such as zebrafish and *Drosophila* [7, 37], no such comprehensive data currently exist for mammals. In this regard, it will be very interesting in the future to define normal targeting and arborization patterns of individual RGC types and assess the degree to which regenerating axons recapitulate this process. In light of different transgenic mouse lines in which distinct RGC subtypes including ipRGCs are labeled, initiation of such analysis may be feasible [35, 46].

In summary, our data highlight the limitation of shRNA technology in fully mimicking KO regeneration phenotypes, and indicate that combining AAV, shRNA, and pharmacotherapy represents an alternative and effective strategy to improve axon regeneration and importantly, target reconnection in WT animals. Further, extended application of whole brain imaging underscores technical improvement in conducting a systematic evaluation of axon targeting and uncovers heterogeneous and distinct terminal patterns by the individual regenerating axons.

MATERIALS AND METHODS

Cloning and generation of AAV2-shPTEN, AAV2-Cre and AAV2-CNTF: To suppress PTEN expression, we adopted a shRNA strategy, based on SIBR vectors [8] in which shRNA is located in an intron and flanked by sequences derived from mir155, an endogenous intronic shRNA. To maximize the probability of effectively targeting PTEN, four separate shRNA sequences, each targeting a different region of PTEN were concatenated in a single plasmid, which was then used to produce adeno-associated virus (AAV-shPTEN). Four sequences that target both mouse and rat PTEN were designed using siDIRECT website and design rules [47]: four targeted sequences for PTEN are: GCAGAAACAAAAGGAGATATCA;GATGATGTTTGAAACTATTCCA;GTAGAGTTCTTC CACAAACAGA;GATGAAGATCAGCATTCACAAA. Oligonucleotides encoding hairpin loops that included these sequences and deliberate mis-matches in the non-target strand were synthesized, annealed, inserted into the SIBR knockdown vector, and concatenated into a single plasmid as described [8]. A region of the SIBR knockdown vector comprising the ubiquitin promoter, intronic sequences, knockdown cassette, and EGFP open reading frame was cloned into an AAV-compatible plasmid (AAV-MCS, Stratagene), from which the CMV promoter, intron and MCS were removed. SIBR anti-luciferase control shRNA was transferred to AAV plasmid similarly. To construct AAV expressing a secretable form of CNTF, an AAV-compatible SIBR vector was created by PCR-amplifying the knockdown cassette of a SIBR vector with primers that created 5' Mlu1 (ACGCGTTTAAACTGGCCTCCGCGCC) and 3' Cla1 (ccgccgATCGATTCACTTGTACAGCTCGTCCA) sites. This cassette was inserted into a Stratagene AAV plasmid, replacing the CMV promoter and B-globin intron. The resulting AAV-SIBR plasmid was then modified via bridge PCR to create KpnI and BglII sites to flank the

EGFP open reading frame. Plasmid DNA encoding human CNTF was purchased from OpenBiosystems (Accession: BC068030) and the open reading frame was amplified using a forward primer that incorporated both a 5' Kpn1 restriction site and the NGF signal peptide sequence (GGTACCATGTCCATGTTGTTCTACACTCTGATCACAGCTTTTCTGATCGGCATACAG GCGGCTTTCACAGAGCATTCACCGC) and a reverse primer that incorporated 3' BglII site (AGATCTCTACATTTTCTTGTTGTTAGCAA). PCR-amplified CNTF was then used to replace the EGFP ORF in the AAV-SIBR vector via standard restriction digest and ligation. All enzymes were purchased from New England Biolabs. Plasmids were then used to produce adeno-associated virus serotype-2 (AAV2) (1-4x10^{13} particles/ml) at the University of Miami Viral Vector Core. For making AAV2 expressing Cre recombinase, the cDNA of Cre was inserted downstream of the CMV promoter/β-globin intron enhancer in the plasmid pAAV-MCS (Stratagene), containing the AAV2 inverted terminal repeats and a human growth hormone polyA signal. pAAV-RC (Stratagene) that encodes the AAV2 genes (rep and cap) and the helper plasmid (Stratagene) that encodes E2A, E4 and VA were used for co-transfection in 293T cells to generate recombinant AAV. Plasmids were then used to produce adeno-associated virus serotype-2 (AAV2) (1-4x10^{13} particles/ml) at the University of Miami Viral Vector Core.

Animals: All animal procedures were performed with the approval of IACUC at University of Miami. C57BL/6 (male or female; Charles River Laboratory) mice were used in this study, except for the wheat germ agglutinin (WGA) experiment in Figure 8 in which iZ/WAP mice (B6;129-Tg(CMV-Bgeo,-WGA,-ALPP)1Mgmj/J, Jackson Laboratory; Stock number, 017524)[24] were used. The age of animals used at the start of each experiment was between 4-6 weeks.

Animals were randomly assigned to different treatment groups. The investigator who analyzed the data was not blinded to the animal identity. The numbers of animals (n/group) used for each experiment range from 3 up to 14 depending on the type of experiment and are listed in the figure legends.

Intraorbital optic nerve crush: The optic nerve was exposed intraorbitally and crushed with jeweler's forceps (Dumont #5; Roboz) for 10 seconds approximately 1 mm behind the optic disc. To preserve the retinal blood supply, care was taken not to damage the underlying ophthalmic artery. After the surgical procedure, mice received a subcutaneous injection of buprenorphine (0.05 mg/kg, Bedford Lab) as post-operative analgesic. Eye ointment containing atropine sulphate was applied preoperatively to protect the cornea during surgery.

Intravitreal injection: For each intravitreal injection, a glass micropipette was inserted into the temporal eye posterior to the ora serrata and deliberately angled to avoid lens damage. Approximately 2 µl of vitreal fluid were withdrawn before injection to accommodate the same volume of either virus mix or cholera toxin β-subunit (CTB) conjugated with Alexa 555 (Invitrogen). AAV was administered either 2 weeks before or immediately after crush. cpt-cAMP (8-(4-chlorophenylthio) adenosine-3′,5′-cyclic monophosphorothioate; Sigma Aldrich; 50 µM) was injected intravitreally on the day of crush and biweekly (i.e. every other week) thereafter until euthanasia [25]. CTB (2 µg/µl) was injected 2-4 days prior to euthanasia. To visualize RGC projection in normal mice, CTB was injected and animals were euthanized 2-4

days later. After the completion of eye injection, animals received the same post-operative treatment as described above.

Immunohistochemistry/immunocytochemistry: Animals were perfused transcardially with PBS followed by 4% paraformaldehyde (PFA) in PBS, then tissues dissected and post-fixed with 4% PFA in PBS for 1 hour at room temperature. For histological sectioning, samples were cryoprotected by incubating in 30% sucrose in PBS for 48 hours. Optic nerves and retinae were cryosectioned to 10 and 20 μm thickness, respectively. Tissue sections were blocked in 5% normal goat serum and 0.3% Triton X-100 in PBS for 1 hour and incubated with primary antibodies diluted in blocking buffer overnight at 4ºC, followed by 1 hour incubation with secondary antibodies at room temperature. For cortical neuron immunocytochemistry, cells were fixed for 15 minutes in 4% PFA, washed with PBS and stained as described above. Primary antibodies used were anti-βIII-tubulin (1:800; Covance; #PRB-435P), PTEN (1:200; CST; #9559S), vesicular glutamate transporter 2 (Vglut2) (1:500; Synaptic Systems; #135304), wheat germ agglutinin lectin (WGA) (1:100; Sigma Aldrich; #T4144-1VL) and GFP (1:1,000; Abcam; #ab13970). All secondary antibodies (used at dilution of 1:400; Cy2, Cy3 or Cy5) were purchased from Jackson ImmunoResearch.

Measurement of PTEN immunoreactivity: The mean PTEN staining intensity in RGCs was measured using ImageJ software. Values for PTEN were based on 8 cells per section, 2 sections per case, and 3 per groups. Only GFP^+ cells in the ganglion cell layer with visible axon projection (i.e. RGCs) were selected for measurement. As negative controls, we omitted the

primary antibody. Individual mean values were corrected by staining levels in the corresponding negative controls (i.e. background subtracted) and then averaged across each group.

Cortical cell culture: Mixed cortical cultures from P2 rat pups were prepared as previously described [48]. Briefly, cells were dissociated by sequential digestion in papain (20 U/mL, Worthington) and trypsin (2.5%, Invitrogen), then cultured in supplemented Neurobasal media (Invitrogen) in 24-well Falcon plates on a substrate of PDL (100µg/mL, Sigma) and laminin (100µg/mL, Cultrex) at a density of 50,000 cells per well. AAV2-shPTEN or AAV2-anti-luciferase ($4x10^8$ total particles) were applied. Cultures were maintained at 37º C in a humidified CO^2 incubator for six additional days, with media exchanged every other day, then fixed in 4% paraformaldehyde (PFA, Sigma)/4% Sucrose (Sigma).

Western blot: Cortical cells were lysed with RIPA buffer. The protein concentration of the supernatant was determined using the Bio-Rad (Hercules, CA) protein assay reagent. Approximately 20 µg of protein was loaded and separated in a 10% acrylamide–Bis solution (Bio-Rad) gel. The protein was transferred onto Hybond-C Super membrane (Amersham Biosciences, Little Chalfont, UK) and blocked with 5% skim milk in 0.1% Tween 20 in PBS (TPBS). The membranes were incubated with anti-PTEN (1:1000; CST; #9559S) or anti-βIII tubulin (1:2000; Covance; #PRB-435P) in 5% BSA in TPBS overnight at 4°C. The membranes were incubated in biotinylated secondary antibody at a 1:5,000 dilution for 1 hour at room temperature. The membranes were incubated with HRP-conjugated antibody (Babco) before the labeled proteins were detected using the ECL agent (Pierce, Rockford, IL), following the

supplier's manual. The intensity of each band was quantified using the Image J. The relative level of PTEN was expressed as the ratio to βIII-tubulin. The quantification was the average calculated from three biological replicates (i.e. three independent cortical cell preparations).

Cell survival and axon regeneration quantification: To quantify regenerating axons, the crush site was identified by tissue morphology and CTB signal intensity, and the number of CTB^+ axons that projected various distances from the lesion was recorded. At least 4 sections were counted for each animal. To quantify RGCs, the number of $TUJ1^+$ cells in the ganglion cell layer of at least 4 non-consecutive retina sections per animal was counted.

Tissue clearing: Optic nerves and brains were prepared as described above and post-fixed overnight. Detailed description of tissue clearing is provided in our recent manuscripts [22]. Samples underwent dehydration by incubation in increasing concentrations of tetrahydrofuran (THF, Sigma-Aldrich) solutions. Optic nerves were incubated for 15 minutes each in 50% THF (diluted in water v/v), 80% THF, and 100% THF. Dehydrated optic nerves were rendered clear by incubating in BABB (a mixture of benzyl alcohol and benzyl benzoate (Sigma-Aldrich) at a ratio of 1:2) for 20 minutes. Adult mouse brains were gradually dehydrated with 50% THF for 12 hours, 80% THF for 12 hours, and 100% THF for 3 x 12 hours, and cleared in BABB for 12 hours with constant shaking before imaging.

Light Sheet Fluorescence Microscopy (LSFM) and axon tracing: LSFM was performed as previously described [21, 49]. For each optic nerve and brain between 100 and 500 optical slices were imaged with LSFM (LaVision) at a scan speed of 0.5–1.5 s per slice. Images were collected at 2 to 5µm increments in the Z axis. Images, and 3D volume rendering were prepared using Imaris software v7.6.1 (Bitplane). CTB-labeled RGC axons in the brain were traced using Imaris Filament Tracer Module and SCN boundaries were marked with Imaris Surface Module. Axons were identified and manually traced in individual 2D optical slices (z stacks) and compiled to give a 3D reconstruction.

Examination of trans-synaptic WGA labeling in iZ/WAP mice: Transgenic mice (B6;129-Tg(CMV-Bgeo,-WGA,-ALPP)1Mgmj/J, Jackson Laboratory; Stock number, 017524)[24] that express Cre recombinase-inducible WGA under the direction of the CMV, cytomegalovirus, promoter received optic nerve crush followed immediately by AAV-EGFP or PCC injection. One weeks following injury, AAV-Cre was injected intravitreally to induce WGA expression in RGCs. Five weeks after AAV-Cre injection, animals were perfused and tissues were collected for WGA immunohistochemistry.

Statistics: Data were analyzed using ANOVA and the Bonferroni within-groups comparison with additional testing using Dunnett's test or student's t-test. Significant differences required P values <0.05. Values were displayed as mean+ standard error of mean (SEM). Sample size (up to 14/group) was chosen in accordance to several previous studies of optic nerve regeneration[1, 4, 18].

Acknowledgments: This work was supported by grants from U.S Army W81XWH-05-1-0061 (KKP), W81XWH-12-1-0319 (KKP), NEI 1R01EY022961-01 (KKP), Ziegler Foundation (KKP), Pew Charitable Trust (KKP), Craig H. Neilsen Foundation (KKP), and the Buoniconti Fund (KKP). We thank Imaging, and Viral Vector Core at the Miami Project to Cure Paralysis, Dr. David Turner for SIBR vector, Dr. Vance Lemmon and Dr. John Bixby for guidance with shRNA vector, Dr Bryan Luikart for shPTEN plasmid.

Conflict of interest: Authors declare no conflict of interest.

References

1. Park KK, Liu K, Hu Y, Smith PD, Wang C, Cai B *et al.* Promoting axon regeneration in the adult CNS by modulation of the PTEN/mTOR pathway. *Science* 2008; **322**(5903)**:** 963-6.

2. Smith PD, Sun F, Park KK, Cai B, Wang C, Kuwako K *et al.* SOCS3 deletion promotes optic nerve regeneration in vivo. *Neuron* 2009; **64**(5)**:** 617-23.

3. Sun F, Park KK, Belin S, Wang D, Lu T, Chen G *et al.* Sustained axon regeneration induced by co-deletion of PTEN and SOCS3. *Nature* 2011; **480**(7377)**:** 372-5.

4. de Lima S, Koriyama Y, Kurimoto T, Oliveira JT, Yin Y, Li Y *et al.* Full-length axon regeneration in the adult mouse optic nerve and partial recovery of simple visual behaviors. *Proc Natl Acad Sci U S A* 2012; **109**(23)**:** 9149-54.

5. Kotterman MA, Schaffer DV. Engineering adeno-associated viruses for clinical gene therapy. *Nat Rev Genet* 2014; **15**(7)**:** 445-51.

6. Alsina B, Vu T, Cohen-Cory S. Visualizing synapse formation in arborizing optic axons in vivo: dynamics and modulation by BDNF. *Nat Neurosci* 2001; **4**(11)**:** 1093-101.

7. Robles E, Laurell E, Baier H. The retinal projectome reveals brain-area-specific visual representations generated by ganglion cell diversity. *Curr Biol* 2014; **24**(18)**:** 2085-96.

8. Chung KH, Hart CC, Al-Bassam S, Avery A, Taylor J, Patel PD *et al.* Polycistronic RNA polymerase II expression vectors for RNA interference based on BIC/miR-155. *Nucleic Acids Res* 2006; **34**(7)**:** e53.

9. Zukor K, Belin S, Wang C, Keelan N, Wang X, He Z. Short Hairpin RNA against PTEN Enhances Regenerative Growth of Corticospinal Tract Axons after Spinal Cord Injury. *J Neurosci* 2013; **33**(39)**:** 15350-61.

10. Luikart BW, Schnell E, Washburn EK, Bensen AL, Tovar KR, Westbrook GL. Pten knockdown in vivo increases excitatory drive onto dentate granule cells. *J Neurosci* 2011; **31**(11)**:** 4345-54.

11. Hellstrom M, Harvey AR. Retinal ganglion cell gene therapy and visual system repair. *Curr Gene Ther* 2011; **11**(2)**:** 116-31.

12. Leaver SG, Cui Q, Bernard O, Harvey AR. Cooperative effects of bcl-2 and AAV-mediated expression of CNTF on retinal ganglion cell survival and axonal regeneration in adult transgenic mice. *Eur J Neurosci* 2006; **24**(12)**:** 3323-32.

13. Leaver SG, Cui Q, Plant GW, Arulpragasam A, Hisheh S, Verhaagen J *et al.* AAV-mediated expression of CNTF promotes long-term survival and regeneration of adult rat retinal ganglion cells. *Gene Ther* 2006; **13**(18)**:** 1328-41.

14. Pernet V, Joly S, Dalkara D, Jordi N, Schwarz O, Christ F *et al.* Long-distance axonal regeneration induced by CNTF gene transfer is impaired by axonal misguidance in the injured adult optic nerve. *Neurobiol Dis* 2013; **51:** 202-13.

15. Pernet V, Joly S, Jordi N, Dalkara D, Guzik-Kornacka A, Flannery JG *et al.* Misguidance and modulation of axonal regeneration by Stat3 and Rho/ROCK signaling in the transparent optic nerve. *Cell Death Dis* 2013; **4:** e734.

16. Muller A, Hauk TG, Leibinger M, Marienfeld R, Fischer D. Exogenous CNTF stimulates axon regeneration of retinal ganglion cells partially via endogenous CNTF. *Mol Cell Neurosci* 2009; **41**(2)**:** 233-46.

17. Park K, Luo JM, Hisheh S, Harvey AR, Cui Q. Cellular mechanisms associated with spontaneous and ciliary neurotrophic factor-cAMP-induced survival and axonal regeneration of adult retinal ganglion cells. *J Neurosci* 2004; **24**(48)**:** 10806-15.

18. Moore DL, Blackmore MG, Hu Y, Kaestner KH, Bixby JL, Lemmon VP *et al.* KLF family members regulate intrinsic axon regeneration ability. *Science* 2009; **326**(5950)**:** 298-301.

19. Hellstrom M, Pollett MA, Harvey AR. Post-injury delivery of rAAV2-CNTF combined with short-term pharmacotherapy is neuroprotective and promotes extensive axonal regeneration after optic nerve trauma. *J Neurotrauma* 2011; **28**(12)**:** 2475-83.

20. Hellstrom M, Harvey AR. Cyclic AMP and the regeneration of retinal ganglion cell axons. *Int J Biochem Cell Biol* 2014.

21. Luo X, Yungher B, Park KK. Application of tissue clearing and light sheet fluorescence microscopy to assess optic nerve regeneration in unsectioned tissues. *Methods Mol Biol* 2014; **1162:** 209-17.

22. Luo X, Salgueiro Y, Beckerman SR, Lemmon VP, Tsoulfas P, Park KK. Three-dimensional evaluation of retinal ganglion cell axon regeneration and pathfinding in whole mouse tissue after injury. *Exp Neurol* 2013; **247:** 653-62.

23. Pernet V, Schwab ME. Lost in the jungle: new hurdles for optic nerve axon regeneration. *Trends Neurosci* 2014; **37**(7)**:** 381-387.

24. Louis GW, Leinninger GM, Rhodes CJ, Myers MG, Jr. Direct innervation and modulation of orexin neurons by lateral hypothalamic LepRb neurons. *J Neurosci* 2010; **30**(34)**:** 11278-87.

25. Kurimoto T, Yin Y, Omura K, Gilbert HY, Kim D, Cen LP *et al.* Long-distance axon regeneration in the mature optic nerve: contributions of oncomodulin, cAMP, and pten gene deletion. *J Neurosci* 2010; **30**(46)**:** 15654-63.

26. Lewandowski G, Steward O. AAVshRNA-mediated suppression of PTEN in adult rats in combination with salmon fibrin administration enables regenerative growth of corticospinal axons and enhances recovery of voluntary motor function after cervical spinal cord injury. *J Neurosci* 2014; **34**(30)**:** 9951-62.

27. Ohtake Y, Park D, Abdul-Muneer PM, Li H, Xu B, Sharma K *et al.* The effect of systemic PTEN antagonist peptides on axon growth and functional recovery after spinal cord injury. *Biomaterials* 2014; **35**(16)**:** 4610-26.

28. Christie KJ, Webber CA, Martinez JA, Singh B, Zochodne DW. PTEN inhibition to facilitate intrinsic regenerative outgrowth of adult peripheral axons. *J Neurosci* 2010; **30**(27)**:** 9306-15.

29. Xu XM, Yoo MH, Carlson BA, Gladyshev VN, Hatfield DL. Simultaneous knockdown of the expression of two genes using multiple shRNAs and subsequent knock-in of their expression. *Nat Protoc* 2009; **4**(9)**:** 1338-48.

30. Fraser MM, Bayazitov IT, Zakharenko SS, Baker SJ. Phosphatase and tensin homolog, deleted on chromosome 10 deficiency in brain causes defects in synaptic structure, transmission and plasticity, and myelination abnormalities. *Neuroscience* 2008; **151**(2)**:** 476-88.

31. Hellstrom M, Muhling J, Ehlert EM, Verhaagen J, Pollett MA, Hu Y *et al.* Negative impact of rAAV2 mediated expression of SOCS3 on the regeneration of adult retinal ganglion cell axons. *Mol Cell Neurosci* 2011; **46**(2)**:** 507-15.

32. Gao Y, Deng K, Hou J, Bryson JB, Barco A, Nikulina E *et al.* Activated CREB is sufficient to overcome inhibitors in myelin and promote spinal axon regeneration in vivo. *Neuron* 2004; **44**(4)**:** 609-21.

33. Park KK, Hu Y, Muhling J, Pollett MA, Dallimore EJ, Turnley AM *et al.* Cytokine-induced SOCS expression is inhibited by cAMP analogue: impact on regeneration in injured retina. *Mol Cell Neurosci* 2009; **41**(3)**:** 313-24.

34. Wyatt C, Ebert A, Reimer MM, Rasband K, Hardy M, Chien CB *et al.* Analysis of the astray/robo2 zebrafish mutant reveals that degenerating tracts do not provide strong guidance cues for regenerating optic axons. *J Neurosci* 2010; **30**(41)**:** 13838-49.

35. Osterhout JA, El-Danaf RN, Nguyen PL, Huberman AD. Birthdate and outgrowth timing predict cellular mechanisms of axon target matching in the developing visual pathway. *Cell Rep* 2014; **8**(4)**:** 1006-17.

36. McFarlane S, McNeill L, Holt CE. FGF signaling and target recognition in the developing Xenopus visual system. *Neuron* 1995; **15**(5)**:** 1017-28.

37. Cohen-Cory S, Fraser SE. Effects of brain-derived neurotrophic factor on optic axon branching and remodelling in vivo. *Nature* 1995; **378**(6553)**:** 192-6.

38. Aviles-Trigueros M, Sauve Y, Lund RD, Vidal-Sanz M. Selective innervation of retinorecipient brainstem nuclei by retinal ganglion cell axons regenerating through peripheral nerve grafts in adult rats. *J Neurosci* 2000; **20**(1)**:** 361-74.

39. Vidal-Sanz M, Aviles-Trigueros M, Whiteley SJ, Sauve Y, Lund RD. Reinnervation of the pretectum in adult rats by regenerated retinal ganglion cell axons: anatomical and functional studies. *Prog Brain Res* 2002; **137:** 443-52.

40. Wizenmann A, Bahr M. Growth characteristics of ganglion cell axons in the developing and regenerating retino-tectal projection of the rat. *Cell Tissue Res* 1997; **290**(2)**:** 395-403.

41. Sauve Y, Sawai H, Rasminsky M. Topological specificity in reinnervation of the superior colliculus by regenerated retinal ganglion cell axons in adult hamsters. *J Neurosci* 2001; **21**(3)**:** 951-60.

42. Carter DA, Bray GM, Aguayo AJ. Regenerated retinal ganglion cell axons form normal numbers of boutons but fail to expand their arbors in the superior colliculus. *J Neurocytol* 1998; **27**(3)**:** 187-96.

43. Sauve Y, Sawai H, Rasminsky M. Functional synaptic connections made by regenerated retinal ganglion cell axons in the superior colliculus of adult hamsters. *J Neurosci* 1995; **15**(1 Pt 2)**:** 665-75.

44. Carter DA, Bray GM, Aguayo AJ. Regenerated retinal ganglion cell axons can form well-differentiated synapses in the superior colliculus of adult hamsters. *J Neurosci* 1989; **9**(11)**:** 4042-50.

45. Li S, He Q, Wang H, Tang X, Ho KW, Gao X *et al.* Injured adult retinal axons with Pten and Socs3 co-deletion reform active synapses with suprachiasmatic neurons. *Neurobiol Dis* 2014; **73C:** 366-376.

46. Hattar S, Kumar M, Park A, Tong P, Tung J, Yau KW *et al.* Central projections of melanopsin-expressing retinal ganglion cells in the mouse. *J Comp Neurol* 2006; **497**(3)**:** 326-49.

47. Ui-Tei K, Naito Y, Takahashi F, Haraguchi T, Ohki-Hamazaki H, Juni A *et al.* Guidelines for the selection of highly effective siRNA sequences for mammalian and chick RNA interference. *Nucleic Acids Res* 2004; **32**(3)**:** 936-48.

48. Blackmore MG, Wang Z, Lerch JK, Motti D, Zhang YP, Shields CB *et al.* Kruppel-like Factor 7 engineered for transcriptional activation promotes axon regeneration in the adult corticospinal tract. *Proc Natl Acad Sci U S A* 2012.

49. Erturk A, Mauch CP, Hellal F, Forstner F, Keck T, Becker K *et al.* Three-dimensional imaging of the unsectioned adult spinal cord to assess axon regeneration and glial responses after injury. *Nat Med* 2012; **18**(1)**:** 166-71.

Figure Legends

Figure 1. AAV-shRNA mediated suppression of PTEN (**a**) A map of AAV2-shPTEN4 construct. Control and shPTEN constructs contain EGFP reporter. (**b**) Immunocytochemistry showing expression of GFP, PTEN, and beta III tubulin (TUJ1) in cultured cortical neurons incubated with either AAV-anti-luciferase-EGFP (control) or AAV-RNA against PTEN (AAV-shPTEN4) for 7 days. These are representative micrographs from 2 separate experiments. (**c**) Retina sections following control AAV2-EGFP (EGFP) or AAV2-shPTEN4 injection show PTEN knockdown in ganglion cell layer. (**d**) Flat-mounted retina 2 weeks following intravitreal injection of AAV2-shPTEN4, stained with antibodies against GFP and TUJ1 shows >90% transduction efficiency in RGCs. (**e**) Western blot of protein lysates extracted from cultured cortical neurons showing PTEN level at 7 days after the addition of AAV-shPTEN4 or AAV-EGFP. (**f**) Quantification of PTEN level from the western blot. Values are represented as ratio of PTEN to βIII-tubulin (n=3 biological replicates). (g) Quantification of PTEN expression in RGCs in retinal sections, measured by ImageJ densitometry method. Intensity unit is an arbitary value. Error bars, SEM. Scale bars, 20 μm.

Figure 2. Assessment of RGC axon regeneration following AAV-shRNA mediated knockdown of PTEN. (**a**) Representative optic nerve sections of mice receiving AAV2-shPTEN4 or control AAV2–EGFP injection. Red asterisk, lesion site. (**b**) Quantification of regenerating axons in control and shPTEN treated animals (n=5/group) at different distances from the lesion site. The data are represented as mean number of axons per section. (**c**) Representative images of TUJ1 stained wholemount retinae for both groups. (**d**) Quantification of RGC density (n=5/group). Error bars, SEM; ****: $p<0.0001$; ***: $p<0.001$, *$p<0.05$ ANOVA

with Bonferroni correction (b) and student's unpaired t-test (d). Scale bars, 100 μm (a); 20 μm (b).

Figure 3. AAV-shPTEN, AAV-CNTF and cpt-cAMP further improves lengthy RGC axon regeneration. (**a**) Representative optic nerve sections of mice receiving various AAV treatments. Control, AAV2-EGFP; shPTEN4, AAV2-shPTEN4; CNTF, AAV-CNTF; CNTF/cAMP, AAV2-CNTF/cpt-cAMP; PCC, AAV2-shPTEN4/AAV2-CNTF/cpt-cAMP. Red asterisk, lesion site. (**a'**) Higher-magnification images of the boxed area in A. (**b**) Quantification of regenerating axons at different distances from the lesion site (n=6-8/group). *: $p<0.05$, Bonferroni test (PCC significantly different to AAV-CNTF and AAV-CNTF/cpt-cAMP groups). (**c**) Representative images of TUJ1 stained wholemount retinae from mice receiving various AAV treatments. (**d**) Quantification of RGC density (n=6/group). Error bars, SEM. Scale bars, 100 μm (a); 20 μm (d).

Figure 4. Tissue clearing and ultramicroscopic assessment of axonal trajectories in the optic chiasm of PCC animals. (**a**) Adult mouse brains with and without tissue clearing. The eyes and optic nerves are attached to the brain. (**b**) Top view of an intact mouse brain. Brain from an uninjured mouse shows the entire trajectory of CTB-labeled RGC axons: all visual targets are visible, including the suprachiasmatic nucleus, lateral geniculate nucleus, and superior colliculus, ipsi- and contralaterally to the injected eye. (**c**) A horizontal optical slice from an unsectioned brain of a PCC-treated animal shows CTB-labeled axons in the optic chiasm. (**c'**) Higher-magnification of the boxed area in c. (**d**) Reconstruction of traced axons through the chiasm. (**e**) Quantification of axonal trajectories into different regions in 5 different cases (i.e. ipsi- and contralateral optic tracts, contralateral optic nerve, and hypothalamic regions). Contra,

contralateral; Hypothal. Hypothalamic region; Ipsi, ipsilateral; IOT, ipsilateral optic tract; LGN, lateral geniculate nucleus; ON, optic nerve; OT, optic tract; OX, optic chiasm; 3rd V, 3rd ventricle; SC, superior coliculus; SCN, suprachiasmatic nucleus. Scale bars, 100 µm.

Figure 5. Ultramicroscopic visualization of axonal projections in mouse visual target. (**a**) Optic chiasm, optic tract and SCN shown by CTB labeling in a cleared, uninjured brain. (**b**) Bottom view of a brain containing the SCN (i.e. dotted circles) imaged from a brain of an injured control mouse subjected to AAV-EGFP injection. None of the control animals had regenerating axons in the brain. (**c**) and (**d**) Bottom view of brains of two different PCC-treated animals showing regenerated axons in the chiasm and SCN. Yellow arrowhead indicates a regenerating axon extending into the SCN. Yellow arrow indicates distal end of the same axon showing continued growth beyond the SCN. White arrows in d indicate extensive arborization. (**e-j**), reconstructions of single axons showing various growth patterns. In (**e**), an axon bypasses the target. In (**f**) and (**g**), axons traverse the target. In (**h**), axon terminals are found within the SCN. In (**i**) and (**j**), axons enter the SCN and form complex arborization. ON, optic nerve; Uninj, uninjured; SCN, suprachiasmatic nucleus. Scale bars, 100 µm.

Figure 6. Regenerate axons following PCC treatment form synapses in the SCN. (**a**) Schematic coronal brain section showing the SCN marked in a dotted red rectangle. (**b**) CTB-labeled axons (red) in the SCN express presynaptic marker Vglut2 (green). (**b'**) High-magnifications of the boxed area in (**b**), with XZ and YZ projections at the yellow crosshairs. (**c**) Retinal cross section showing RGCs expressing WGA (green) six weeks following AAV-Cre injection in iZ/WAP mice. DAPI (blue) is used in these tissue sections for nuclear staining. (**d**)

WGA^+ cells in the SCN of an uninjured animal. WGA (green) and DAPI (blue). (**e**) WGA^+ cells in the LGN (as marked by dotted line) of an uninjured animal. WGA (green) and DAPI (blue). (**f**) No WGA^+ cells are detected in the injured AAV-EGFP control mice (n=5). (**g**) Low magnification coronal brain section showing the SCN of an injured PCC animal, marked in a yellow circles immunostained with antibodies against WGA. CTB, red; DAPI, blue. (**h**) High magnification of the dotted area in (**g**) showing CTB^+ axons (red) wrapping or making close contact with WGA^+ cells in the SCN. Scale bars, 50 μm.

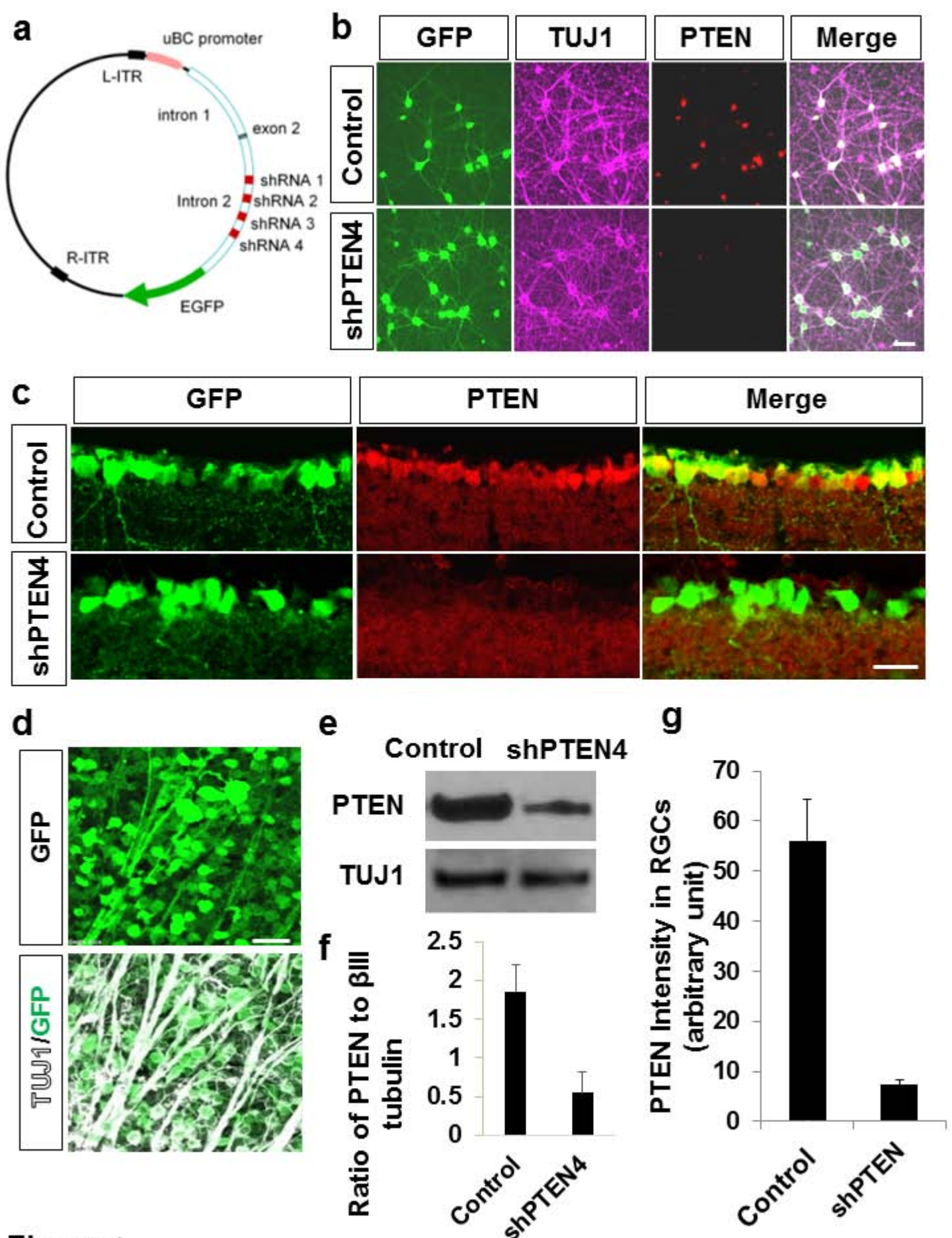
a
uBC promoter
L-ITR
intron 1
exon 2
shRNA 1
shRNA 2
shRNA 3
shRNA 4
Intron 2
R-ITR
EGFP
b
GFP
TUJ1
PTEN
Merge
Control
shPTEN4
c
GFP
PTEN
Merge
Control
shPTEN4
d
GFP
TUJ1/GFP
e
Control
shPTEN4
PTEN
TUJ1
f
Ratio of PTEN to βIII tubulin
2.5
2
1.5
1
0.5
0
Control
shPTEN4
g
PTEN Intensity in RGCs (arbitrary unit)
70
60
50
40
30
20
10
0
Control
shPTEN

Figure 1

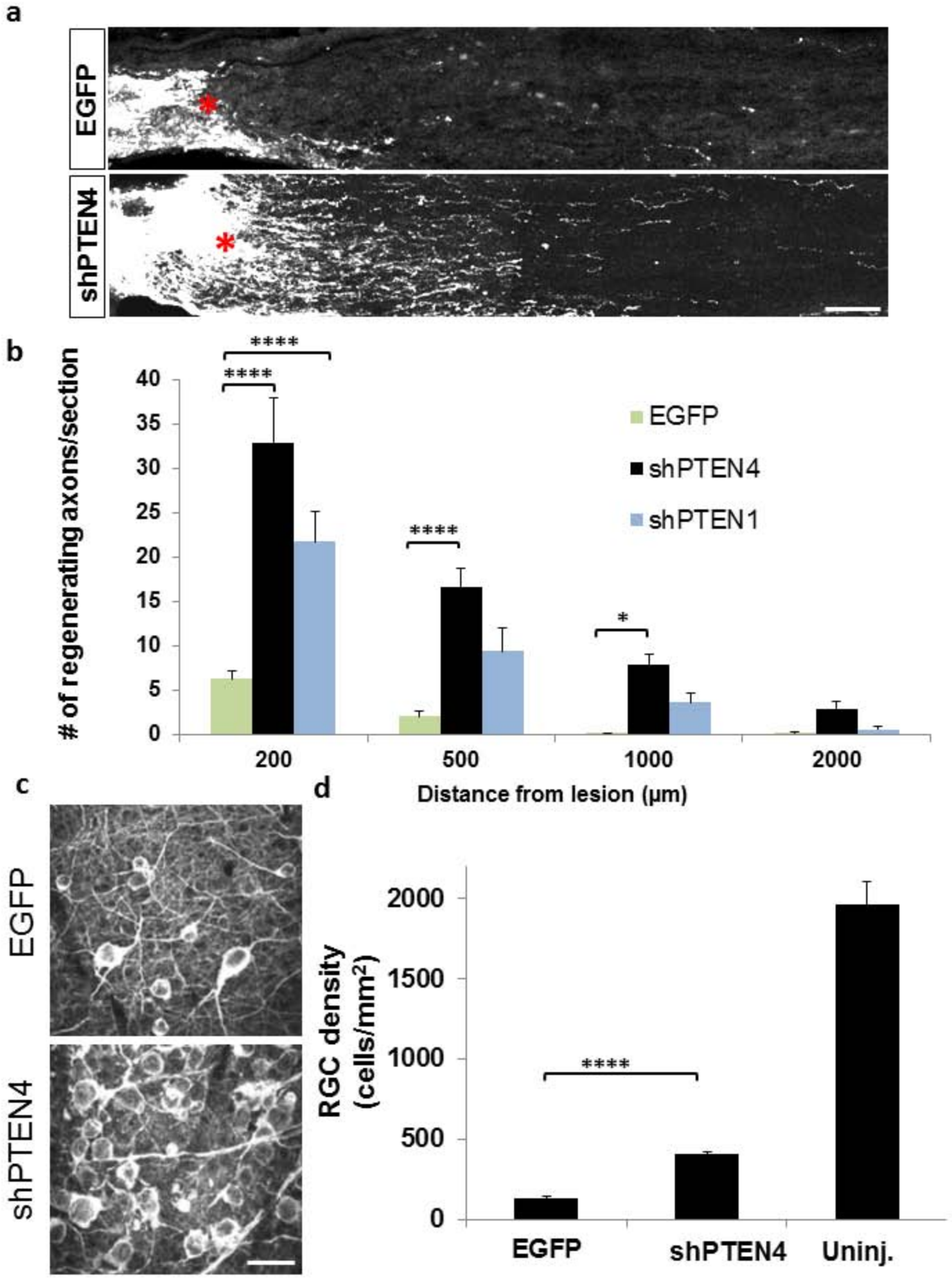
a
EGFP
shPTEN4
b
# of regenerating axons/section
40
35
30
25
20
15
10
5
0
****
****
****
*
EGFP
shPTEN4
shPTEN1
200
500
1000
2000
Distance from lesion (µm)
c
EGFP
shPTEN4
d
RGC density (cells/mm²)
2000
1500
1000
500
0
****
EGFP
shPTEN4
Uninj.

Figure 2

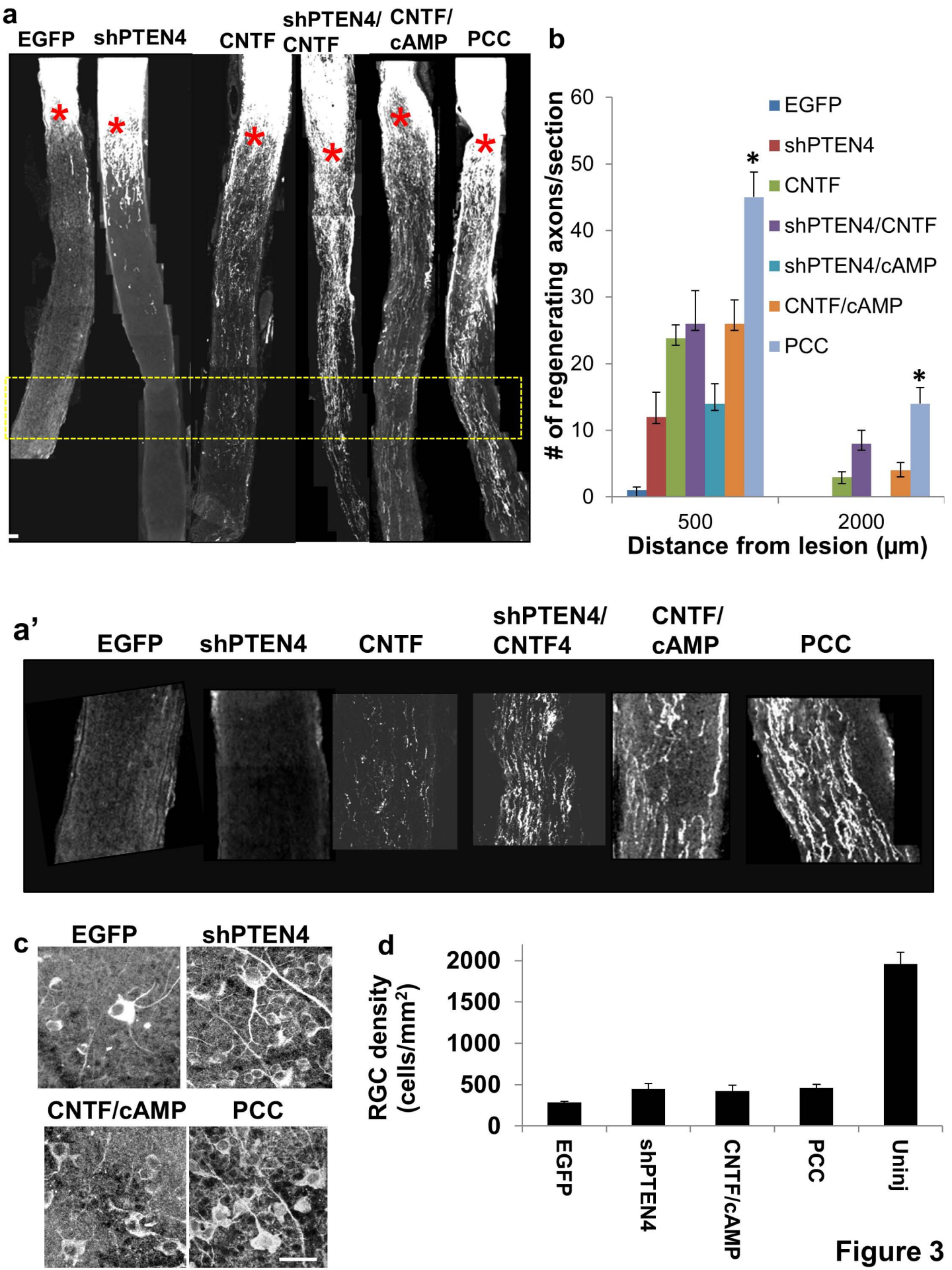
a
EGFP
shPTEN4
CNTF
shPTEN4/ CNTF
CNTF/ cAMP
PCC
b
# of regenerating axons/section
60
50
40
30
20
10
0
EGFP
shPTEN4
CNTF
shPTEN4/CNTF
shPTEN4/cAMP
CNTF/cAMP
PCC
500
2000
Distance from lesion (µm)
a'
EGFP
shPTEN4
CNTF
shPTEN4/ CNTF4
CNTF/ cAMP
PCC
c
EGFP
shPTEN4
CNTF/cAMP
PCC
d
RGC density (cells/mm²)
2000
1500
1000
500
0
EGFP
shPTEN4
CNTF/cAMP
PCC
Uninj

Figure 3

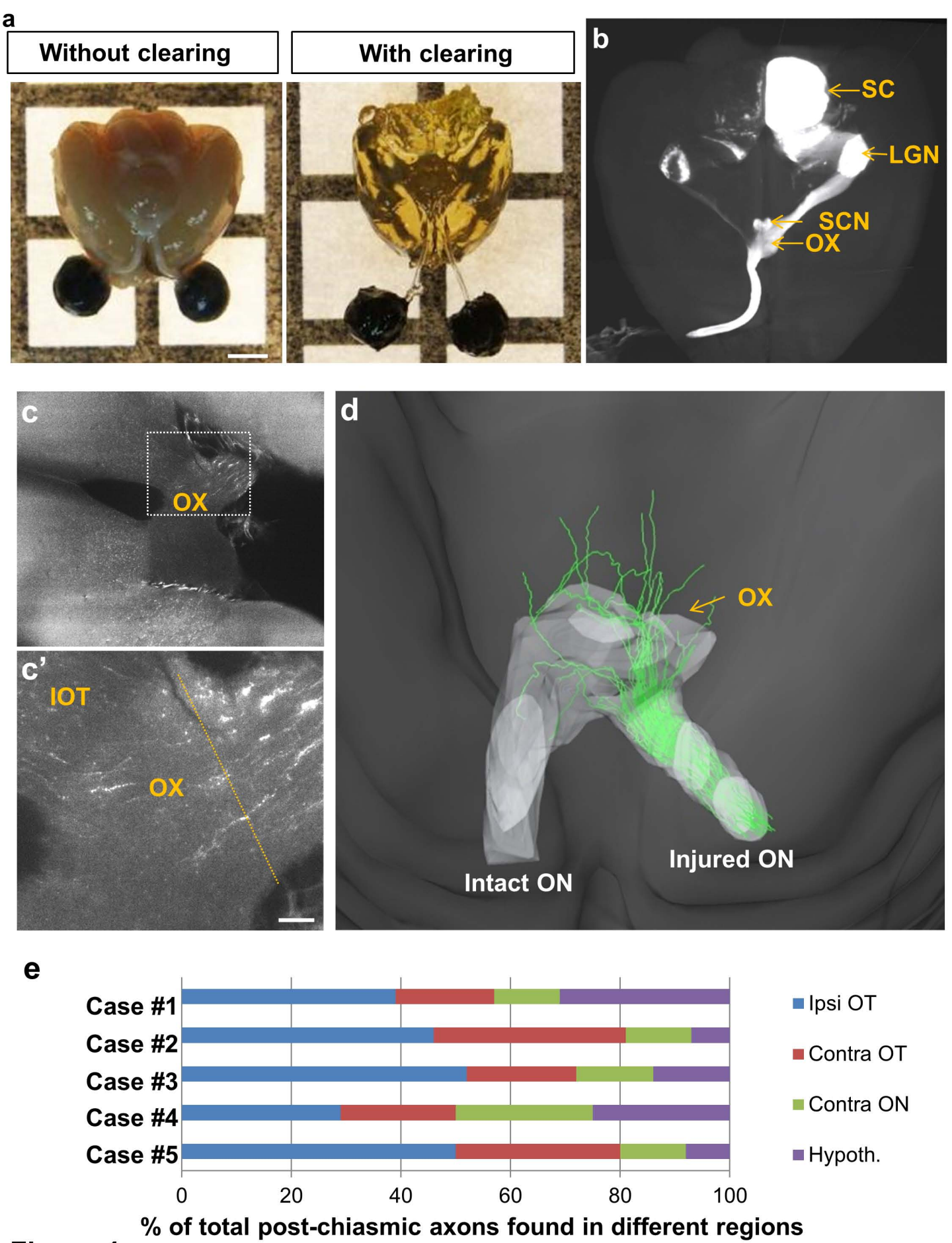
a
Without clearing
With clearing
b
SC
LGN
SCN
OX
c
OX
c'
IOT
OX
d
OX
Intact ON
Injured ON
e
Case #1
Case #2
Case #3
Case #4
Case #5
0
20
40
60
80
100
% of total post-chiasmic axons found in different regions
Ipsi OT
Contra OT
Contra ON
Hypoth.

Figure 4

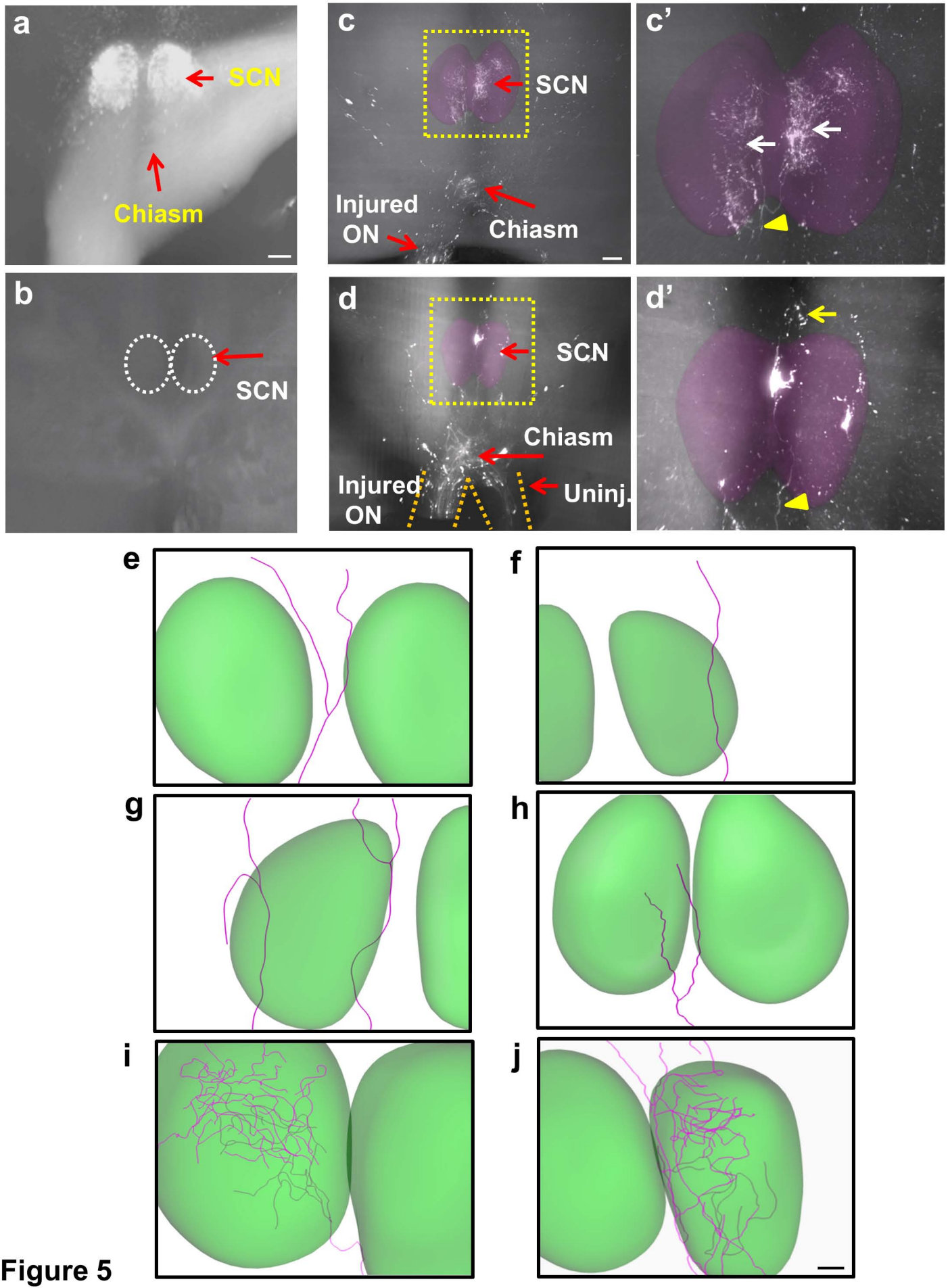
a
SCN
Chiasm
b
SCN
c
SCN
Injured
ON
Chiasm
c'
d
SCN
Chiasm
Injured
ON
Uninj.
d'
e
f
g
h
i
j

Figure 5

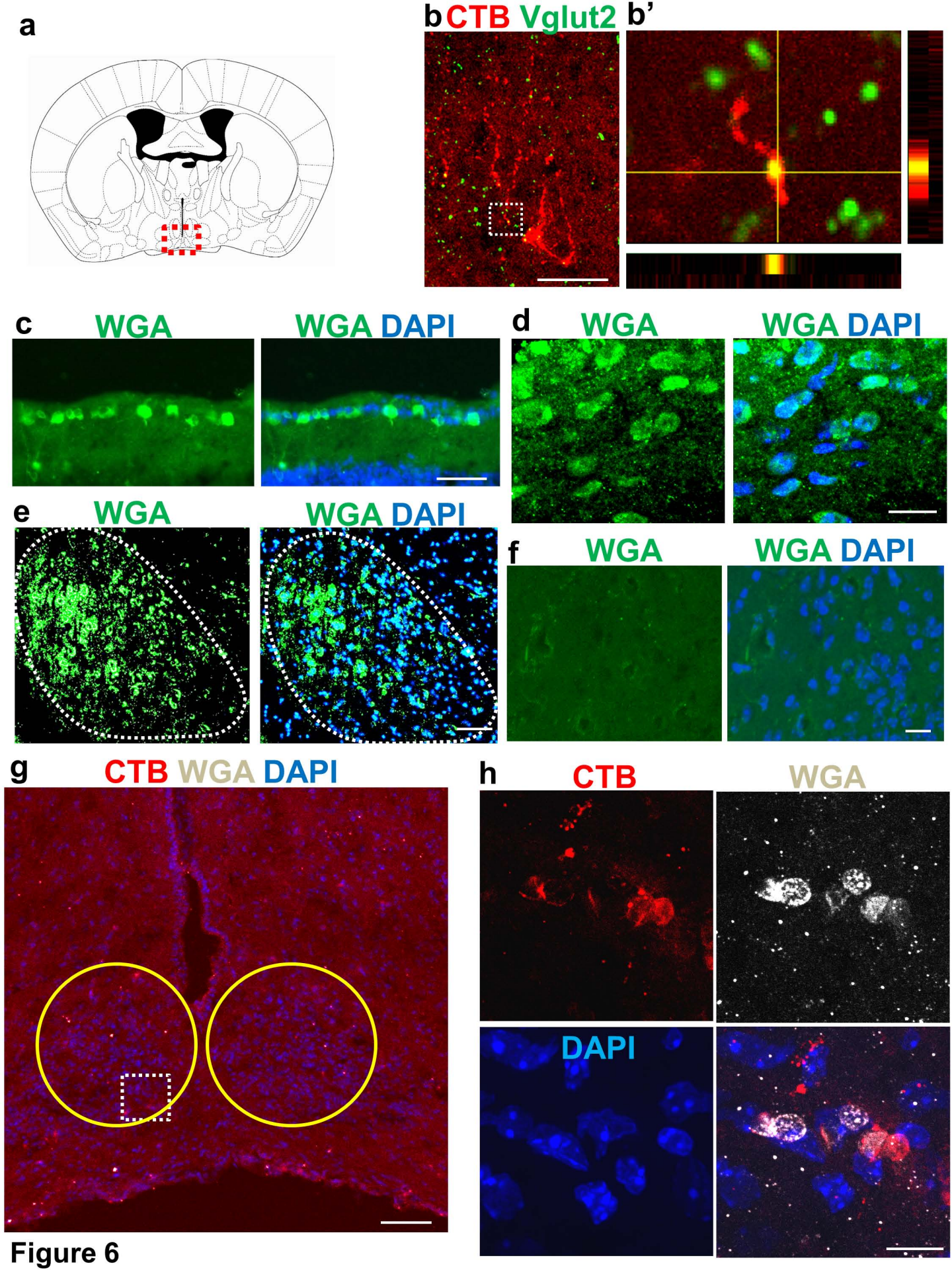
a
b CTB Vglut2
b'
c WGA
WGA DAPI
d WGA
WGA DAPI
e WGA
WGA DAPI
f WGA
WGA DAPI
g CTB WGA DAPI
h CTB
WGA
DAPI

Figure 6